Construction and analysis of the receiver for a solar thermal cooker system

by

Paulene Govender

June, 2013

Submitted in fulfilment of the academic
requirements for the degree of
Master of Science in the
School of Chemistry and Physics,
University of KwaZulu-Natal,
Durban.

The financial assistance of the National Research foundation (NRF) towards this research is hereby acknowledged. Opinions expressed and conclusions arrived at, are those of the author and are not necessarily to be attributed to the NRF.

Abstract

One of the key components in a solar thermal cooker system is the receiver since the performance of the receiver greatly affects the entire system. Absorption of the maximum amount of reflected radiation is crucial for ensuring the system is operating at high efficiency. A small-scale solar thermal cooker was constructed and tested. The main focus was the design, construction and analysis of a receiver for the solar cooker. The receiver was constructed from mild steel and contains water as the heat transfer fluid. The receiver consists of two half shells fixed to either end of a short cylinder to form an elongated boiling chamber for the water as it is heated by concentrated solar radiation. One of the half shells is exposed to the concentrated solar radiation and is coated with a high-temperature resistant black paint. The size of the receiver was determined by the method of ray-tracing. The maximum temperature the water attained within the receiver during solar heating was 136 °C. The highest receiver efficiency was 66%. It was shown that there has been effective heat transfer within the system.

Preface

The experimental work described in this dissertation was carried out in the School of Chemistry and Physics, University of KwaZulu-Natal, Westville, Durban, from January 2011 to June 2013, under the supervision of Dr. A.P. Matthews and Professor Jørgen Løvseth.

These studies represent original work by the author and have not otherwise been submitted in any form for any degree or diploma to any tertiary institution. Where use has been made of the work of others it is duly acknowledged in the text.

Declaration-Plagiarism

I, Paulene Govender declare that

1. The research reported in this thesis, except where otherwise indicated, is my original research.
2. This thesis has not been submitted for any degree or examination at any other university.
3. This thesis does not contain other persons' data, pictures, graphs or other information, unless specifically acknowledged as being sourced from other persons.
4. This thesis does not contain other persons' writing, unless specifically acknowledged as being sourced from other researchers. Where other written sources have been quoted, then:
   (a) Their words have been re-written but the general information attributed to them has been referenced.
   (b) Where their exact words have been used, then their writing has been placed in italics and inside quotation marks, and referenced.
5. This thesis does not contain text, graphics or tables copied and pasted from the Internet, unless specifically acknowledged, and the source being detailed in the thesis and in the Bibliography section.

Signed: .....

Acknowledgements

Firstly, I would like to express my sincere gratitude to my supervisor Dr Alan Matthews for his contribution towards the completion of this thesis. Your invaluable help, guidance and patience throughout this project is highly appreciated.

To my co-supervisor, Professor Jørgen Løvseth, thank you for all your constructive criticism and advice during the course of this project. I really appreciate all of your guidance and assistance whenever it was needed.

Special thanks to Principal Technician, Enock Chekure for his valuable time, support and assistance whenever it was needed. I am truly grateful for your willingness to help with all of my requests.

To the staff at the central academic workshop: Danny Padayachee, Sagie Pillay and Logan Pillay, I would like to thank you for your help with the construction and realization of the system.

I would also like to thank, Evans Zhandire, Robert van den Heetkamp, Michael Brooks, Luke Philogene and Myron Nobin for their assistance.

To my colleagues, Heiko Heilgendorff, Rakesh Mohanlal, Sharlene-Asia Naicker and Marcelino Macome for their unwavering assistance and support.

Thanks to our Norwegian collaborators Professor Ole Jørgen Nydal, Maximme Mussard and Fong Chee Woh at the Norwegian University of Science and Technology (NTNU) for their assistance.

To my family, thank you for all the encouragement and immense support that you have always given me.

To Professor Sadha Pillay who could not be here to see the finalization of this work, thank you for your guidance during the time of your supervision.

Lastly, I would also like to thank the National Research Foundation (NRF) for financial support.

Contents

List of Figures

List of Tables

Chapter 1

Introduction

The need for sustainable and clean energy is of crucial importance for the reduction of carbon dioxide (CO_2) emissions, partially caused by the burning of fossil fuels. The rapid depletion and limited availability of fossil fuels makes the utilization of renewable resources more critical. Solar energy enters the earth's atmosphere in the form of shortwave radiation and is emitted in the form of longwave radiation. The burning of fossil fuels emit greenhouse gases such as CO_2 and methane (CH_4) which prevent longwave solar radiation from leaving the earth's atmosphere and entering into space. This results in excess thermal energy being trapped in the atmosphere, raising the temperature of the earth. This process is known as global warming [1]. In order to counteract the effects of global warming a significant decline in the burning of fossil fuels is required and more environmentally friendly energy alternatives have to be considered. Some of which include solar, wind, hydro, wave, tidal and geothermal.

Solar radiation is the most plentiful source of renewable energy, and those technologies that utilize the solar resource can be categorized into photovoltaics or solar thermal power. The latter can be further classified as either concentrating or non-concentrating, based on the type of collector used. Non-concentrating systems are generally used for low temperature applications such as water heating, while concentrating systems are employed for larger scale, high temperature applications such as electricity generation. For solar thermal electricity generation, the four main components are the concentrator, receiver, working fluid and some form of power conversion unit such as a steam turbine or Stirling engine. The solar thermal technologies with the highest potential are the parabolic trough, central receiver and parabolic dish/Stirling engine systems. The major advantage of these systems is their non-pollution of the environment. Every square meter of reflector surface within a solar field is sufficient to prevent the annual production of 150 to 250 kilograms of CO_2 [2]. This makes solar thermal

technology a viable alternative to fossil fuels for cleaner energy production.

South Africa is fortunate to have one of the best solar resources in the world, with an average annual Direct Normal Irradiation (DNI) of more than 2500 kWh/m^2 [3]. This makes South Africa an ideal location for implementing solar powered technologies such as concentrating solar power (CSP) and photovoltaics (PV). Figure 1.1 illustrates the DNI distribution for South Africa. Of the nine provinces KwaZulu-Natal is one of the areas with the lowest annual average DNI of less than 6.0 kWh/m^2/d. The Northern Cape has the highest DNI of more than 7.0 kWh/m^2/d, making this area an appropriate location for implementing CSP technologies such as parabolic dish and trough, central receiver and linear Fresnel [4].

Solar thermal power is not restricted to large scale applications but can also be used for domestic applications such as solar thermal cookers. The components of a solar thermal cooker are similar to those used in solar thermal electricity generation, with the exception of the power conversion unit. However, one of the key components in a solar thermal cooker system is the receiver since the performance of the receiver greatly affects the entire system. This is due to the fact that the receiver is responsible for absorbing the concentrated radiation and transferring the thermal energy to either the heat transfer fluid or to the cooking surface. Absorption of the maximum amount of radiation is crucial for ensuring the system is operating at high efficiency. Therefore, scientists and engineers spend much effort on the design, analysis and optimization of the receiver system, to ensure that most of the absorbed energy is passed to the heat transfer fluid and minimal energy is lost to the environment.

The energy harnessed during the day needs to be made available at night and during periods of low insolation. Therefore, in addition to the receiver, storage of thermal energy is also an important part of solar thermal systems. The latent and sensible heat storage of thermal energy is possible by the use of materials such as phase change material (PCM), rock, water, concrete and ceramics. These materials are usually employed due to their high heat storage capacity. PCMs however, have become an attractive thermal energy storage medium due to their high energy storage density, ability to store thermal energy at a constant temperature and the fact that they are able to store 5-14 times more thermal energy than sensible storage materials [5].

If solar thermal cookers are to provide an alternative to the burning of fossil fuels we must be able to design, construct, analyze and optimize receivers for these cookers, such that they can convert the maximum amount of concentrated radiation available into useful thermal energy. For this project a solar thermal cooker system was constructed, with emphasis on

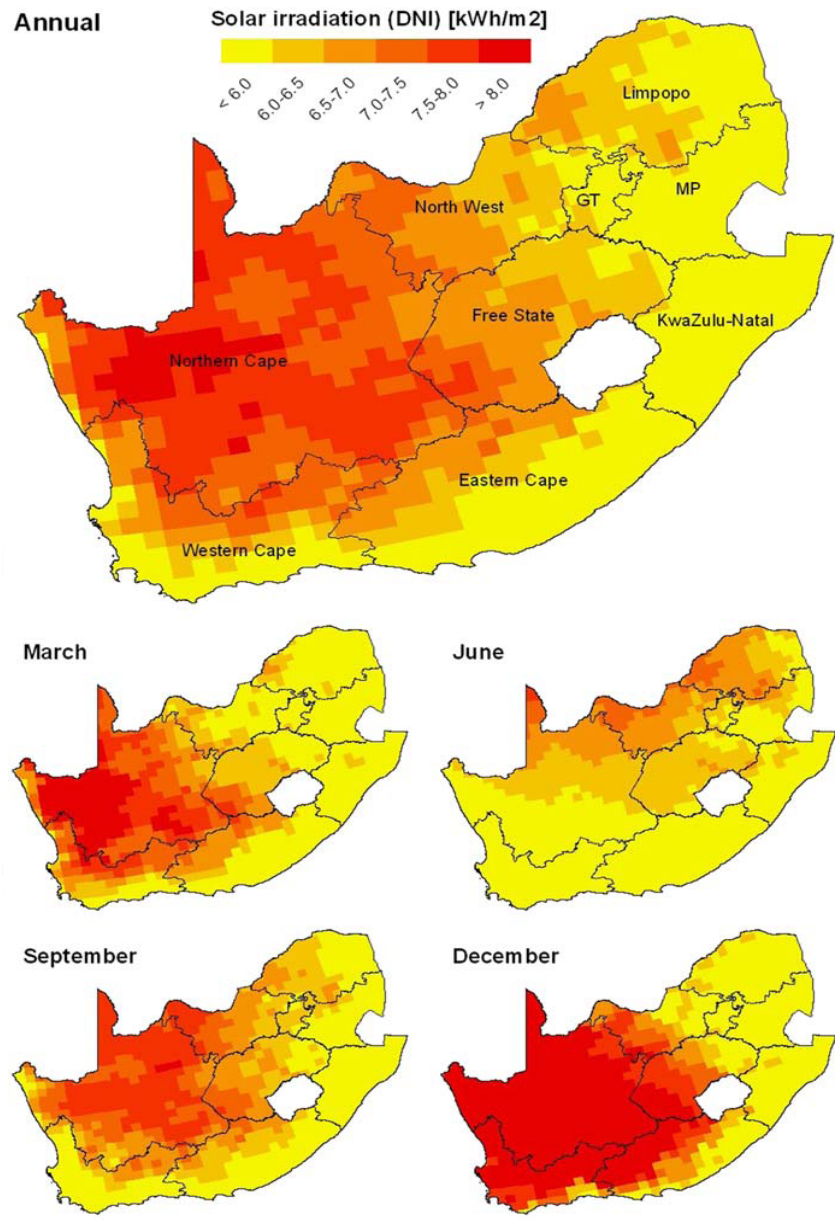

Figure 1.1: Annual average Direct Normal Irradiation (DNI) for South Africa for the entire year and for the months of March, June, September and December. Winter and Summer are experienced during the months of June and December, respectively. Adapted from Fluri [4].

investigating the efficiency of the receiver. There are various factors that are considered when designing and optimizing a receiver. Some of these include the geometric concentration ratio, receiver shape and size, as well as material strength and thermal properties. In order to optimize the receiver, adequate knowledge of the receiver's efficiency is required. This will provide an insight as to what improvements should be made to the receiver to increase its efficiency by limiting heat loss.

1.1 Research aim

The aims of this research were to:

- Construct a small-scale solar thermal cooker system, with emphasis on the testing of the receiver.
- Determine the efficiency of the receiver.
- Carry out a heat transfer analysis to determine the amount of heat loss from the receiver.
- Determine whether effective heat transfer occurs within the system.

1.2 Brief history of solar cookers

There are various types of solar cookers that have been designed, constructed and tested over several decades. These can be broadly classified into two main groups: direct and indirect cookers. Direct cookers use solar radiation directly in the cooking process while indirect cookers use a heat transfer fluid to transfer the absorbed thermal energy from the receiver to the cooking unit. Two commercially successful direct solar cookers are the box type and the concentrating type cookers [6]. The solar box cooker was developed as early as the 1700's by the French-Swiss scientist Horace-Benedict de Saussure (1740-1799). De Saussure investigated how effective glass was in trapping the sun's heat and achieved temperatures as high as 87.5 °C in his first design. This temperature was sufficient to allow him to cook fruit, and he later improved his design by adding insulation around the box to reduce heat loss. After this modification he had managed to achieve a temperature of 108.8 °C, which was almost 22 °C higher than his first experiment. The device was later named the"hot box"due to its ability to retain a large amount of heat [7].

The first solar energy book, *Solar Energy and its Industrial Applications* was published

by French inventor Augustin Mouchot (1821-1912) in 1869. However, by 1866 Mouchot had already developed the first parabolic trough solar collector which was later exhibited in 1878 at a Paris exhibit. Mouchot had also designed and built solar cookers which were used by French soldiers in Africa. The first solar cooker that was reported to have been used in South Africa was by Sir John Herschel in 1885, at the Cape of Good Hope. The box was constructed from mahogany, blackened on the inside, covered by two sheets of glass and buried in sand for better insulation [8]. In 1945, Indian pioneer Sri M.K. Ghosh designed the first commercial box type solar cooker. During the 1950s, Indian scientists designed and manufactured solar ovens and reflectors which were not readily accepted due to lower-cost alternatives [9, 10]. The first practical oven, a box type solar cooker with four reflectors, reached a temperature of 225 °C. This was done in 1959 by Maria Telkes. Telkes also published a book in 1968 titled *Solar Ovens*. During the 1970s, Barbara Kerr developed various types of concentrating and box type solar cookers using recycled materials [10].

The invention of a parabolic fixed focus reflector was first developed in 1982 by German inventor Wolfgang Scheffler. The technology was developed to provide developing countries with a simple method of solar cooking [11]. The device was later named the Scheffler reflector, and since 2008 more than 2000 units have been built and distributed worldwide [12]. Scheffler systems do not make use of heat transfer fluid since solar radiation is focused directly onto the cooking pot. The unique design feature of the Scheffler system is its ability to bend and flex the reflecting surface to focus the incoming sunlight from different angles. This method ensures that a small hot focus area is achieved during all seasons [13].

The major advantages of the box type solar cooker over concentrating cookers are simple construction, easy operation and the fact that it requires little attention during the cooking process. On the other hand, one of the disadvantages is that the cooking process is rather slow, due to low cooking temperatures [6]. In order to achieve higher efficiencies there have been many modifications to the box cooker over the years. Some of these modifications include the addition of reflectors to the sides of the box, the use of glazed glass covers to prevent excessive convective heat loss, and the use of insulation and PCMs.

In addition to the box cookers there have been various other types of solar cookers designed and developed. These include the panel, the collector and the concentrating type cookers. The operation of the panel cooker is similar to the box cooker. However, instead of an insulated box the panel cooker uses multi-faceted reflective panels that focus the sunlight on a cooking vessel. Panel cookers are able to achieve temperatures above 80 °C [14].

By the year 2000, Paul Funk developed an international standard by which the testing and performance of solar cookers can be reported [15]. Since the development of the hot box, many variations of solar cookers have been explored and compared with each other and previous designs. The main characteristic which all of these cookers have in common is the use of a highly reflective surface that directs the incoming radiation onto a focus area. Each of these cookers have their advantages and disadvantages. For example, concentrating type cookers are able to achieve significantly higher temperatures than the box cooker. However, they are more expensive to construct and in some cases more difficult to operate [14].

There are many factors that need to be considered before choosing the appropriate cooker for a particular location or application. Most cookers such as the box and panel type take 2-4 hours to cook for approximately 4-5 people which is inappropriate in the modern context. Therefore, the cooker constructed for this project needs to satisfy requirements such as generating high temperatures (above 100 °C) so that the cooking time is reduced, automatic tracking of the collector and a method of storing the thermal energy so that cooking or water heating can be done during periods of little or no sunshine.

1.3 Literature review

Solar thermal concentrating systems require medium to high-temperature receivers for the conversion of sunlight to thermal energy. Depending on the type of concentrator optics used, these receivers operate from temperatures of 150 °C to 1000 °C, and in some cases higher. The high operating temperatures of the receiver leads to greater heat losses which drastically affect the performance of the system. The amount of heat lost from a receiver is influenced by its size and operating temperature. At high temperatures it becomes more difficult to reduce the factors that contribute to heat loss.

The three heat loss mechanisms, i.e conductive, convective and radiative, have to be considered in order to obtain high thermal energy conversion efficiencies. Heat loss by conduction can be limited by using insulation material on parts of the receiver that are not exposed to concentrated radiation. Materials with high thermal conductivity such as carbon steel, aluminium and copper should be used to construct the receiver. This will increase the heat transfer throughout the receiver so that a uniform heat distribution can be obtained. In addition utilizing materials that have high thermal conductivity will allow the heat to be transferred to the working fluid more effectively. Heat loss due to natural convection can be minimized by the use of a glass covering over the receiver especially in the case of volumetric receivers. Radiative loss becomes the most dominant heat loss mechanism at a temperature in the range of approximately 500-800 °C. This is one of the main challenges that affects high-temperature receivers. Therefore, this category of receivers must be designed such that they are able to absorb as much of the concentrated radiation as well as limit the amount of re-radiation to its surroundings. One of the methods employed in reducing re-radiation is the use of a solar-selective coating on the receiver surface. The purpose of a solar-selective coating is to promote high absorptance of radiation while reducing the long-wave emittance. Many of the materials used in selective coatings are metal oxides such as copper, nickel or zinc, and the surface on which the coating is applied is usually metal [16].

The primary goal for high-temperature receivers is to absorb as much radiation as possible while keeping heat loss to a minimum, resulting in highly efficient systems. Factors such as geometry, materials of construction and operating temperatures significantly determine the amount of heat lost from the receiver and hence its efficiency. Over the years there have been many advancements in high-temperature receiver technology. Some of the techniques used to achieve this include vacuum sealing, solar-selective absorber coatings, durable materials and insulation, as well as low iron content and antireflective glass.

There are three main categories of receivers. These are the cavity receiver, volumetric receiver and tubular receiver. The cavity receiver is an insulated enclosure with a small opening called the aperture that allows the solar radiation to enter. Within the cavity multiple reflections take place among the inner walls. The thermal losses from the cavity receiver include conductive loss from the receiver surface and convective and radiative loss from the receiver aperture. At low temperatures conductive heat loss is the most significant. At higher temperatures convective and radiative heat losses become the most dominant.

Volumetric receivers are usually used in solar towers and constructed from materials such as ceramic foams, grids, honeycombs and pin-fin arrays, metallic mesh and fibers and ceramics such as silicon carbide (SiC), reaction-bonded silicon infiltrated SiC (SiSiC) or pressureless sintered alpha SiC (SSiC) [17]. One of the significant features of volumetric receivers is that the radiation is allowed to penetrate the absorber material making it possible for heat exchange to occur over a larger area rather than just on the surface of the material [18]. Volumetric receivers usually use air as the heat transfer fluid while the cavity and tubular receivers use either oil or water. However, depending on the operating temperature, molten nitrates can be used as heat transfer fluid in cavity and tubular receivers since they are able to withstand temperatures up to 400 °C.

A tubular receiver is a pipe or tube made from material of high thermal conductivity, such as carbon steel or copper, that can be used as is or coiled into a specific shape. Convective heat loss can play a significant role in reducing the operating temperature of this type of receiver. One of the methods used to overcome the natural convective heat loss is to enclose the pipe or coiled pipe assembly with a glass covering. Some high temperature receivers, including the tubular receiver, that have been designed, constructed and tested will be discussed below.

The most established concentrating solar thermal powered technology is the parabolic trough [19]. The largest parabolic trough facility in the world was first built by the Israeli company Luz Industries, called the Solar Energy Generating Systems (SEGS) and consists of nine power plants situated in the Mojave Desert. This parabolic trough technology, operating since 1985, has been proven to be the most low cost large-scale solar powered technology. The size of the nine commercial-scale parabolic trough plants ranges from 14-80 MW with a collective installed capacity of 354 MW. By 2001 the SEGS facility had been successfully operated daily for 18 years, proving the ability of this technology to operate in a large-scale commercial power plant environment [20].

The most significant advancements in solar thermal receiver design have been made to the

parabolic trough systems at the SEGS facility. Initially the receivers had been manufactured by Luz Industries. The tubular receiver/heat collecting element (HCE) of the parabolic trough system, which has the ability of attaining temperatures as high as 390 °C, is one of the main reasons for the high efficiency of the Luz collector design. The receiver consists of a stainless steel tube with an outside diameter of 70 mm and coated with a cermet solar-selective absorber on the surface [20]. Cermets are highly absorbing metal-dielectric composites that consist of fine metal particles in a dielectric or ceramic matrix [21]. The receiver tube is enclosed by an antireflective glass cover with an outside diameter of 115 mm. The space between the steel tube and the glass cover contains a vacuum, to reduce heat loss at high temperatures as well to protect the selective absorber coating from degrading. Later, Solel Solar Systems developed the *Universal Vacuum* (UVAC) HCE which had an improved selective absorber coating and incorporated an internal reflective shield used to protect the inside of the glass-to-metal seal during the time the sun is at a low angle [20]. The UVAC design is considered to be a significant advancement for parabolic trough plants and could be the receiver of choice for future systems.

Parabolic dish concentrators have significant advantages over other types of concentrators, such as the absence of cosine losses, higher geometric concentration ratios and higher operating temperatures [22]. Therefore, parabolic dish receivers need to be designed to withstand these high temperatures while maintaining their efficiency. Geometric concentration ratio is defined as the ratio of aperture area to the receiver (or absorber) area and it determines the solar radiation intensity intercepted by the receiver [23]. The higher the geometric concentration ratio the higher the heat flux absorbed by the receiver, hence a higher temperature is achieved. Cosine losses (or cosine effect) represents difference between the amount of energy falling on a surface that is pointing at the sun, and a surface that is parallel to the earth's surface. For a parabolic dish the cosine loss is eliminated since the concentrator uses two-axis tracking and is always pointed at the sun.

The receiver for a parabolic dish concentrating cooker is a crucial component in the system since it is responsible for absorbing the maximum radiation and transferring the energy either directly to the cooking utensil or to a heat transfer fluid. Some experimental work that has involved direct cooking include Kalbande et al.[24], Habeebullah et al.[25], and Sonune and Phillip [26]. Various receiver configurations for parabolic dish concentrators have been investigated with the aim of increasing the amount of radiation absorbed and limiting the factors contributing to heat loss.

The experimental investigation to determine the efficiencies of three solar thermal receivers for a SK-14 parabolic dish indirect cooker, was conducted by Mlatho [27]. A SK-14 is a parabolic concentrator that has a diameter of 1.4 m. The Volumetric Flask (VF) and Volumetric Box (VB) receivers were of the volumetric type and the Conical Tube (CT) receiver was a cavity type. All three receivers used oil as the heat transfer fluid.

The VF receiver, shown in Figure 1.2, consists of a 500 ml round-bottom glass flask surrounded by a reflecting steel plate mounted to the flask neck till halfway to the round-bottom. The plate is insulated with aluminium foil on the inside and glass wool on the outside. The purpose of the foil is to increase the reflectance of the steel plate. The concentrated radiation is absorbed by the oil through the glass flask and from the reflecting plate.

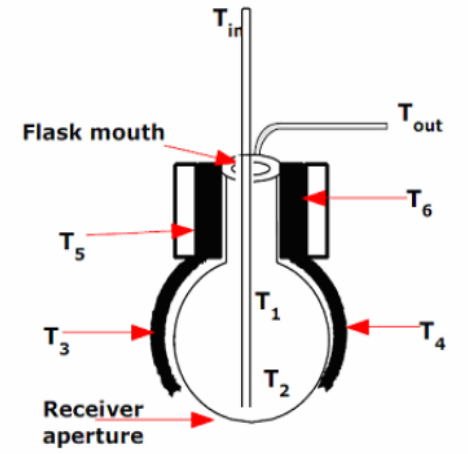

Figure 1.2: Volumetric flask receiver. Adapted from Mlatho [27].

The VB, shown in Figure 1.3, is the second receiver design and is a cavity with a flat glass aperture. The cavity is fabricated from aluminium and painted black on the outside for increased absorption. The cavity is left unpainted on the inside to allow for multiple reflections of the incident concentrated radiation. Glass wool is used to partly insulate the outside of the cavity.

The third design was the CT receiver which comprises a copper pipe coiled onto a solid copper cone to form one unit, as shown in Figure 1.4. The concentrated radiation enters at the bottom of the cone, and the oil flows within the coiled pipe from the vertex of the cone to the cylindrical bottom. It was found that, for the same flow rate, the CT receiver had a maximum efficiency of $\approx 42\%$ while the VF and VB receivers had a maximum efficiency of $\approx 35\%$. The volumetric flask and box receivers were modified by having a porous material

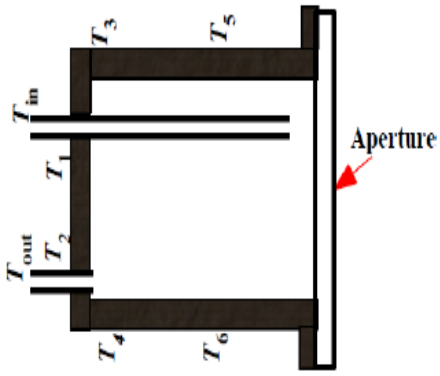

Figure 1.3: Volumetric box receiver. Adapted from Mlatho [27].

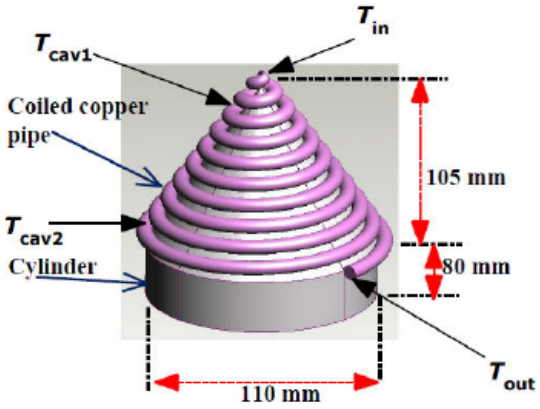

Figure 1.4: Conical tube receiver. Adapted from Mlatho [27].

placed inside the cavity. Porosity of a material is a measure of the void spaces in the material. It is expressed either as a fraction of the volume of voids over the total volume, in the range 0-1 or as a percentage in the range 0-100%. Coarse-textured materials have a lower porosity than fine-textured materials. The porous material used for the VF and VB receivers were blackened wire mesh. The mesh had a porosity of approximately 0.90 and had been made from stainless steel pot scourer.

Tests were then carried out to determine the efficiencies for the modified receivers. It was found that the use of the wire mesh with the VF and VB receivers showed an increase in their efficiencies, since the mesh increases the heat absorption by the oil by increasing the solid-fluid interface area inside the receiver. It has been recommended by the author that these receivers be used in this way to improve their performance.

In addition, testing of the conical tube receiver was carried out for when the cone was

painted with black matte paint. The painted CT receiver was found to have a higher efficiency than the unpainted CT receiver but at the same time reduces the stagnation temperature. This was because the black paint does not allow for reflections from the cone onto the copper pipe through which the oil flows. Therefore, in order to ensure better performance of the CT receiver, only the coiled pipe should be painted black allowing the reflected radiation to reach the pipe which leads to a higher stagnation temperature. When using this design for a receiver there must be good thermal contact between the coiled pipe and the cone. It was concluded that the CT receiver is the best design for use with a SK-14 parabolic dish.

There have not been many studies that have employed volumetric receivers with air as the heat transfer fluid, for parabolic dish concentrators. This type of receiver is usually reserved for solar tower technology. Volumetric receivers for solar tower technology have been investigated by several authors and many designs have been experimentally tested. Some of these are Kribus et al.[28, 29], Karni et al.[30], Hischier et al.[17], Taumoefolau et al.[31] and Fend et al.[32]. Many of these authors focused on design and optimization of the receiver with respect to its structure, materials of construction, thermal efficiencies etc. A test bed provided at the Platforma Solar de Almeria (PSA) or the Weizmann Institute of Science (WIS) allows these receivers to be exposed to conditions similar to those in the field. Some of the significant achievements in volumetric receiver technology can be found in Ávila-Marín [33]. Although these receivers are mainly designed for use in solar tower technology, many of their features can be applied to parabolic dish concentrators.

One such device involving a volumetric receiver and a parabolic concentrator was a solar oven designed for rural communities. This system was constructed and tested at the Norwegian University of Science and Technology (NTNU), under the initiatives of Professor Jørgen Løvseth [34]. The system employed a volumetric receiver made of blackened steel fibres and using air as the heat transfer fluid. Efficiency of the receiver is the ratio of thermal energy absorbed by the receiver to the energy received by the aperture of the concentrator. For this system, receiver efficiencies between 75-80% were obtained. The energy was stored using a rock-bed storage system to enable cooking and water heating during periods of little or no sunshine.

Similarly, a cooker using a 2.4 m parabolic satellite TV dish (called ST-H1) was designed, constructed and tested by Van den Heetkamp [18]. Air was heated to temperatures up to 400 °C and transferred to a pebble-bed storage system. The volumetric receiver for the system consisted of a brush-like configuration where 0.12 mm diameter bristles made of brass

wire are attached to a central bush. Brass has a thermal conductivity that is higher than stainless steel but lower than aluminium and copper. The air in the receiver was allowed to flow from the periphery through the ends of the bristles along its length, to the outlet pipe located at the center. It was observed that the brass bristles of the receiver become brittle after repeated use indicating that a durable type of material such as stainless steel or nichrome should be used as an alternative. Most of the radiation was focused on the receiver within a diameter of 200 mm.

The parabolic reflective surface of the ST-H1 consisted of 3 mm thick acrylic back-silvered mirror material. Mirror strips of 100 mm width were fixed to the concentrator, therefore taking the shape of any irregularities that the satellite dish surface may have had. An image taken of the illuminated receiver showed irregularities in the flux distribution and hence a non-uniform flux distribution. The non-uniformity of the flux distribution on the receiver is due to the concentrator optics. The non-uniform flux distribution may be overcome by cutting trapezoidal shaped tiles and fixing them individually to the dish surface. This way each tile can be raised or lowered by the thickness of its backing to reflect incoming light more accurately, so obtaining a sharper focus within the focal region becomes possible. This could increase the amount of radiation absorbed by the receiver and hence its efficiency.

The use of a smaller off-set satellite TV dish as a parabolic concentrator was carried out by Zeghib [35]. Temperatures higher than 200 °C were obtained using a cylindrical receiver made from copper having a diameter and length of 100 and 200 mm, respectively. One of the possible applications for the device was the sterilization of medical instruments.

The cavity receiver has been a popular design and the optimization of this receiver type has been investigated by many authors. Using a fuzzy-focal dish concentrator, Kaushika and Reddy [36] investigated the use of semi-cavity and modified cavity receivers fabricated from stainless steel tubes. A fuzzy focal dish concentrator is one that has imperfections on the optical surface which results in a focal image that is fuzzy and imprecise. Due to this a larger receiver is required. A solar to steam conversion efficiency of 70-80% was achieved, at a temperature of 450 °C. Figure 1.5 shows the cavity, semi-cavity and modified cavity receiver designs.

Since one of the significant thermal losses from a cavity type receiver is due to convection, Sendhil Kumar and Reddy [37] investigated the natural convection heat loss at 400 °C from the cavity, semi-cavity and modified cavity receiver, for a fuzzy focal parabolic dish concentrator. It has been found that the inclination of the receiver affects the amount of convective heat

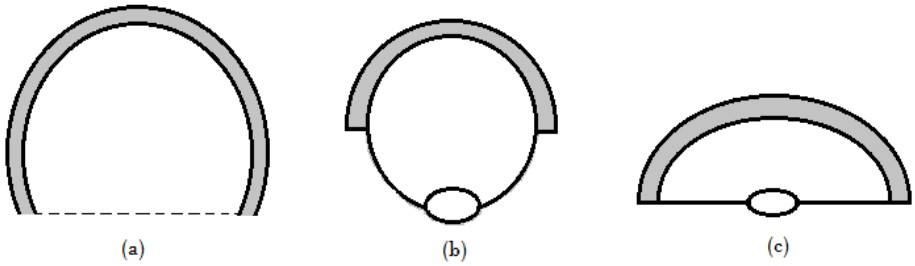

Figure 1.5: (a) Cavity. (b) Semi-cavity. (c) Modified cavity receiver. Adapted from Kaushika and Reddy [36].

lost through the aperture. This is due to an increase in the stagnant zone as the inclination increases from 0 to 90 °. More hot air occupies the secondary reflector at 90 ° than at 0 °, therefore indicating a decrease in the convection heat loss at larger inclinations. The convective heat loss from the above receiver designs were analyzed at receiver inclinations of 0 °, 30 °, 60 ° and 90 °. It was found that the modified cavity receiver had a lower natural convective heat loss than the other types. In addition, the natural convective heat loss for the cavity and modified-cavity receivers were significantly increased for different receiver inclinations. Even though the natural convective heat loss experienced from the modified-cavity receiver was significant, it was found that this receiver geometry was still the most appropriate for the fuzzy focal dish concentrator. The temperature contours for the cavity, semi-cavity and modified cavity receiver at 400 °C and an angle of 90 ° is shown in Figure 1.6.

Secondary reflectors coupled to the cavity receiver have been shown to improve the geometric concentration ratio as well as minimize the convective heat loss by reducing the size of the receiver aperture [37]. In order to further investigate the effect of secondary reflectors on receivers, Reddy and Sendhil Kumar [22] studied various secondary reflector configurations for the cavity receiver. These were the cone, trumpet and CPC reflectors as shown in Figure 1.7. Keeping the inclination constant at 0 °, their convection heat loss respectively was found to be 29, 19 and 20%, lesser than the previously designed modified cavity receiver. However, it was concluded that the modified cavity receiver coupled to a trumpet receiver showed a 60% lower heat loss than the other receiver configurations.

An experimental and numerical investigation of the convective heat loss from a cavity receiver for a parabolic dish system was conducted by Prakash et al.[38]. The receiver, shown in Figure 1.8, was constructed from a helical copper tube of 0.33 and 0.5 m in diameter and height, respectively. The copper tube of diameter 9 mm is coiled 39 times along the height

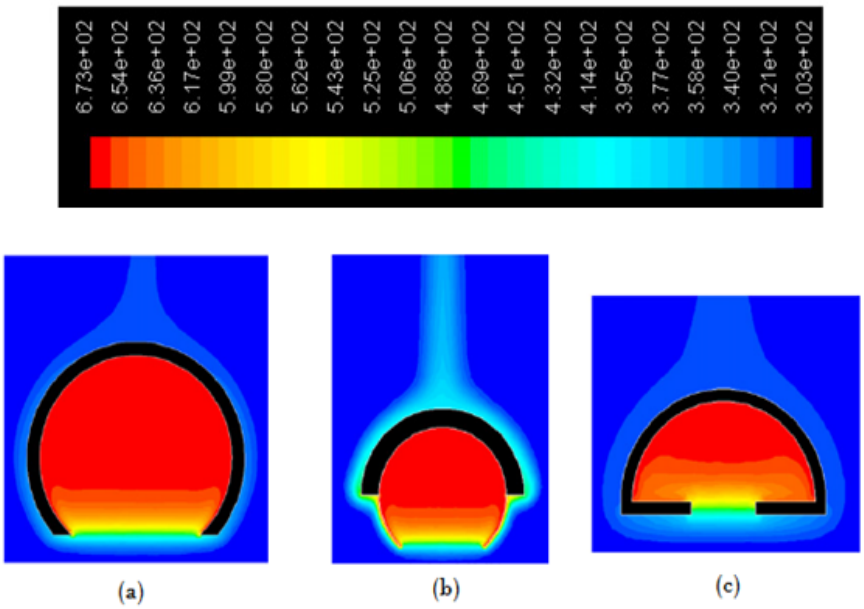

Figure 1.6: Temperature contours for the (a) Cavity, (b) Semi-cavity and (c) Modified cavity receiver at 400 °C and an angle of 90 °. Adapted from Sendhil Kumar and Reddy [37].

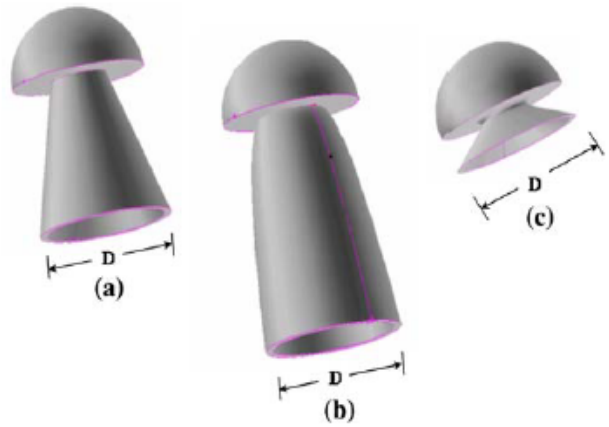

Figure 1.7: (a) Conical reflector. (b) CPC reflector. (c) Trumpet reflector. Adapted from Reddy and Sendhil Kumar [22].

of the receiver with a spacing of 3-4 mm between each coil. A wind skirt was incorporated in this receiver design. The wind skirt has an aperture diameter of 0.5 m consisted of 9 coils. A polyurethane coating that is capable of withstanding temperatures of up to 350 °C is used on the coils. A 75 mm thick mineral wool and aluminium cladding covers the outside of the coil assembly while aluminium foil is used on the inside. During experimental testing water was circulated through the receiver tubes. In Figure 1.8 the cavity receiver is shown without

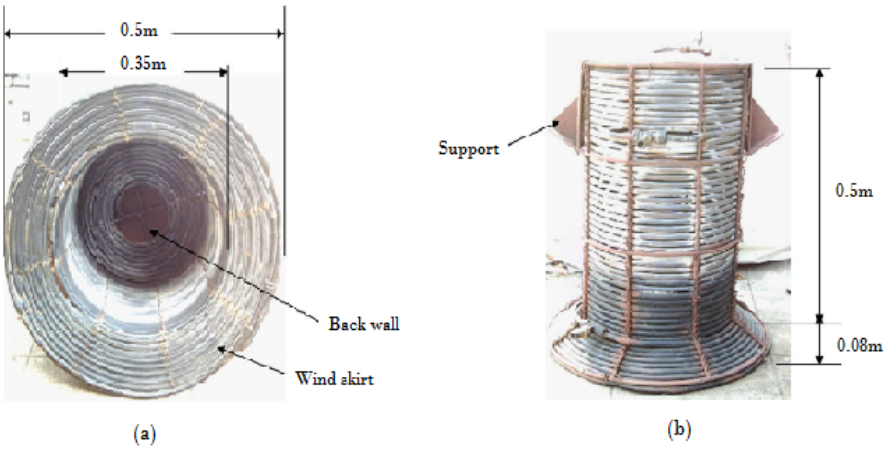

Figure 1.8: (a) Cavity receiver constructed from copper tube as seen from front. (b) Cavity receiver as seen from the side. Adapted from Prakash et al. [38].

the insulation layer. It was concluded that the experimental and numerical convective loss estimates agree reasonably well with a maximum deviation of approximately 14%.

In order to create a device that provided more than one purpose, Badran et al.[39] incorporated a solar cooker and water heater in one portable unit. The receiver for the water heating mode consisted of an absorber which was two circular stainless steel sheets positioned 25 mm apart with a stainless steel envelope. The absorber aperture was shielded by a glass cover. It was found that the temperature of 30 liters of water increased from 20 °C to 50 °C in just over 2 hours.

The determination of the thermal characteristics of parabolic dish receivers was performed by Bellel [40]. The two receivers under test were both made from steel, and cylindrical in shape, with one being a closed cylinder and the other having a coiled copper pipe within its cavity. Water was used within the cylinder cavity and the coiled pipe to monitor the heat transfer. Receiver temperatures above 500 °C were measured.

Scheffler reflectors have been developed for use in remote areas where there is limited access to electricity. These reflectors have been built in a range of sizes, from 0.5 m^2 to 50 m^2 of reflector surface and are able to deliver temperatures in the range of 300 °C. This is was done so that there would be different size options for various applications. Some of the applications included cookers for school canteens, community cookers and even industrial heating [13, 41]. Reflector sizes include 2.0, 2.7 8.0, 9.7, 12.6 and 16 m^2 of reflector area. A 2.7 m^2 reflector is able to boil 1.2 liters of water in 10 minutes. Within the same amount of time, a 9.7 m^2 reflector is able to boil 4.5 liters of water [13]. Most of these cookers are direct cookers and

the cooking vessels are stationary. The production of low pressure steam is also possible with the use of Scheffler reflectors.

In addition to cooking, the Scheffler reflector has allowed applications such as industrial heating and manufacturing processes to be possible so as to limit the use of conventional fossil fuels. Bhirud and Tandale [41] investigated the use of Scheffler reflectors for industrial heating applications. The heating of mild steel plates to 135 °C was done in an oven using two-fixed focus Scheffler reflectors, each having a reflector aperture area of 10 m^2. For mild steel plates of mass 100 kg, the heating time required for the plates to reach 135 °C was 27 minutes. The system was able to deliver 2.5 kWh of energy during the heating process.

Jayasimha [42] reported on the use of Scheffler reflectors for steam generation to be used for commercial laundry and dry cleaning. There was a total of 15 reflectors each with an area of 16 m^2. The second application was the generation of steam for washing compressor components. This system made use of 4 reflectors and is shown in Figure 1.9. One of the planned projects included steam generation for the evaporation of water from milk for the production of sweets. This would require 8 reflectors in total.

Figure 1.9: The four 16 m^2 Scheffler reflectors used to generate steam for washing compressor components. Adapted from Jayasimha [42].

As reported by Pulfer [11], a marmalade factory employed a 4.5 m^2 Scheffler reflector for the manufacturing of jams, marmalades and stewed fruits, in order to limit their use of liquid petroleum gas (LPG) due to its high cost. It was found that when the pot was filled with

40 liters of water at an initial temperature of 29 °C, the temperature had risen to 92 °C in 2 hours and 10 minutes.

For a rather different application, a 50 m^2 Scheffler reflector was developed by Wolfgang Scheffler [43], for use in a solar crematorium in India. This was to reduce the 200-300 kg of wood that would normally have to be used in a cremation. The reflector was designed to heat a cremation chamber 2 m in length to a temperature greater than 700 °C. When the chamber was pre-heated a temperature above 900 °C was reached. This enabled the burning of 4 kg of goat meat in 35 minutes. The solar crematorium concept seems to be a viable alternative to using wood. However, it can pose problems during cloudy weather and a backup option such as gas or wood should always be available. Considering the climate in India where there are approximately 300 sunny days per year [42], the Scheffler crematorium is an attractive technology.

Many Scheffler systems do not incorporate storage to allow for cooking, water heating or steam generation during periods of low insolation. This was taken into account when Tyroller [44] developed a solar steam sterilizer with heat storage for use in rural hospitals. A 10 m^2 Scheffler reflector was used to focus energy onto a 230 kg block of iron. The iron block serves as the receiver and storage unit. The block is heated to temperatures of up to 500 °C. The system is able to run a 76 liter sterilizer 4 times a day.

A compound parabolic concentrator (CPC) for the purpose of in situ steam generation was constructed by Oommen and Jayaraman [45]. As an alternative to other CPC designs, the current CPC module was designed with oversized reflectors to reduce gap losses and accommodate a cylindrical absorber. The absorber assembly consisted of five selectively coated copper pipes of outside diameter 19.5 mm and length 1060 mm. The pipe assembly was enclosed by a borosilicate glass cover. The application to steam cooking was possible by connecting the system to a pressure cooker. Experiments were carried out with a pressure cooker that had a capacity of 5 liters. The pressure cooker started giving off steam after 55 minutes. The cooking of 1 kg of rice with 1.5 liters of water was completed in 125 minutes.

Senthilkumar et al.[46] also used a CPC for low pressure steam generation. However, there were no oversized reflectors incorporated as with the design by Oomen and Jayaraman. The absorber was a copper sphere of 100 mm radius covered with a dull black paint. Copper tubes were used as transport pipes into and out of the absorber, with water as the heat transfer fluid. Since the losses from the absorber were mainly due to re-radiation, the authors decided to eliminate a glass covering around the absorber. Since one of the possible applications for

the present device was steam generation tests were carried out to investigate its performance. Experiments showed that when the absorber was filled with 3.5 liters of water, the temperature had risen to 80 °C in a period of 70 minutes. When the output temperature reached 98 °C, a steady output of steam was observed. The steam generation efficiency was calculated to be approximately 38%. Some of the applications of the CPC module includes steam cooking and water and oil heating. As one of the ways to improve the absorber efficiency and hence steam generation efficiency, the use of a selective coating on the absorber was suggested by some authors.

Contrary to the above and other designs, Popoola and Ayanda [47] chose to use a conical shaped concentrator for their solar concentrating system with oil as the heat transfer fluid. One of the factors influencing their choice was that the energy received by the absorber using a conical concentrator is greater than any other concentrator of equal aperture area. The receiver was a cylindrical structure fabricated from copper. A copper sheet was rolled into a cylinder and fixed at the joining ends by a zinc metal alloy. Copper has a thermal conductivity of 386 W/mK [48], which is significantly higher than stainless steel and aluminium. The cylinder was painted black to enhance the absorption of radiation. The highest receiver temperature recorded was 166 °C. The system lacked automatic tracking, making it difficult for applications such as steam generation to be achieved. Automatic tracking would have allowed the system to be constantly pointing at the sun so that a larger amount of radiation could be absorbed hence higher receiver temperatures would have been achieved.

Perfectly-shaped parabolic dish concentrators are complicated to design and construct in an experimental setting. This is because it is difficult to produce an accurately curved object from flat sheets of metal. The accuracy of the parabolic shape determines how well a sharp point focus can be achieved. The point focus is the main reason that parabolic dish concentrators have the ability of achieving significantly higher temperatures than other types of concentrators. It is their ability to achieve higher operating temperatures i.e temperatures in excess of 1500 °C, that makes the parabolic dish concentrator the most efficient of all concentrating systems [1]. For cooking purposes however, such high temperatures are not necessary and instead Fresnel concentrators are able to provide adequate temperatures. Fresnel concentrators have become popular for solar cooking applications since they provide adequate cooking temperatures and may be easier and cheaper to fabricate [6]. With this in mind, Sonune and Philip [26] developed and tested a Fresnel type SPRERI concentrating cooker for domestic cooking. This direct solar cooker was able to reach temperatures above 90 °C,

allowing various types of food items to be cooked. However, this system required manual tracking which was considered to be quite problematic since the women using it were taken away from completing other household chores. Manual tracking requires re-positioning of the concentrating system by 15 ° every hour.

Franco et al.[49, 50] constructed a communal Fresnel type cooker for use in boarding schools and communal centres. The design allowed for interchanging of receivers for different purposes such as boiling, baking and frying. The first receiver was a blackened stainless steel coil pipe of 10 cm diameter placed within a Pyrex glass cover. The Pyrex cover was used to limit the natural convective heat loss. For an irradiance of 1000 W/m^2, it was found that 1.5 kg of steam was produced. With this boiler-type receiver the duration needed to heat the water until it boils was 10 minutes.

The second receiver alternative comprised black aluminium triangular shaped bars again contained in a Pyrex vessel. The triangular bars were arranged radially to form the shape of a cylinder within the Pyrex vessel. Once the bars are heated they can be removed and placed on a rack or tray, with the cooking pot on top of them. Heating the pot through conduction allows this method to be used for cooking or baking. Aluminium was used for this purpose since it has a higher thermal conductivity than stainless steel. This would allow the cooking pot to reach a higher temperature. The coiled pipe receiver and aluminium cylinder receiver are shown in Figure 1.10.

The last receiver alternative was to use a blackened pot placed at the focus. The walls of the pot reached temperatures higher than 200 °C, making frying possible. This option was found to be best for larger families.

Franco et al.[50] also used the boiler-type coil receiver for the pasteurization of goat milk. The receiver was able to reach a temperature of 65 °C after 75 minutes. This temperature was sufficient for low-temperature pasteurization. The pasteurization of 10 liters of milk was done in approximately 1 hour.

In general, for parabolic dish concentrators a cavity or tubular receiver is preferred over a flat receiver. The shape of the cavity receiver could be hemispherical, cylindrical or box-shaped with the aperture facing the incoming concentrated radiation. Cavity receivers have been found to have a lower convective heat loss and an increased geometric concentration ratio by the inclusion of secondary reflectors at the aperture. A tubular receiver is usually coiled into either a cylindrical, cone or hemispherical shape to promote absorption of reflected radiation from all directions. Volumetric receivers are enclosed by a glass covering to reduce

(a) (b)

Figure 1.10: (a) Blackened stainless steel coil receiver. (b) Blackened triangular aluminium bars. Adapted from Franco et al. [49, 50].

heat loss from the absorbing medium to its surroundings and to prevent damage to the absorbing medium. The receivers are usually painted black and parts that are not exposed to the concentrated radiation are well insulated.

The materials used in the construction of the receivers are generally metals with high thermal conductivity. These metals include carbon steel, aluminium, cast iron and copper. The properties of these materials such as their thermal conductivity, density, chemical composition and mechanical strength depend on the grade of the material. The most appropriate type of material and grade should be carefully chosen before being used as part of any solar thermal system.

Many of the receiver designs reviewed in this section involve bending and coiling of pipes and employing glass covers to limit convective heat loss. The use of insulation is important in reducing conductive losses from the receiver. Therefore, the type of insulation used should be carefully selected. It has also been established that the use of selective coatings or black paint significantly improves the amount of radiation absorbed. Selective coatings are usually more expensive, which is why black paint is a popular alternative. However, a crucial requirement of the ordinary black paint used on the high-temperature receivers is that they need to withstand the heat. This problem can be overcome by using high-temperature resistant black paint which is specially designed for this purpose.

Chapter 2

Solar radiation and solar technology

The solar radiation emitted from the sun is in the form of electromagnetic energy. The radiation has wavelengths, λ, ranging from 300 (gamma rays) to 3000 nm (microwaves). Most of these wavelengths are screened from the earth's surface by different layers of the atmosphere. The main wavelength that does reach the surface is that of visible light ($380 < \lambda < 780$ nm). However, portions on either side of the visible spectrum are not completely cut off and are able to pass through the atmosphere. These are the ultra-violet ($\lambda < 380$ nm) and infrared ($\lambda > 780$ nm) ranges. The infrared range has wavelengths which are too long to be seen by the naked eye, whereas the ultra-violet region contains wavelengths which are too short. The solar spectrum is approximately equal to that of a black body at a temperature of 5800 K. Due to the absorption of certain frequencies by water vapour, dust particles and other molecules in the air, the spectrum that is received by the earth's surface is significantly altered [16]. Figure 2.1 shows the solar energy spectrum.

Irradiance is the term given to the amount of radiant energy received on a surface per unit area per unit time. The amount of solar radiation reaching the surface of the earth is greatly reduced by the absorption, reflection and scattering of light. Factors such as air molecules, clouds, dust particles and water vapour contribute to the reduction of the amount of sunlight received. Radiation that experiences any of these processes is referred to as *diffuse* solar radiation. The radiation that does not undergo scattering, absorption or reflection is known as *direct* or *beam* radiation [16]. The direct and diffuse solar radiation can be summed to give the *global* solar radiation. The global (sky+solar disk) radiation, G, incident on a horizontal surface is the sum of the direct beam, B, projected onto the surface modified by the cosine of the incidence angle of the beam, i, and sky radiation, D, from the dome of the sky excluding

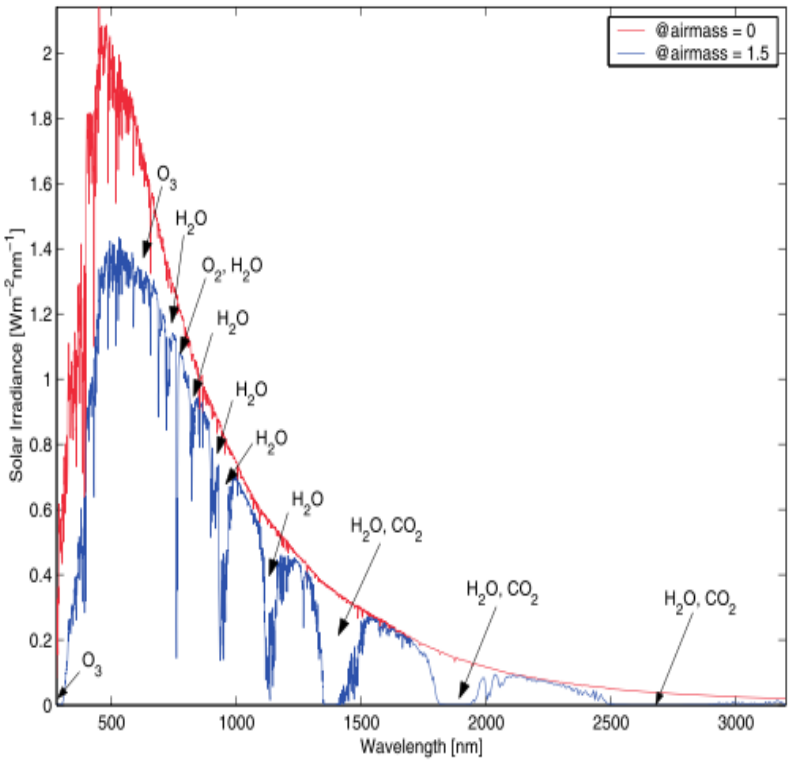

Figure 2.1: Spectral distribution of solar energy above the atmosphere (red) at zero airmass and the altered spectrum (blue) that reaches the surface of the earth at airmass equal to 1.5 (reproduced by Lysko [51]).

the sun [52]. This relationship is expressed by [52]:

$$G = B\cos i + D. \tag{2.1}$$

2.1 Sun-Earth geometry

The elliptical orbit of the earth's path around the sun is shown in Figure 2.2. It indicates the position of the earth relative to the sun at different times of the year. The *declination,* δ, angle is the angle between the sun's direction and the equatorial plane. This angle varies through the year and is at its extreme during the solstices (longest or shortest length of day) and at zero during the equinoxes (equal day and equal night). The North-South (N-S) pole axis is normal to the equatorial plane whilst the declination axis is at an angle of δ_o=23.45 ° away from the normal to the plane of revolution. The variation of the declination angle is shown in Figure 2.3 can be expressed by

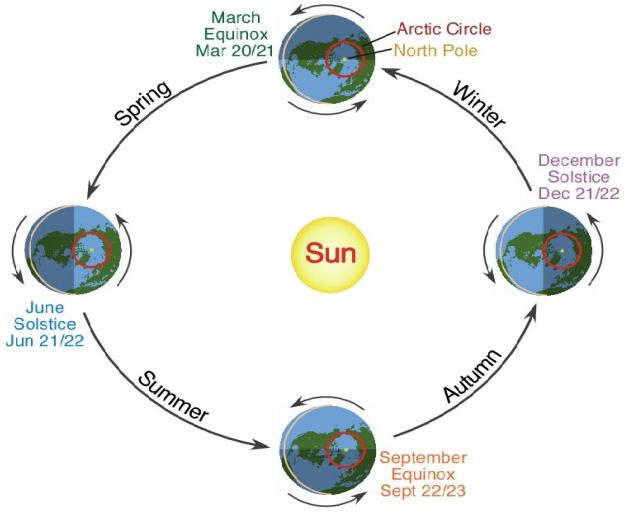

Figure 2.2: Sun-Earth geometry throughout the year [53].

$$\delta = \delta_o \sin\left(\frac{360\,^\circ(284+n)}{365}\right), \tag{2.2}$$

where δ_o varies between $+\delta_o = +23.45\,^\circ$ (for mid-summer in the northern hemisphere) and $-\delta_o = -23.45\,^\circ$ (for mid-winter in the northern hemisphere). The day in the in the year is represented by n where $n = 1$ for 1 January [54].

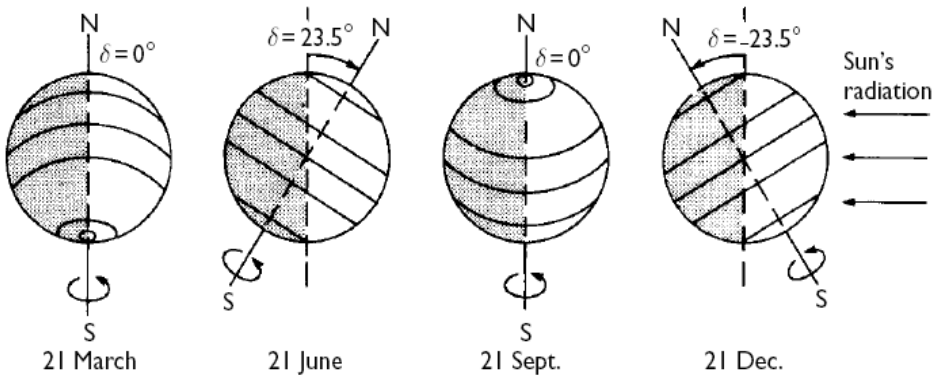

Figure 2.3: Variation of the declination angle through the year. The earth's circles of latitude are shown. A declination angle of $0\,^\circ$ denotes the two equinoxes [54].

For solar energy calculations, apparent *solar time* (ST) is used to express the time of day. Apparent solar time is based on the apparent angular motion of the sun across the sky and does not coincide with clock time [16]. The time when the sun crosses the meridian of

the observer is the local solar noon. The relationship between apparent solar time and *local standard time* (LST) is calculated using the following equation

$$ST = LST + EOT + (l_{st} - l_{local}).4min/degree, \tag{2.3}$$

where l_{st} and l_{local} is the standard meridian of the local time zone and local longitude, respectively and EOT is time in minutes given by

$$EOT = 9.87 \sin 2B - 7.53 \cos B - 1.5 \sin B, \tag{2.4}$$

where $B = 360(n - 81)/364$ degrees [55].

2.2 Solar radiation measurement instruments

The measurement of solar radiation is referred to as *radiometry* [56]. Assessment of the solar resource at a particular location is needed in order to design and construct efficient and cost effective solar energy systems. Terrestrial solar radiation is measured using instruments such as pyranometers and pyrheliometers. Pyrheliometers measure shortwave direct solar radiation, whereas pyranometers measure shortwave global radiation and diffuse radiation by the use of a shadow band or shading ball across the sensor. The World Radiometric Reference (WRR) provides a standard measurement scale for all the radiometers in the world. The WRR is maintained by the World Meteorological Organisation (WMO) situated at the Physical Meteorological Observatory in Davos, (PMOD), Switzerland. A group of absolute cavity pyrheliometers (ACP) comprise the WRR, and all other radiometers are calibrated against these ACPs since they provide the most accurate and precise radiometric reference [52]. All radiometers must be traceable to the WRR. The radiometry instruments mounted onto a Solys 2 solar tracker at the Westville radiometry station at UKZN can be seen in Figure 2.4.

2.2.1 Pyrheliometers

Pyrheliometers are used to measure the direct solar radiation received at a particular location. They measure the nearly collimated radiation within a narrow field of view, typically between 5.0 and 5.8 ° [52]. The Absolute Cavity Radiometer (ACR) is of the highest class and all other pyrheliometers are calibrated against it. A Kipp and Zonen Normal Incidence Pyrheliometer (NIP) was used for obtaining measurements in this thesis. The angle of aperture for the

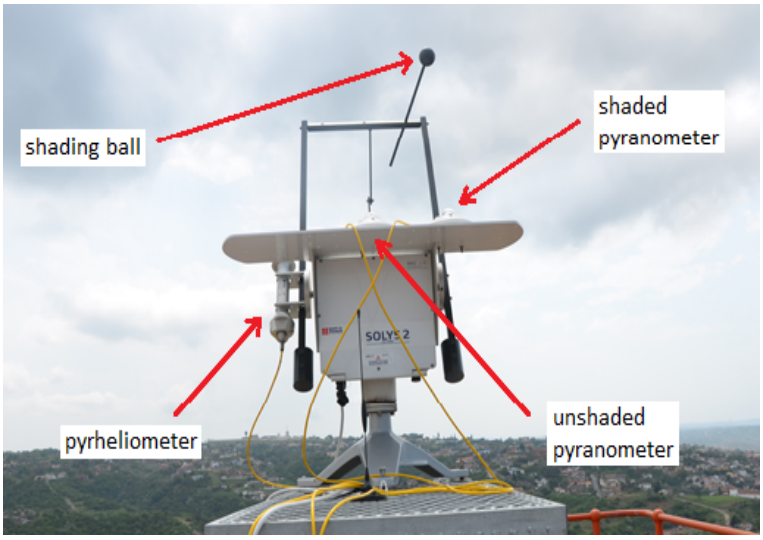

Figure 2.4: Radiometry instruments at the Westville station. The pyrheliometer, shaded and unshaded pyranometers are mounted onto a Solys 2 solar tracker. The tracker is shown facing North.

instrument is $5.0 \pm 0.2\,^{\circ}$ and has a sensitivity of approximately 7.4 μV/Wm^{-2} [57]. To continuously measure the direct solar radiation the pyrheliometer has to be constantly following the sun. This is achieved by the use of a solar tracker. The pyrheliometer is mounted onto the tracker and allowed to track the sun throughout the day. There are different categories of solar trackers: passive, microprocessor and electro-optically controlled. The microprocessor-based tracker is considered to have a higher level of accuracy compared to the passive and electro-optical systems. Trackers can be further specified by the axis of rotation, whether one axis of rotation, or two and three axes of rotation [58]. Commonly used solar trackers are Eppley's ST-1 or ST-3, Solys and BRUSAG's INTRA. The Kipp and Zonen pyrheliometer was mounted onto a Solys 2 tracker, as shown in Figure 2.5.

2.2.2 Pyranometers

Global and diffuse solar radiation can be measured by the use of pyranometers. They measure the radiation that is incident on them within the solid angle 2π. It consists of a copper-constantan thermopile sensing element which is housed in a domed structure. The copper-constantan thermopile converts the temperature to a voltage [16]. The function of the dome cover is to shield the sensing element from wind and rain, as this may affect its temperature. However, the dome still allows transmission of the solar radiation equally from all directions. Measurement of the diffuse component can be achieved by the use of a shadow band or shading ball covering the sensing element. The direct component of the solar radiation is blocked by the

shading device so that only the scattered radiation can be received by the sensor. Alternatively, if the direct component is known the diffuse component can be calculated using equation (2.1). For this research, the Kipp and Zonen shaded and unshaded pyranometers used to measure the direct and diffuse components have sensitivity values of 9.1 and 9.3 $\mu V/Wm^{-2}$ respectively, and are shown in Figure 2.5.

2.3 Current solar technology

Many countries around the world have recognized the growing necessity of solar technology for electricity generation. As the world's population continues to grow and the need to provide a sustainable future becomes critical, closer attention is being drawn to the development of new, efficient and sustainable solar powered systems. Many applications of solar technology exist in many parts of the world. Below is a brief discussion of some of these technologies.

2.3.1 Photovoltaic (PV) cells

PV cells consist of semiconductors that convert solar radiation into an electric current by the photoelectric effect. Several photovoltaic cells form a photovoltaic module or a panel which is the main component of a solar generator. Solar panels are usually installed on the rooftops of homes and buildings [59].

2.3.2 Concentrating solar power (CSP)

Parabolic trough concentrator (PTC)

Parabolic trough concentrating (PTC) systems make use of linear parabolic mirrors that reflect light onto a tubular receiver through which a heat transfer fluid flows. The receiver is normally coated with a selective absorber and encased within a glass covering. The troughs are mounted next to each other on a north-south axis to form an array and are allowed to track the sun throughout the day. The heat transfer fluid used for PTC systems is usually a synthetic oil that can reach temperatures of approximately 400 °C. The heated oil flows through a heat exchanger where water is heated to produce steam. The steam is then used to power turbines.

The largest array of PTCs is the Solar Electric Generating Systems (SEGS) plant (Figure 2.6) situated in Southern California. The SEGS power plant has a total installed capacity of 354 MW [3]. Nevada Solar One is another operational plant with a capacity of 64 MW. An ap-

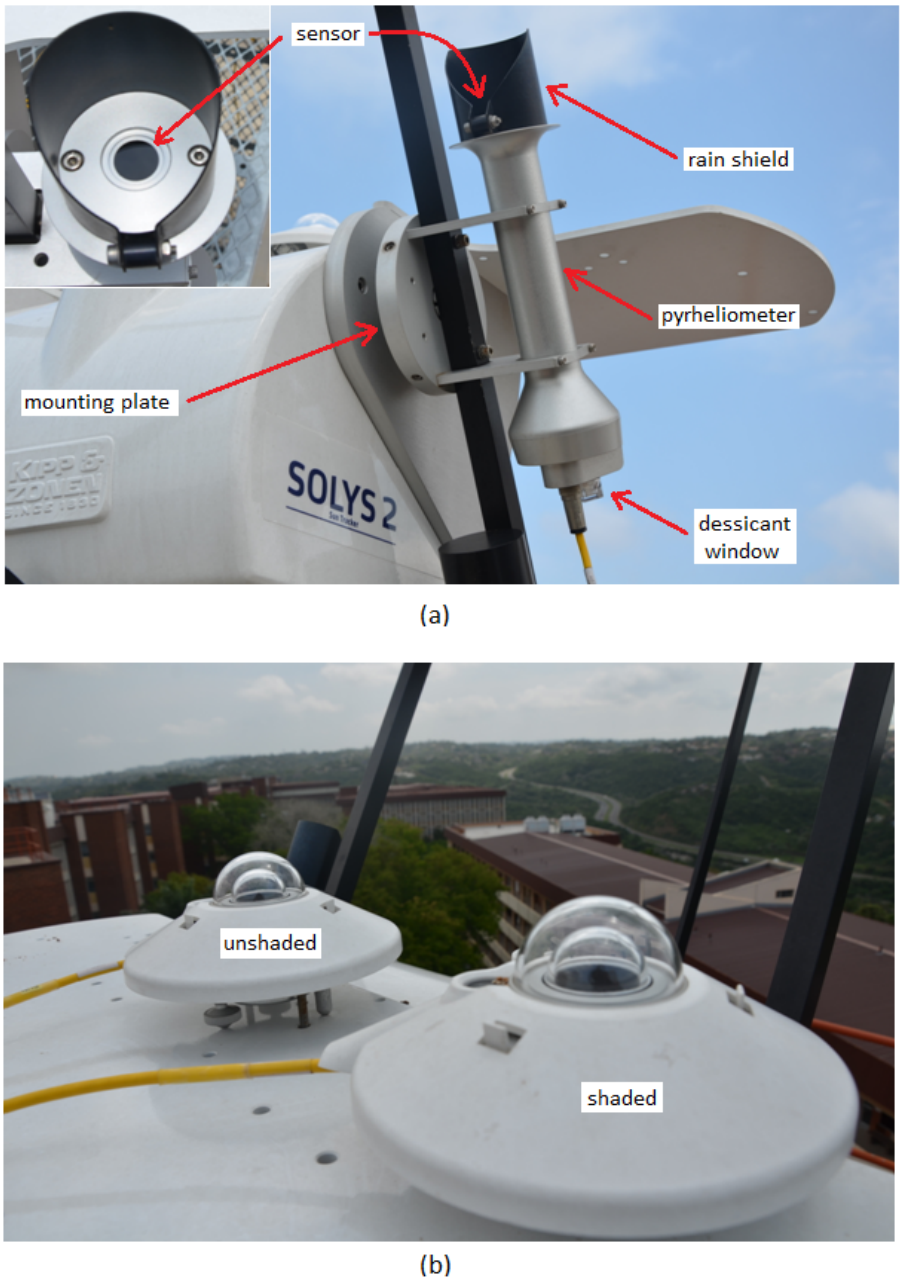

Figure 2.5: (a) Pyrheliometer mounted onto the Solys 2 tracker measures the direct radiation. Inset: Front view of the pyhreliometer that is constantly pointed at the sun. (b) Shaded and unshaded pyranometers mounted on a stationary plate on top of the Solys 2 tracker. The diffuse component is measured by the shaded pyranometer, which uses a shadow ball to cover the sensing element.

plication of the PTC technology in Southern Spain is the Plataforma Solar de Almeria (PSA), which consists of several 50 MW parabolic trough systems. Some of these include Anadasol 1, 2 and 3, Solnova, Palma del Rio and Puertollano. The Andasol plants are operational while the remaining ones are under construction [60]. South Africa's first CSP plants are currently

under construction. One of these include a 100 MW parabolic trough called KaXu Solar One. It is located in the Northern Cape and will have a storage capacity of three hours [61].

Figure 2.6: SEGS III parabolic trough plant at Kramer Junction, California [62].

Parabolic dish/Stirling engine

Parabolic dish/Stirling engines use large dish type receivers that focus light onto a small area above the center of the dish. The parabolic dish is covered by mirrors to concentrate light onto the receiver allowing the heat transfer fluid within the receiver to reach temperatures of 750 °C and above. The heated fluid drives either a steam or a Stirling engine. These dishes require accurate two-axis tracking in order to keep them focused at the sun at all times. Stirling engines have been designed to be used as off-grid systems for remote and undeveloped areas. A 1.75 GW solar farm consisting of Stirling engines has been planned for the California Mojave Desert [3]. Figure 2.7 shows dish/Stirling technology.

Central receiver

Central receiver systems require independently-tracking mirrors positioned in an array to focus light onto a central tower. Within the towers a nitrate salt combination is used to store the heat allowing temperatures of up to 650 °C to be reached. Nitrate salts have high heat

Figure 2.7: Dish/Stirling engine technology [60].

capacity which allows them to store a large amount of thermal energy. In addition they are non-flammable and non-toxic. The reflective mirrors used for these systems are flat, significantly lowering manufacturing costs since they do not require specialized machinery to be bent accurately into curved shapes. The first commercial central receiver plant providing electricity to several thousand homes is called the PS10 and is situated in Seville, Spain. The plant was built in 2007 and has an installed capacity of 11 MW. This was followed by a second 22 MW plant, with an additional capacity of 600 MW being planned [3]. Shown in Figure 2.8 is the Solar 2 central receiver plant which was an upgrade from Solar 1. The Solar 2 plant had succeeded in proving the technical feasibility of a central receiver plant with molten salt storage. This provided critical data which later influenced the design for one of the most significant achievements in Spain, which was the 20 MW Gemasolar tower plant. This plant generates energy continuously and has a 15 hour molten salt storage. Gemasolar has higher working temperatures than previous tower plants such as the PS10 [60]. Khi Solar One is a 50 MW solar tower plant that is under construction in South Africa, that will have a two hour storage capacity [61].

Figure 2.8: Solar 2 tower plant, Mojave Desert, California [63].

Linear Fresnel reflector (LFR)

Linear Fresnel Reflector systems use flat rings of mirrors to reflect light onto receivers suspended above the reflecting surface [3]. Athough LFRs are not as efficient as parabolic dish and trough systems, they may be favourable when it comes to reducing manufacturing costs due to flat mirrors being cheaper to fabricate than curved mirrors. The first concentrating linear Fresnel prototype was the 5 MW Kimberlina plant which was built in Bakersfield, California in 2008 [60].

Chapter 3

Solar thermal cooker system

One of the small scale applications of solar thermal power is a solar thermal cooker. This chapter describes a solar thermal cooker system that was designed and constructed for the work of this thesis. Included are the different components of the system and their functions, with emphasis on the receiver. Each of the components will be discussed separately.

A solar thermal cooker system generally comprises a concentrator, receiver, heat transfer fluid and an optional storage system. A schematic of the cooker system for this thesis is shown in Figure 3.1. The system constructed consists of an off-axis concentrator, a receiver, water as the heat transfer fluid and a latent thermal energy storage system.

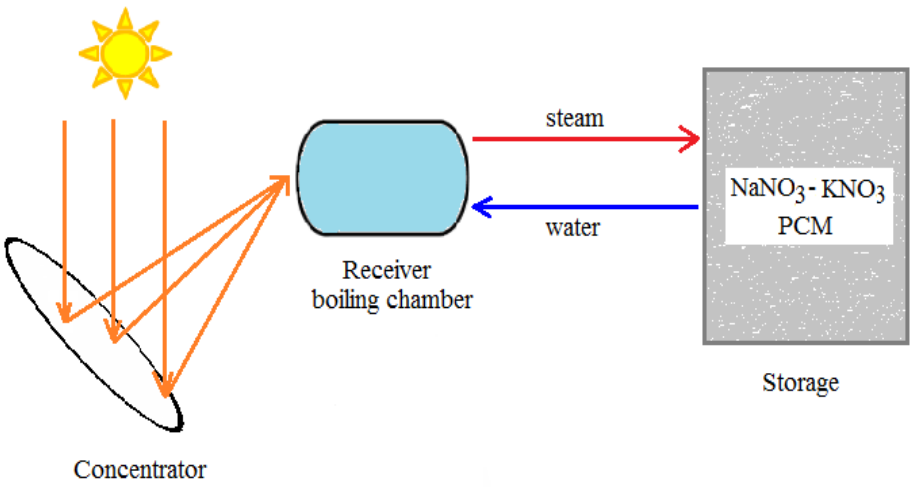

Figure 3.1: Schematic of the experimental setup of the system with the parabolic concentrator, receiver and storage container with $NaNO_3$-KNO_3 phase change material (PCM). The dish concentrates the incoming radiation onto the receiver which heats the heat transfer fluid. The heat transfer fluid is circulated through the storage to heat the PCM.

The general idea of the system is that water is heated in the receiver by concentrated radiation until it becomes superheated. The steam produced from the superheated water circulates through a pipe clamped beneath the storage top-plate. The steam condenses within the pipe and heats the thermal storage which consists of $NaNO_3$-KNO_3 PCM. The condensate flows back to the receiver where it is re-heated.

3.1 Concentrator

The purpose of a solar concentrator (or collector) is to direct the incoming radiation onto a small receiving area or focal region located on the parabola optical axis. Concentrating systems are generally associated with higher operating temperatures than non-concentrating systems, since they are able to produce a higher heat flux by converging the incoming radiation into a small area. To obtain optimal dimensions of a concentrator and the receiver several factors must be taken into account. These include geometric concentration ratio, C_R, ratio of the focal length, f, to concentrator aperture diameter, d, and rim angle, ϕ, which is the angle between a line that extends from the rim of the dish to the focal point, F, and a vertical line through the focal point. Of these, the concentration ratio is the most important factor since it provides a method of estimating the optimal size of the concentrator and receiver to obtain the highest energy output [64].

The concentration ratio, defined as the ratio of aperture area, A_a, to absorber area, A_{abs}, of the solar concentrator determines the intensity of the solar radiation intercepted by the receiver [23]. The quantity A_{abs} is defined as the absorbing area of the receiver normal to the incoming radiation. A high heat flux makes it possible to attain medium to high temperatures suitable for applications such as cooking and steam generation. The heat losses from the concentrator are proportional to the area of the absorber and inversely proportional to the concentration. The concentration ratio, C_R, is given by

$$C_R = \frac{A_a}{A_{abs}} = \frac{Aperture\ area}{Absorber\ area}. \tag{3.1}$$

For concentrating collectors, C_R is always greater than 1 [64].

The curvature of the concentrator can be described by focal length-to-diameter ratio, f/d, and rim angle. The relationship between them is illustrated in Figure 3.2, which shows several concentrators with the same diameter. It can be seen that the rim angle decreases as the f/d

ratio increases. A concentrator with a small rim angle has little curvature with the focal point located far from the reflecting surface. As shown in Figure 3.3, concentrating solar power (CSP) systems using cavity receivers with small apertures should make use of concentrators with small rim angles. This will allow the outermost reflected rays to reach the aperture of the cavity receiver. Conversely, CSP systems using tubular receivers should use concentrators with large rim angles and shorter focal lengths [64]. Placing the receiver closer to the concentrator will allow reflected radiation to be intercepted from all directions.

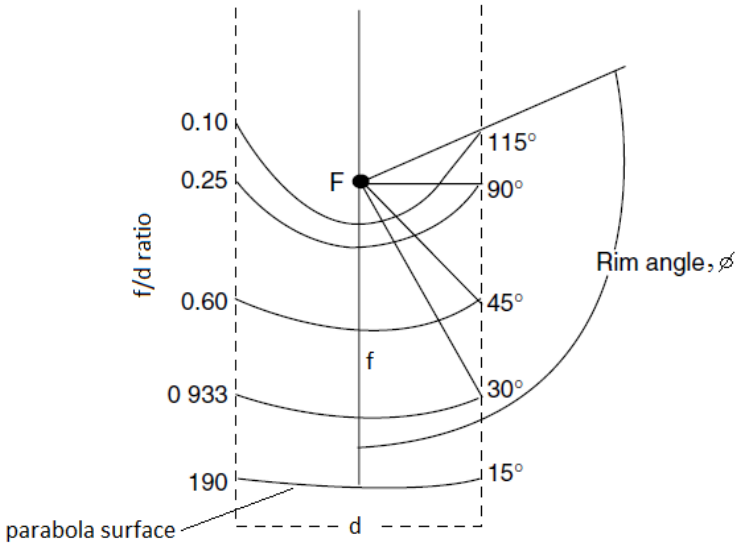

Figure 3.2: Relationship between f/d ratio and parabola rim angle. For several parabola surfaces with the same aperture diameter and common focal point, as the rim angle increases the parabola surface becomes more curved and the focal length becomes shorter. Adapted from Romero-Alvarez and Zarza [64].

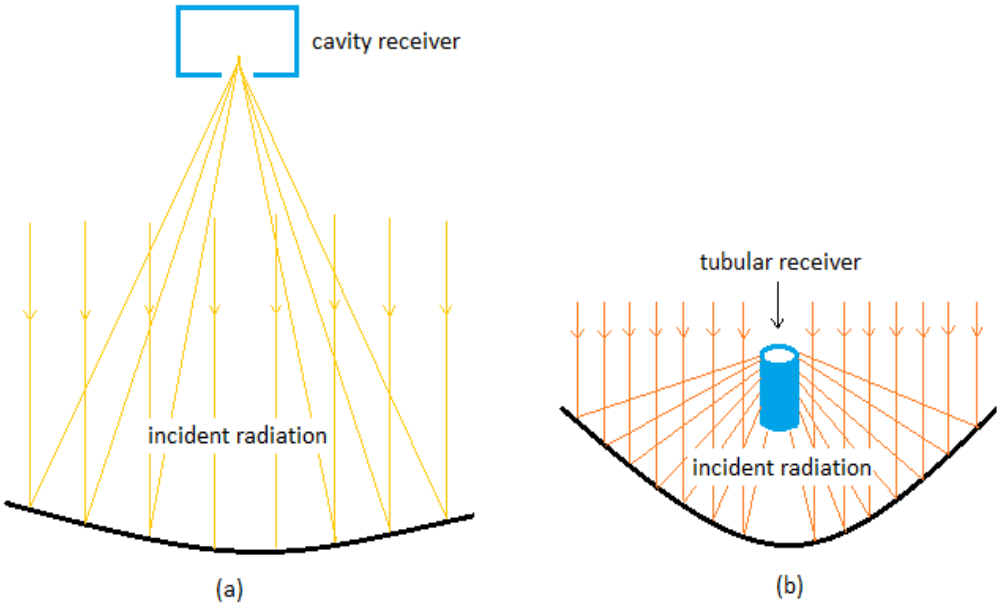

Figure 3.3: The effect of the parabola rim angle on the type of receiver used. (a) A parabola with small rim angle has less curvature and a focal point far away, and therefore a cavity type receiver should be used since this enables the outermost reflected rays to reach the cavity aperture. (b) A parabola with large rim angle and a closer focal point makes better use of a tubular/cylindrical receiver which allows reflected radiation to be intercepted from all directions.

3.1.1 Geometry of an off-axis parabolic dish

The central parabolic dish is regarded as the 'parent' parabola and the off-axis (or off-set) parabolic dish is a lateral section of this parent parabola [65]. A lateral section refers to a section or surface that does not form a base. This is depicted in Figure 3.4. The focus (or focal point) is the point at which the reflected radiation converges. The focal length, f, is the distance between the vertex and the focus of the parabola. The parent and off-axis parabolas share the same focal point. However, the position of the focal point for the off-axis parabola is situated near the lower part of the dish instead of in the center, as in the case of the parent parabola. The touch point of a line (ab) tangent to the off-axis parabola indicates the lowest point of this parabola. The angle, α, between the tangent line and the horizontal is the off-axis angle. Positioning the off-axis parabola at this angle will give a flux distribution that can be contained within the smallest focal region.

A parabola that is symmetric about the y-axis can be described by equation (3.2). The rays of sunlight parallel to the y-axis will intersect at a point called the focus or focal point.

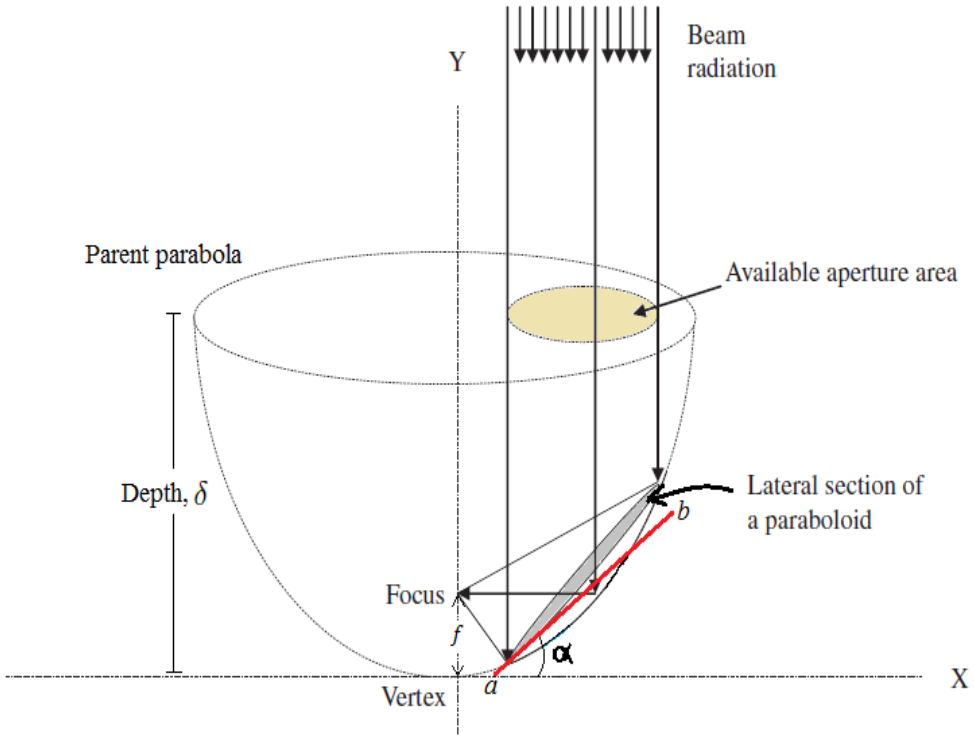

Figure 3.4: Schematic depicting the off-axis segment (grey portion) relative to the parent parabola. The touch point of the tangent line (red) to the off-axis parabola indicates its lowest point. The parent and off-axis parabolas have a common focus and the same focal length. Focal region of the off-axis segment is toward the lower part of the off-axis dish. Adapted from Munir et al. [65].

The focal length is found by equation (3.4) [66]:

$$y = ax^2, \tag{3.2}$$

where

$$a = \frac{1}{4f}, \tag{3.3}$$

which gives

$$f = \frac{x^2}{4y}. \tag{3.4}$$

Alternatively, the focal length can be obtained from the diameter and the depth, δ, of the parabolic dish using [66]:

$$f = \frac{d^2}{16\delta}. \tag{3.5}$$

ReflecTech Mirror Film

ReflecTech Mirror Film is a silvered polymer film that was developed by ReflecTech Inc. and the National Renewable Energy Laboratory (NREL). This highly reflective film of 0.1 mm thickness has a specular reflectance and a solar weighted-hemispherical reflectance of 93% and 94%, respectively. It is highly durable to withstand harsh outdoor conditions, extremely lightweight, moisture resistant and is not susceptible to breakage as is the case with glass reflectors [67].

For the work of thesis, the concentrator comprises a 1200 mm off-axis (or off-set) parabolic dish covered with lightweight Reflectech mirror film. This was a commercially available satellite television dish manufactured by Visiosat (Model: SMC 120). The Reflectech film was chosen due to its curveability, light weight material and high specular reflectance. The film was cut into strips of 55 mm in width. The film strips were fixed to the dish surface such that three separate strips were used to cover the width of the dish instead of one complete strip. This had to be done so that the film will take the shape of the dish as closely as possible and there will be no creasing or overlapping of the film. The concentrator has an off-axis angle of 22.3 ° and a focal length of 780 mm.

3.1.2 Determination of the flux distribution by the method of Ray-tracing

The geometric precision and optical quality of the concentrator significantly impacts the amount of radiation absorbed by the receiver and hence the overall performance of the system. Optical losses can be caused by imperfections of the shape of the concentrator, the reflecting surface or both. Therefore, it is imperative that the concentrator be assessed with respect to its optical performance.

In order to determine the focal region of the collector the method of ray-tracing was used. There were five red lasers (laser class IIIa) mounted onto a movable horizontal arm and pointing perpendicularly to the horizontal. The lasers were first calibrated against a flat mirror to ensure that the beam was exactly vertical to the horizontal. The experimental setup for the ray-tracing procedure is presented in Figure 3.5. The film surface was separated into three panels i.e a left, right and center panel. Each of these panels was scanned separately and is indicated by a different colour on the ray-tracing pattern. The mid-section of the concentrator was scanned first to determine the mid-point of the focal region and thereafter, every second foil strip in each panel. The reflections were studied on a screen tilted at an angle of 45 ° to the horizontal, as depicted in the schematic in Figure 3.6. The incident rays strike the

concentrator surface and converge at the focal point. The theoretical focal point as specified by the manufacturer is 780 mm. However, scans were done at focal lengths of 688, 723, 790 and 800 mm to verify the manufacturer's specification. The distribution of the reflections at the focal length of 780 mm is shown in Figure 3.7. The reflections from the left, center and right panels were indicated on the screen in blue, red and green, respectively. More than 90% of the reflections can be contained within a circle of 100 mm diameter. The extreme points (top, bottom, left and right) of the concentrator are indicated by an 'X' in Figure 3.7. For this focal length the extremities were also within the focal region of 100 mm diameter circle.

An advanced method used to characterize concentrators is by digital Photogrammetry, which was developed by Shortis and Johnston [68]. It involves the use of a network of multiple photographs of a targeted object taken from a range of viewing positions, to obtain high-accuracy, 3D coordinate data for the object being measured. An advantage of using digital photgrammetry as a measurement device is that it is a rapid technique that does not require any contact with the object and can accommodate objects of different sizes.

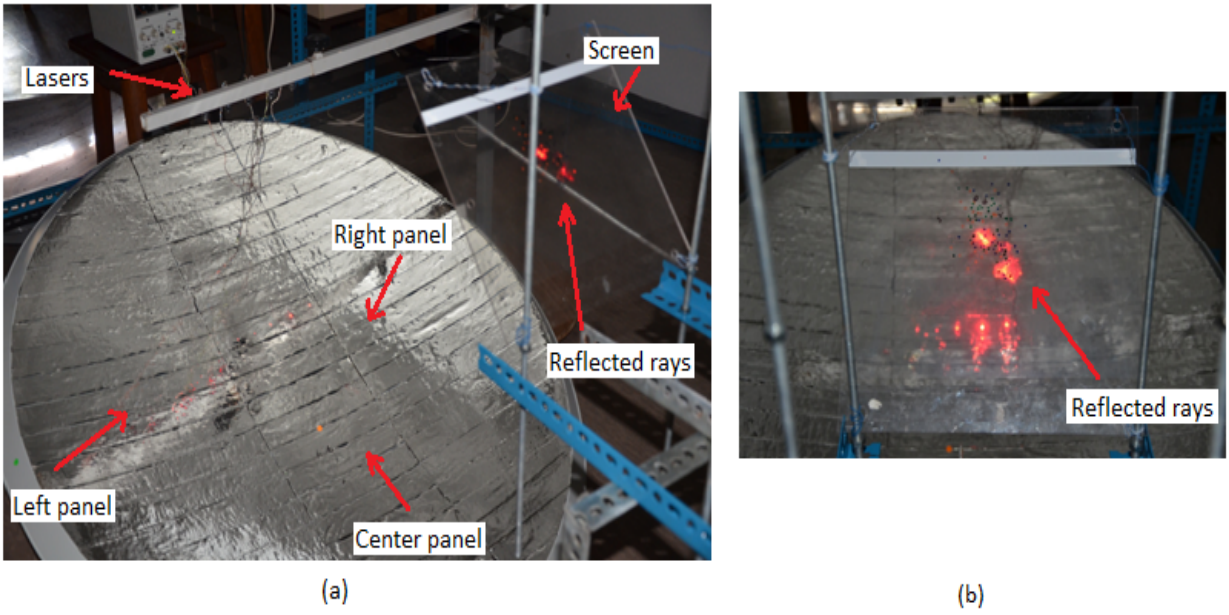

Figure 3.5: (a) Experimental setup for the ray-tracing of the off-set parabolic concentrator with red lasers. Parallel incident rays from the laser diodes strike the surface of the concentrator, and the reflected rays are marked on the screen positioned at 45 ° to the horizontal. (b) Front view of reflected rays as seen on screen.

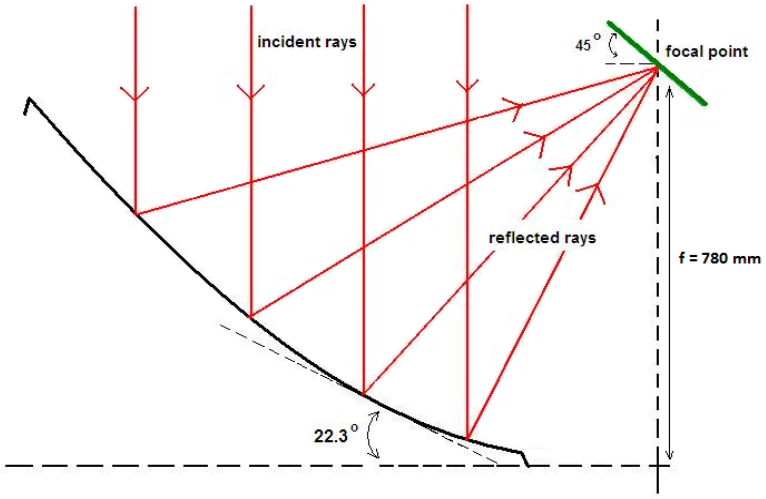

Figure 3.6: Schematic of the incident and reflected rays from an off-set parabolic concentrator. The concentrator is inclined at 22.3 ° to the horizontal. The screen on which the flux distribution is studied is inclined at 45 ° to the horizontal and placed at a height of 780 mm.

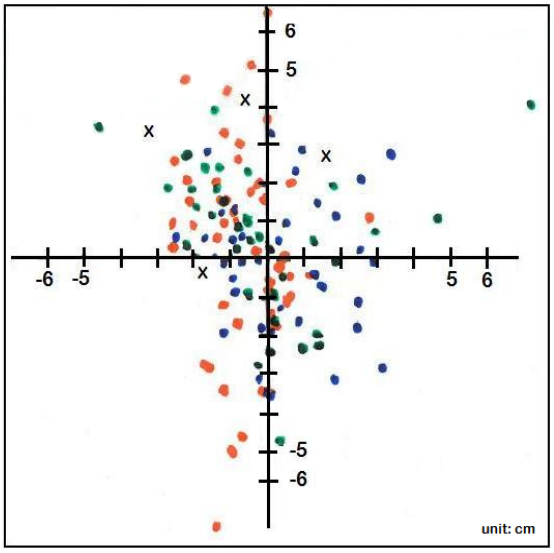

Figure 3.7: Ray-tracing pattern for focal length of 780 mm with screen at an angle of 45 ° to the horizontal. More than 90% of the reflections can be contained within a circle of 100 mm diameter. Left, center and right panels indicated in blue, red and green, respectively. Points marked with 'X' indicate the four extreme points of the dish.

3.2 Receiver

A device that is used in high temperature solar concentrators for the conversion of concentrated solar radiation to heat is called a *receiver* [69]. The purpose of the receiver is to absorb as much

radiation as possible and transfer this energy to the heat transfer fluid. The receiver is therefore an important component of any solar concentrating system. In the case of a parabolic dish concentrator, the receiver may be designed in various ways to optimize its efficiency. Receivers can be fabricated from different materials such as aluminium, steel, copper and even fibers as in the case for air-based systems. The geometry of the receiver, the use of a selective absorber and the use of glass with low iron content are some of the methods employed to increase the amount of radiation absorbed by the receiver. The amount of heat lost from the receiver can greatly reduce the performance or efficiency of the system. The three main heat loss mechanisms from a receiver are conduction, convection and radiation [37]. This should be considered when designing a receiver to ensure that these losses are kept to a minimum.

3.2.1 Receiver geometry

The design of a receiver depends on factors such as the type of concentrator used, the operating temperature and pressure of the system, working fluid used in the system and the radiation flux available at the receiver surface [29]. However, the shape and size of the receiver are the two factors that greatly influence the amount heat lost to the environment. A schematic of the receiver constructed for the work of this thesis is shown in Figure 3.8.

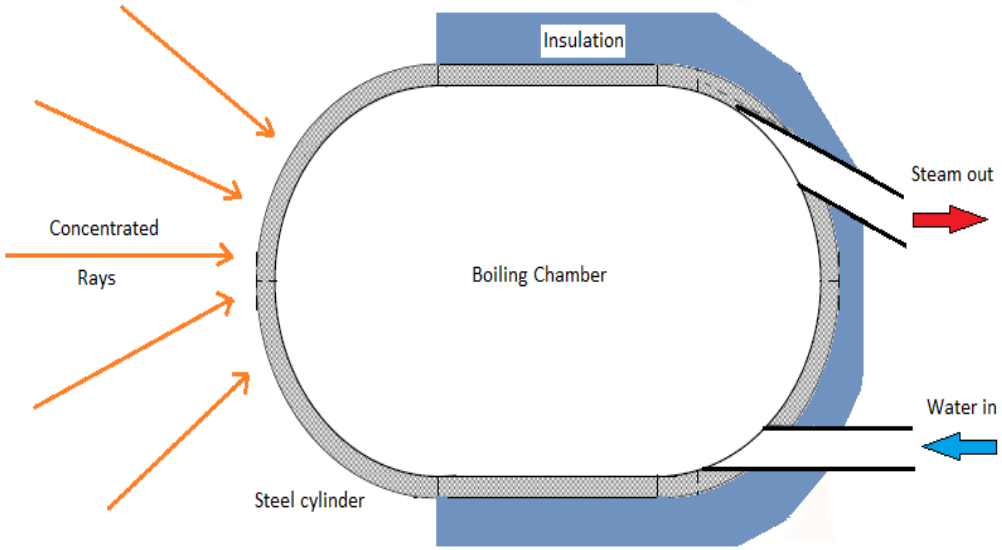

Figure 3.8: Receiver, constructed from mild steel, in the shape of a cylinder serves as a boiling chamber. The water is heated by the concentrated radiation striking the spherical cap. The steam rises toward the top of the cylinder where it leaves the receiver through the steam pipe (red). The condensed water (blue) enters the receiver at the bottom of the cylinder where it is re-heated.

It consists of a mild steel (grade EN8) cylinder 160 mm in length, with a spherical cap of 100 mm in diameter. Water is used within the cylinder as the heat transfer fluid. The cylindrical shape serves as a boiling chamber and contains ceramic boiling chips to facilitate the boiling process. The cylinder and spherical cap have a wall thickness of 4 mm. The cylindrical part of the receiver is insulated and the spherical part which receives the concentrated radiation is coated with *Solvalitt* black paint, which can withstand a temperature of up to 600 °C [70]. The water is heated by the concentrated rays striking the spherical cap. The steam produced by the boiling water rises upward, where it leaves the receiver through the steam pipe (red). The condensed water (blue) enters the receiver at the bottom of the cylinder where it is re-heated. As will be shown in Chapter 4, the receiver is required to produce superheated water at a temperature of approximately 250 °C in order to melt PCM salt in the storage.

Using equation (3.1) and the concentrator and receiver dimensions, listed in Table 3.1, the theoretical concentration ratio was calculated to be 144. The absorbing area of the receiver normal to the concentrated radiation was taken as πr^2. The area of the concentrator, A_{dish}, is given by

$$A_{dish} = \pi ab, \tag{3.6}$$

where a and b are the semi-major and semi-minor axes, respectively. The aperture area, A_a, of the concentrator is defined as the area of the concentrator multiplied by the cosine of the off-axis angle, given as

$$A_a = A_{dish} cos\alpha. \tag{3.7}$$

Table 3.1: Concentrator and receiver dimensions.

	Concentrator	**Receiver**
Semi-major axis (mm)	635	-
Semi-minor axis (mm)	615	-
Diameter (mm)	-	100
Length (mm)	-	160
Focal length (mm)	780	-
Wall thickness (mm)	-	4
Mass (kg)	8.5	2.5
Material	Mild steel with powder coating	Mild steel with black paint

3.2.2 Receiver analysis

Receiver efficiency

The energy balance for the receiver is given as

$$P_{net} = P_{rec} - P_{loss}, \tag{3.8}$$

where

P_{net} = useful energy transferred to the working fluid

P_{rec} = energy collected by the receiver

P_{loss} = total energy loss from the receiver [40].

The power, P_{dish}, captured by the concentrator and the power reaching the receiver, P_{rec}, are given by the following equations:

$$P_{dish} = I_{DNI} A_a, \tag{3.9}$$

$$P_{rec} = \eta_0 P_{dish}, \tag{3.10}$$

where I_{DNI} is the direct normal irradiation in $\mathrm{W/m^2}$ and η_0 is the optical efficiency.

The optical efficiency, η_0, is given by

$$\eta_0 = R_{film} R_{ray}, \tag{3.11}$$

where R_{film} is the film reflectance and R_{ray} is the fraction of reflections contained in a 100 mm diameter from the ray-tracing experiment and α is the off-axis angle. The factor R_{film} is a property that characterizes the concentrator and R_{ray} is a property that characterizes both the concentrator and the receiver.

The heat loss from the receiver is in the form of conduction, convection and radiation, and the total heat loss is a combination of these three mechanisms, given by [40]:

$$P_{loss} = P_{cond} + P_{conv} + P_{rad}. \tag{3.12}$$

The overall efficiency of the receiver, η_{rec}, is obtained by [40]:

$$\eta_{rec} = \frac{P_{net}}{P_{rec}}. \tag{3.13}$$

The heat loss mechanisms vary in the different regions of the receiver and one may be more dominant than the other. The receiver is divided into two parts: the spherical portion (or spherical cap) and the cylindrical portion. The spherical cap is exposed to concentrated

radiation while the cylindrical portion is insulated is 25 mm thick Superwool insulation. Since the receiver comprises spherical and cylindrical geomteries, using the above equations, the heat loss from each part is calculated separately and the total heat loss from the receiver is the sum of the two. The heat loss analysis for this thesis follows closely from Incropera and deWitt [71]. The heat loss mechanisms will be discussed in further detail.

3.2.3 Heat loss mechanisms

Conduction

Conduction is the mode of energy transfer where the heat flow is due to the temperature difference within a body or between bodies in thermal contact, without the involvement of mass flow and mixing [48]. The aim of a conduction analysis is to obtain the temperature distribution within a medium. The temperature distribution is a representation of how the temperature varies with position within the medium. Once the temperature distribution has been determined, the conduction heat flux from any point in the medium or on the surface of the medium may be obtained using *Fourier's law* [71]. Fourier's law states that, *the heat flow by conduction in any direction is proportional to the temperature gradient and area perpendicular to the flow direction and is in the direction of the negative gradient.* The mathematical form of Fourier's law in one dimension is given by

$$P_{cond} = -kA\, dT/dx, \tag{3.14}$$

where A is the cross-sectional area and dT/dx is the temperature gradient. The negative sign in equation (3.14) indicates the transfer of heat in the direction of decreasing temperature. The proportionality constant in the relation is known as thermal conductivity, k, of the material [48]. For engineering applications, knowledge of the temperature distribution allows for the optimization of the thickness of an insulating material, or to determine how compatible special coatings or adhesives may be if used on the medium.

According to Incropera and deWitt [71], one of the ways used to determine the temperature distribution and perform a heat conduction analysis is by the use of the heat equation. Consider a differential control volume $dxdydz$ shown in Figure 3.9. The conduction heat rates at the x, y and z surfaces are indicated by q_x, q_y and q_z, respectively.

From *Fourier's law* the conduction heat rate through each of the surfaces is

$$q_x = -kA\, dT/dx = -kdydz\frac{\partial T}{\partial x}, \tag{3.15}$$

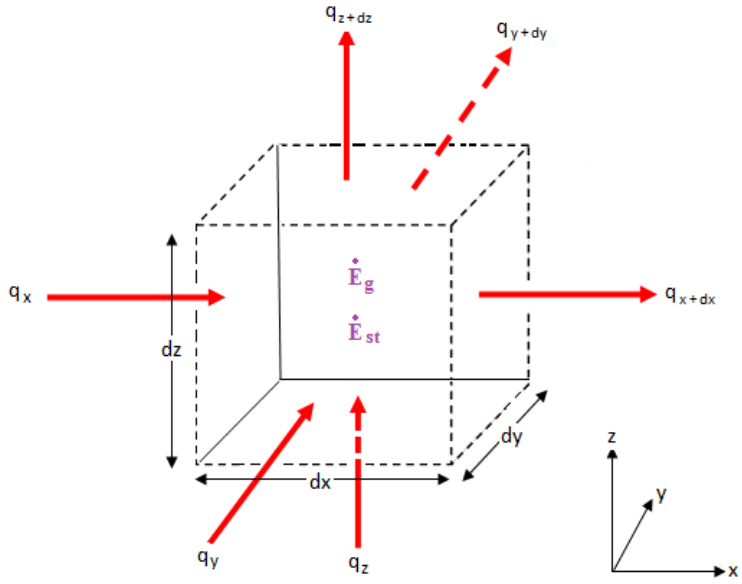

Figure 3.9: Differential control volume depicting the conduction heat rates through the volume in the x, y and z directions. Adapted from Incropera and deWitt [71].

$$q_y = -kA\, dT/dy = -kdxdz\frac{\partial T}{\partial y}, \tag{3.16}$$

$$q_z = -kA\, dT/dz = -kdxdy\frac{\partial T}{\partial z}. \tag{3.17}$$

The conduction heat rates at the opposite sides of each surface can be expressed using a Taylor series

$$q_{x+dx} = q_x + \frac{\partial q_x}{\partial x}dx + \frac{1}{2!}\frac{\partial^2 q_x}{\partial x^2}dx^2 + \frac{1}{3!}\frac{\partial^3 q_x}{\partial x^3}dx^3 + ... \tag{3.18}$$

Neglecting the higher order terms, equation (3.18) becomes

$$q_{x+dx} = q_x + \frac{\partial q_x}{\partial x}dx. \tag{3.19}$$

Similarly,

$$q_{y+dy} = q_y + \frac{\partial q_y}{\partial y}dy, \tag{3.20}$$

$$q_{z+dz} = q_z + \frac{\partial q_z}{\partial z}dz. \tag{3.21}$$

Within the control volume there may be an energy source that can be associated with the rate of thermal energy generation. This energy source term, $\dot{E}_g$, is given by

$$\dot{E}_g = \dot{q}dxdydz, \tag{3.22}$$

where $\dot{q}$ is the rate at which energy is generated per unit volume of the medium in $\mathrm{W/m^3}$. The rate of change of thermal energy stored, $\dot{E}_{st}$, by the material within the control volume

is expressed as

$$\dot{E}_{st} = \rho C_p \frac{\partial T}{\partial t} dxdydz, \tag{3.23}$$

where $\rho C_p \partial T/\partial t$ is the time rate of change of the sensible thermal energy of the medium per unit volume. Using the general form of the conservation of energy which is

$$\dot{E}_{in} + \dot{E}_g - \dot{E}_{out} = \dot{E}_{st}, \tag{3.24}$$

where $\dot{E}_{in}$ and $\dot{E}_{out}$ is the flow of energy into and out of the medium, respectively. Substituting equations (3.15)-(3.17) and equations (3.19)-(3.21) into the energy conservation equation we obtain

$$q_x + q_y + q_z + \dot{q}dx\ dy\ dz - q_{x+dx} - q_{y+dy} - q_{z+dz} = \rho C_p \frac{\partial T}{\partial t} dxdydz. \tag{3.25}$$

Substituting from equations (3.19)-(3.21) again, the above equation becomes

$$-\frac{\partial q_x}{\partial x}dx - \frac{\partial q_y}{\partial y}dy + \frac{\partial q_z}{\partial z}dz = \rho C_p \frac{\partial T}{\partial t} dxdydz. \tag{3.26}$$

Using equations (3.15)-(3.17) in the previous equation and dividing throughout by *dxdydz*, the general form of the heat equation in Cartesian coordinates is

$$\frac{\partial}{\partial x}\left(k\frac{\partial T}{\partial x}\right) + \frac{\partial}{\partial y}\left(k\frac{\partial T}{\partial y}\right) + \frac{\partial}{\partial z}\left(k\frac{\partial T}{\partial z}\right) + \dot{q} = \rho C_p \frac{\partial T}{\partial t}. \tag{3.27}$$

Simplifying the above by removing k as a constant from the first three terms, equation (3.27) becomes

$$\left(\frac{\partial^2 T}{\partial x^2}\right) + \left(\frac{\partial^2 T}{\partial y^2}\right) + \left(\frac{\partial^2 T}{\partial z^2}\right) + \frac{\dot{q}}{k} = \frac{1}{\alpha}\frac{\partial T}{\partial t}, \tag{3.28}$$

where $\alpha = k/\rho C_p$ is the thermal diffusivity [71].

For the purpose of this thesis, the heat equation in cylindrical and spherical coordinates is of more importance since the receiver has these geometries. Using the same method as before and applying an energy balance to the control volume in Figure 3.10 (a) and (b), the heat equation can be derived for cylindrical and spherical coordinates, respectively. These equations are given as

Cylindrical:

$$\frac{1}{r}\frac{\partial}{\partial r}\left(kr\frac{\partial T}{\partial r}\right) + \frac{1}{r^2}\frac{\partial}{\partial \phi}\left(k\frac{\partial T}{\partial \phi}\right) + \frac{\partial}{\partial z}\left(k\frac{\partial T}{\partial z}\right) + \dot{q} = \rho C_p \frac{\partial T}{\partial t}, \tag{3.29}$$

Spherical:

$$\frac{1}{r^2}\frac{\partial}{\partial r}\left(kr^2\frac{\partial T}{\partial r}\right) + \frac{1}{r^2\sin^2\theta}\frac{\partial}{\partial \phi}\left(k\frac{\partial T}{\partial \phi}\right) + \frac{1}{r^2\sin\theta}\frac{\partial}{\partial \theta}\left(k\sin\theta\frac{\partial T}{\partial \theta}\right) + \dot{q} = \rho C_p \frac{\partial T}{\partial t}, \tag{3.30}$$

where r is the radius of the cylinder or sphere [71].

The temperature gradients in cylindrical and spherical symmetries are in the radial direction (r-direction) only and therefore, their conduction may be treated as one-dimensional. For the cylindrical case, eliminating the circumferential and axial directions and for steady-state conditions with no heat generation, gives

$$\frac{1}{r}\frac{\partial}{\partial r}\left(kr\frac{\partial T}{\partial r}\right) = 0. \tag{3.31}$$

Similarly, for the spherical case, equation (3.30), eliminating the polar and azimuthal directions yields [71]:

$$\frac{1}{r^2}\frac{\partial}{\partial r}\left(kr^2\frac{\partial T}{\partial r}\right) = 0. \tag{3.32}$$

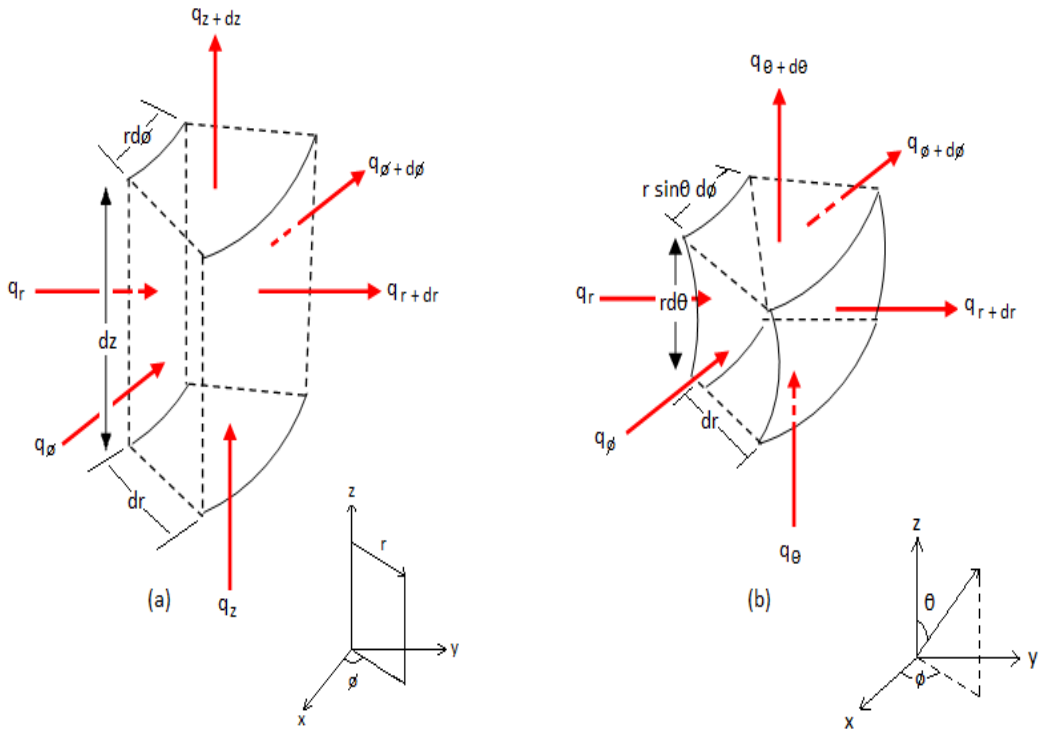

Figure 3.10: Differential control volumes depicting the conduction heat rates for (a) cylindrical geometry. The control volume in (r,ϕ,z) coordinates is $r\,dr{\cdot}d\phi{\cdot}dz$. (b) spherical geometry. The control volume in (r,ϕ,θ) coordinates is $r^2\,dr{\cdot}\sin\theta\,d\phi{\cdot}d\theta$. Adapted from Incropera and deWitt [71].

Under steady-state conditions (temperature at each point is independent of time) with no heat generation, the heat conduction for cylindrical and spherical symmetries may be analyzed either by using the appropriate form of the heat equation (standard method) or by using Fourier's law and integrating the rate equation (alternative method) [71]. The appropriate

form of Fourier's law and the rate at which energy is conducted through a cylinder is given by

$$q_{cond,c} = -k(2\pi rL)\frac{dT}{dr}, \tag{3.33}$$

where $2\pi rL = A$, which is the area through which the heat transfer occurs and L is the length of the cylinder. The temperature distribution within the cylinder may be obtained by solving equation (3.31) and applying boundary conditions. Integrating equation (3.31) twice gives

$$T(r) = C_1 lnr + C_2. \tag{3.34}$$

Applying the following boundary conditions to solve for C_1 and C_2:

$$T(r_1) = T_{s,1} \qquad \text{and} \qquad T(r_2) = T_{s,2}.$$

Substituting the boundary conditions into equation (3.34) we obtain

$$T_{s,1} = C_1 \ln r_1 + C_2 \qquad \text{and} \qquad T_{s,2} = C_1 \ln r_2 + C_2.$$

Solving the above equations for C_1 and C_2 and substituting into equation (3.34) we obtain the temperature distribution in a cylinder:

$$T(r) = \frac{T_{s,1} - T_{s,2}}{ln(r_1/r_2)} ln\left(\frac{r}{r_2}\right) + T_{s,2}. \tag{3.35}$$

Combining equations (3.35) and (3.33) the conduction heat rate through a cylinder is given by

$$q_{cond,c} = \frac{2\pi Lk(T_{s,1} - T_{s,2})}{ln(r_1/r_2)}, \tag{3.36}$$

where r_1 is the inner radius, r_2 the outer radius and $T_{s,1}$ and $T_{s,2}$ are the temperatures of surface 1 and 2, respectively. The quantity $R_{th,cond_c}$ is the thermal resistance due to conduction and is expressed as

$$R_{th,cond_c} = \frac{ln(r_1/r_2)}{2\pi Lk}. \tag{3.37}$$

For spherical geometry the alternative method is used to obtain the heat transfer rate. In this method the heat rate equation is integrated in order to obtain the temperature distribution. Using equation (3.33) and the area for a sphere which is $4\pi r^2$, the appropriate form of Fourier's law that can be used to analyze the conduction through a sphere is

$$q_{cond,sp} = -k(4\pi r^2)\frac{dT}{dr}. \tag{3.38}$$

Since $q_{cond,sp}$ is constant and independant of the radius r, the above equation can be written in integral form as follows

$$\frac{q_{cond,sp}}{4\pi}\int_{r_1}^{r_2}\frac{dr}{r^2} = -\int_{T_{s,1}}^{T_{s,2}} kdT. \tag{3.39}$$

Performing the above integration yields

$$\frac{q_{cond,sp}}{4\pi}\left[\frac{1}{r_1}-\frac{1}{r_2}\right]=k(T_{s,1}-T_{s,2}). \tag{3.40}$$

Assuming k is a constant, the rate of conduction through a spherical shell is given by

$$q_{cond,sp}=\frac{4\pi k(T_{s,1}-T_{s,2})}{(1/r_1)-(1/r_2)}, \tag{3.41}$$

where k, $T_{s,1}$ and $T_{s,2}$ are the same as for the cylindrical case. The thermal resistance, $R_{cond,sp}$, for a spherical shell is

$$R_{th,cond_{sp}}=\frac{1}{4\pi k}\left(\frac{1}{r_1}-\frac{1}{r_2}\right), \tag{3.42}$$

where r_1 and r_2 are inner and outer radii of the sphere, respectively [71].

Convection

This is the mode of energy transfer between a solid surface and the adjacent fluid that is in motion, and it involves the combined effects of conduction and fluid motion. The faster the fluid motion, the greater the convection heat transfer. In the absence of any bulk fluid motion, heat transfer between a solid surface and the adjacent fluid is by pure conduction [72]. Convection can be described as either *natural* or *free* convection or *forced* convection. Forced convection occurs when the fluid flow is due to an external factor such as a fan, pump or even wind. Free convection of the fluid is a result of the buoyancy forces due to density differences caused by temperature variation of the fluid. The convection heat transfer rate is proportional to the temperature difference and the relationship is known as *Newton's law of cooling*, expressed as

$$P_{conv}=hA_s(T_s-T_\infty), \tag{3.43}$$

where h is the convection heat transfer coefficient in $\mathrm{W/m^2K}$, A_s is the surface area over which the convection heat transfer occurs and T_s and T_∞ are the surface temperature and ambient temperature, respectively [71]. The convective heat transfer mode is also subjected to thermal resistance as in the case of the conduction mode. From Newton's law of cooling the general form of the thermal resistance due to convection is

$$R_{th,conv}=\frac{T_s-T_\infty}{Q_{conv}}. \tag{3.44}$$

The thermal resistance due to convection for cylindrical and spherical geometry is given by equation (3.45) and equation (3.46), respectively

$$R_{th,conv_c}=\frac{1}{2\pi rLh}, \tag{3.45}$$

$$R_{th,conv_{sp}} = \frac{1}{4\pi r^2 h}, \tag{3.46}$$

where r is the outer radius of the cylinder or sphere [71].

Radiation

The process by which heat is transferred from a body by virtue of its temperature is called thermal radiation [48]. Radiative heat transfer differs from conductive and convective heat transfer by two significant features: (1) no medium is required and (2) the energy transfer is proportional to the fourth power of the temperatures of the bodies involved [73]. In the study of radiative heat transfer the ideal surface is the *blackbody*, which is one that absorbs all the radiation incident upon it at any wavelength and temperature [48]. The total hemispherical emissive power of a blackbody is given by the *Stefan-Boltzmann* equation

$$E_b = \sigma T^4, \tag{3.47}$$

where σ = 5.67x 10^{-8} W/m^{2}K^4, E_b is the total emissive power and T is the temperature in Kelvin. All other surfaces emit radiation that is less than that of a blackbody and the thermal emission from most surfaces can be expressed as the difference between the power emitted from the surface and the power gained from the environment, according to

$$P_{rad} = \epsilon\sigma A(T_s^4 - T_\infty^4), \tag{3.48}$$

where ϵ is the emissivity of the radiating surface and A is the area. Emissivity values vary from one material to another and ranges from zero to one [73].

3.2.4 Receiver heat loss factor

If the radiative losses are small ($P_{rad} \ll P_{loss}$) such that P_{rad} may be neglected, the power loss by the receiver may be approximated as

$$P_{loss} \simeq P_{cond} + P_{conv}. \tag{3.49}$$

As shown in equations (3.14) and (3.43), P_{cond} and P_{conv} may be expressed as linear functions of the temperature difference T_{rec} - T_{amb}, where T_{rec} is the average receiver surface temperature and T_{amb} is ambient temperature (equal to T_∞ in equations (3.43) and (3.48)). For this case P_{net} may be approximated as

$$P_{net} \simeq P_{rec} - UA_{rec}(T_{rec} - T_{amb}), \tag{3.50}$$

where A_{rec} is the total surface area of the receiver, over which losses occur, and U is the receiver heat loss factor.

If the quantities η_0, U and A_{rec}, which are properties of the concentrator and receiver system, are known then P_{net} may be calculated as a function of P_{dish}, T_{rec} and T_{amb}. However, whereas η_0 and A_{rec} are relatively straightforward to calculate, U requires more complex modelling of the receiver, which is beyond the scope of this thesis. Such modelling would need to take account of the variation of temperature over the surface of the receiver (which itself may vary with T_{rec}), air convection, geometry and fraction of insulation coverage, and other such physical processes. Alternatively, if P_{net} and P_{rec} are known, then U may be estimated empirically using equation (3.50).

3.2.5 Heat transfer fluid (HTF)

Another important component of a solar thermal cooker system is the heat transfer fluid (HTF). The HTF is responsible for absorbing the thermal energy from the receiver and transferring this energy to parts of the system where it is required. The HTF may be used to directly heat a cooking surface or if the energy is required during periods of low insolation, it may be used to charge a storage system. An important factor to consider when choosing HTFs is that they must be non-toxic and non-hazardous. Some of the HTFs commonly used are water, synthetic oils, and air. For the present solar cooker system water has been used as the HTF.

Water

Water is a commonly used heat transfer fluid as it is cheap, widely available and non-toxic. It has a high thermal heat capacity of ~ 4.2 kJ/kg·K. Thermal conductivities of most liquids decrease with increasing temperature. The exception is water, which exhibits increasing thermal conductivity up to about 150 °C and decreasing thermal conductivity thereafter. Water has the highest thermal conductivity of all common liquids except liquid metals [73]. The thermophysical properties for water can be found in Figure B.1 (Appendix B) [71].

For this system, there is a flow of steam from the receiver to the storage system and the condensate is returned to the receiver by gravity. Water is heated within the receiver until it starts to boil and the less dense steam molecules rise to the top of the receiver. The steam leaves the top pipe of the receiver and travels through the pipe clamped beneath the hot-plate. When the energy from the steam is transferred to the hot-plate, it condenses and the

condensate flows back into the receiver where it is re-heated.

3.2.6 Heat transfer in the receiver during boiling

Boiling occurs at a solid-liquid interface when a liquid is brought into contact with a surface maintained at a temperature T_s, which is sufficiently above the saturation temperature, T_{sat}, of the liquid [72]. The boiling process is characterized by vapour bubbles that rapidly form at the solid-liquid interface. Those with enough energy are able to become detached from the surface and rise to the free surface of the liquid. Since the process involves the movement of fluid, it is associated with the convective heat transfer mode. The convection heat transfer process from the solid to the liquid occurs according to the following equation

$$q''_s = h(T_s\text{-}T_{sat}) = h\Delta T_e, \tag{3.51}$$

where, q''_s is the heat flux and ΔT_e is the *excess temperature*. According to the Nukiyama's boiling curve (for saturated water at atmospheric pressure) Figure 3.11, there are four main boiling regimes: free convection, nucleate, transition and film boiling. Each of these regimes are characterized by their excess temperature and the type of bubble formation that is produced [71].

According to the boiling curve nucleate boiling occurs where $\Delta T_{e,C} < 30\,^{\circ}\text{C}$. There are two distinct types of bubble formation in the nucleate boiling regime i.e isolated bubbles and jet/column formation [71]. The former is what occurs in the receiver in order to generate steam. As water is heated in the receiver it approaches its boiling point and bubbles begin to form. This corresponds to region A-B on the boiling curve. Vapour bubbles emerge from distinct sites on a heated surface and their number increases with increasing heat flux density. These distinct sites, referred to as *cavities* or *nucleation* sites, allow for the formation of bubbles by trapping small quantities of gas or vapour [71]. The boiling chips within the receiver provide these cavities to initiate the boiling process. Immediately after a bubble is formed its growth is mainly governed by heat conduction near the vapour-liquid interface. Shortly thereafter, radial convection becomes dominant. After bubble departure heat conduction, and radial and axial convection become the controlling heat transfer mechanisms. During the rising and the departure of the bubbles, their internal energy is transferred from the heated surface to the surrounding fluid [71].

As boiling within the receiver progresses the water changes phase and steam is produced. The density of steam is less than that of water since steam molecules are further apart from each other. Therefore, the space above the water level becomes filled with the less dense steam

molecules, and this allows the steam to rise up the outlet pipe where it is circulated through the hot-plate of the storage container. As the pressure from the steam increases, it exerts pressure on the remaining water causing the boiling point of the water to increase. This is due to the fact that an increased pressure on the water surface makes it difficult for water molecules to escape from the surface. As the water is further heated, steam pressure increases and the temperature of the water is raised to become superheated water. This superheated water, which is water under pressure at temperatures in the range 100-374 °C, is required for heating the thermal energy storage and melting PCM salt at 223 °C, as will be shown in Chapter 4.

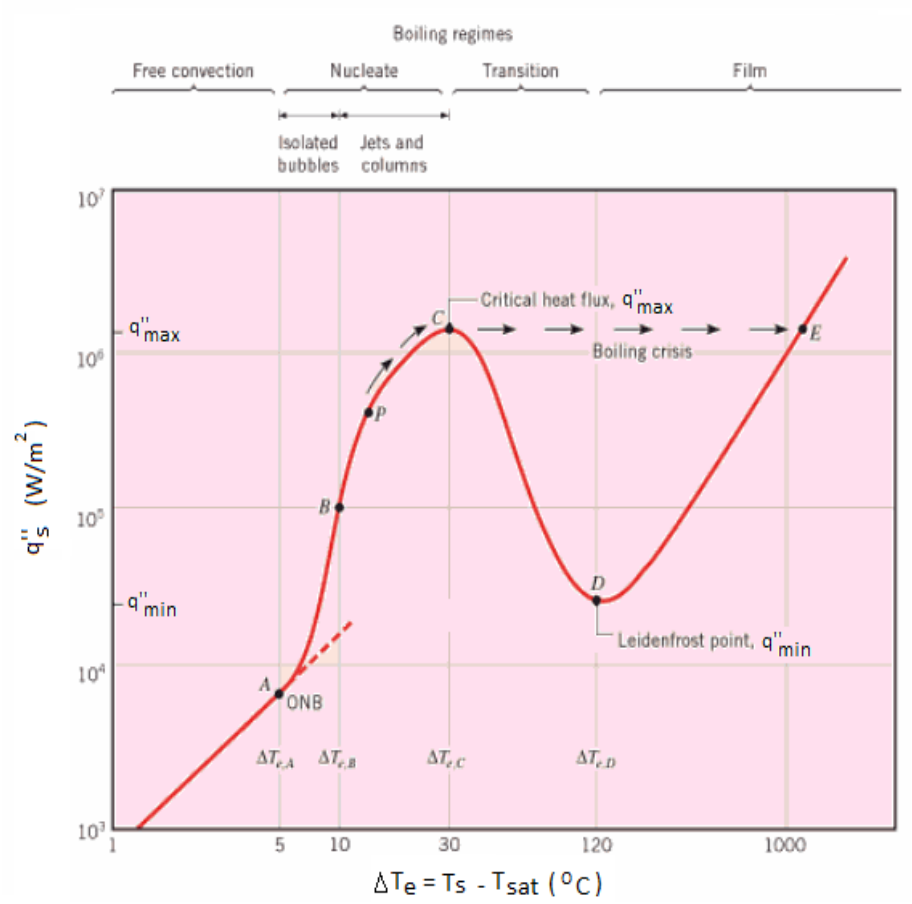

Figure 3.11: Nukiyama's boiling curve. Boiling in the receiver corresponds to points *A* and *B* of the nucleate boiling regime on the boiling curve. Adapted from Incropera and DeWitt [71].

3.3 Tracker

In order to maximize the amount of solar radiation absorbed by the receiver, the concentrator is allowed to track the sun throughout the day. An adequate tracking mechanism needs to follow the sun with a certain degree of accuracy during clear and cloudy conditions, and return the collector to the starting position at the end of the day [74]. An incorrect tracking system will compromise the amount of concentrated radiation being absorbed since the solar flux distribution may not be accurately focused onto the receiver. A decrease in receiver performance will cause a decrease in the overall system performance [75]. The tracking angles that describe the daily motion of the sun are depicted in Figure 3.12.

Solar zenith angle, θ_z: This is also called the *zenith distance* and is the angle between the local zenith and the line joining the observer and the sun. It is an angle between 0 and 90 °.

Solar altitude angle, α: This is the sun's angular height above the horizon. Also referred to as the *solar elevation*, it ranges from 0 to 90 ° and is the compliment of the solar zenith angle.

Solar azimuth angle, ψ: The solar azimuth is the angle at the local zenith, between the plane of the observer's meridian and the plane of a great circle passing through the zenith and the sun. It is measured east positive, west negative, (south zero) and hence varies between 0 ° and ± 180 °.

Hour angle, ω: The hour angle is measured at the celestial pole between the observer's meridian and the solar meridian. Starting from midday, it changes 15 ° per an hour.
The relationship between the solar angles is given by the following equations:

$$\cos\theta_z = \sin\delta\sin\phi + \cos\delta\cos\phi\cos\omega = \sin\alpha, \tag{3.52}$$

$$\sin\psi = \frac{\cos\delta\sin\omega}{\cos\alpha}, \tag{3.53}$$

where δ and ϕ are the declination and latitude angles, respectively [76]. The declination angle is defined in Chapter 2 and the latitude angle defined as the angle between a line from the earth's center to a point on the earth and the equatorial plane.

For this thesis, a polar axis tracking system was constructed. The concentrator was rotated about the polar axis at 15 ° per an hour to keep it focused on the receiver. The polar axis is

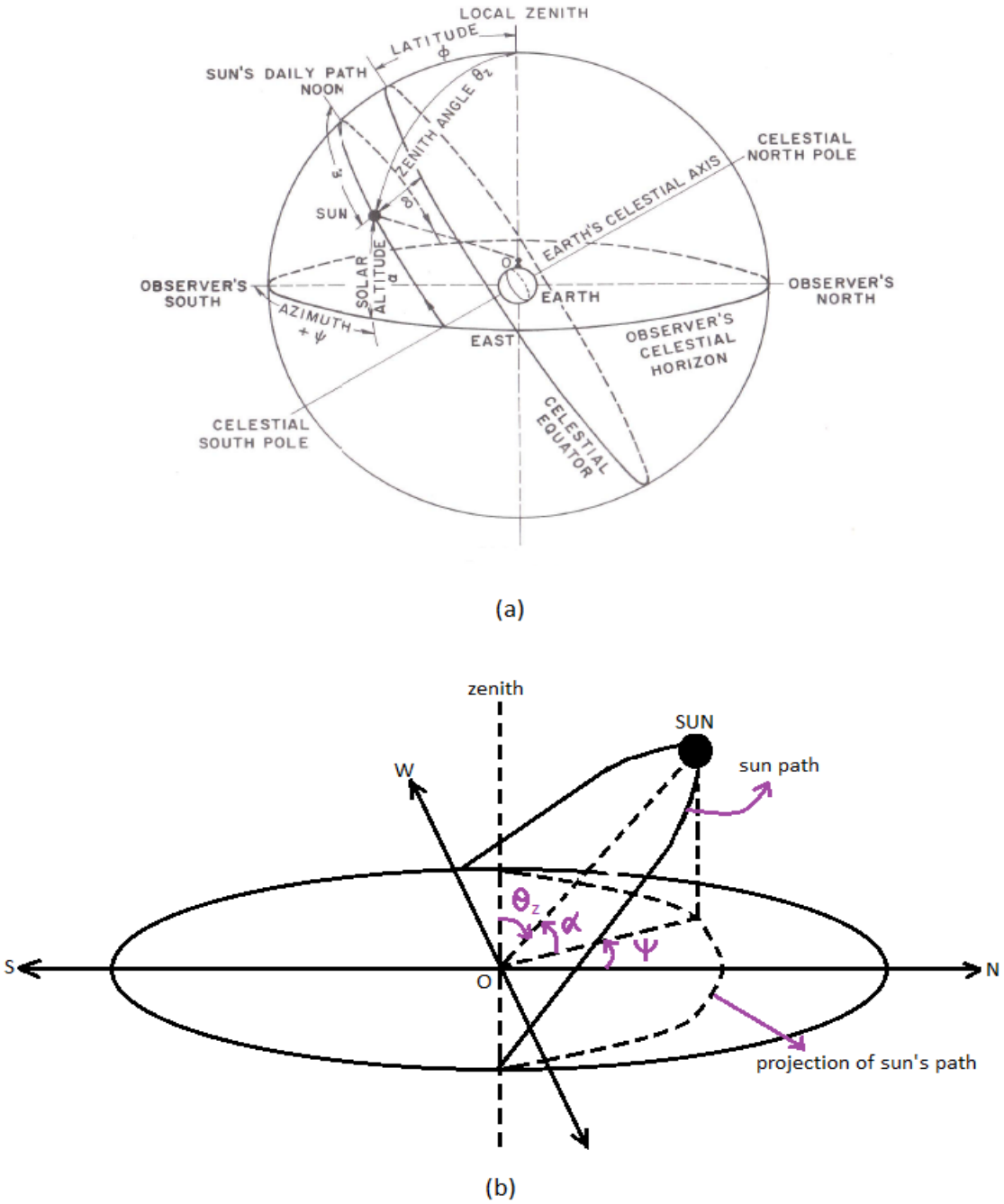

Figure 3.12: (a) Celestial sphere and the sun's coordinates relative to the observer on earth at point O. Adapted from Iqbal [76]. (b) Apparent daily motion of the sun across the sky from sunrise to sunset for the southern hemisphere, with the observer at point O. The angles (θ_z), (α) and (ψ) represent the sun's zenith, altitude and azimuth, respectively.

aligned parallel to the earths N-S axis and is inclined to the horizontal at an angle equal to the local latitude, which for Durban, is approximately 30 °. A chaindrive system consisting of a tracking wheel, bicycle chain and sprocket and a 12 V swing gate motor were positioned onto

the rotating cylinder of the system. This allowed for east-west tracking and the declination was adjusted manually by a screw mechanism. An electronic sun sensor (manufactured by Lingding Energy) was mounted on the top of the concentrator and connected to the motor. As shown in Figure 3.13, the photodiodes positioned on the left, right, top and bottom detects a shadow that the sun casts. Once the shadow is detected it moves in the appropriate direction so that the shadow is no longer present. Once this is the case the sensor is now facing the sun directly. The relays are used to control the message sent to the motor and whether the motor should move depending on the position of the sun. The circuitry is housed in a plastic casing. The motor, which draws very little current, does not run continuously. When the sensor is out of focus it activates the motor and the motor jogs until the sun is in focus again. Once in focus the motor stops and the process is repeated when the sun goes out of focus. At the end of the day the system has to be manually turned back to the starting position.

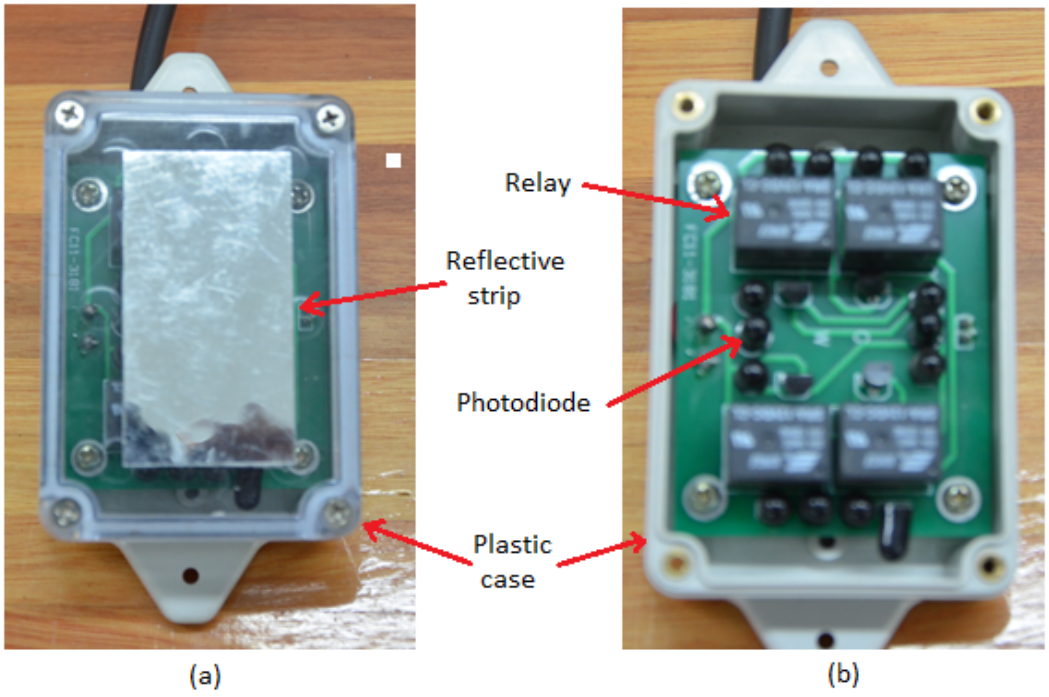

Figure 3.13: Sun sensor for tracking system. (a) Sensor box with cover. Reflective strip prevents the box from over heating. (b) Sensor box without top cover showing the photodiode and relay circuitry.

Chapter 4

Thermal energy storage (TES)

The other important component of a solar thermal system is a thermal energy storage (TES). Storage of thermal energy is important since it reduces the gap between supply and demand, and allows for the utilization of the energy during off-sunshine hours [5]. Since the space for a thermal energy storage system is often limited, optimal design is needed in order to make efficient use of the storage volume. TES systems can be categorized into two broad groups, namely sensible and latent storage. This chapter discusses the distinction between sensible and latent heat storage, and the storage systems designed and constructed for the work of this thesis.

4.1 Sensible heat storage

Sensible heat storage systems are those that exhibit no phase change of the storage material. The thermal energy is stored by raising the temperature of the solid or liquid. This method of heat storage uses the heat capacity and the change in material temperature during charging and discharging [5]. The amount of heat stored is dependent on factors such as the specific heat of the storage medium, operating temperatures, thermal conductivity and diffusivity, vapour pressure, quantity of the storage material etc. This needs to be taken into consideration during the design of the heat storage system [77]. The quantity of energy stored, Q, in a sensible storage medium is given by the following

$$Q = \int_{T_i}^{T_f} mC_p \, \mathrm{d}T = mC_{ap}(T_f - T_i), \tag{4.1}$$

where, m, C_{ap}, T_f and T_i are the mass, heat capacity, final and initial temperatures of the material, respectively [5]. A list of some commonly used sensible energy storage media with

their corresponding melting point, thermal conductivity, specific heat capacity and heat of fusion can be found in Agyenim et al.[78], Sharma et al.[5], Kenisarin [79] and Zalba et al.[80].

4.2 Latent heat storage

Latent heat storage is based on the absorption or release of heat when the storage material undergoes a change of phase, either from solid to liquid, liquid to gas or vice versa.

Phase Change Materials (PCMs) are considered to be latent energy storage materials since the transfer of thermal energy occurs when the material undergoes a change in state or "phase." Compared to sensible storage media, PCMs store energy at a nearly constant temperature and they utilize a significantly smaller volume. PCMs are able to store 5-14 times more energy per unit volume than some sensible storage media such as water, masonry or rock [5]. The phase change process of a PCM from solid phase to liquid phase and vice versa is depicted in Figure 4.1, and the latent energy storage capacity with a PCM medium is given by the following equation

$$Q = \int_{T_i}^{T_m} mC_p \,\mathrm{d}T + ma_m \Delta h_m \int_{T_m}^{T_f} mC_p \,\mathrm{d}T \tag{4.2}$$

which, upon integration, yields

$$Q = m[C_{sp}(T_m - T_i) + a_m \Delta h_m + C_{lp}(T_f - T_m)], \tag{4.3}$$

where C_{sp} is the sensible heat capacity between T_i and T_m, a_m is the fraction melted, Δh_m is the heat of fusion and C_{lp} is the latent heat capacity between T_m and T_f [5].

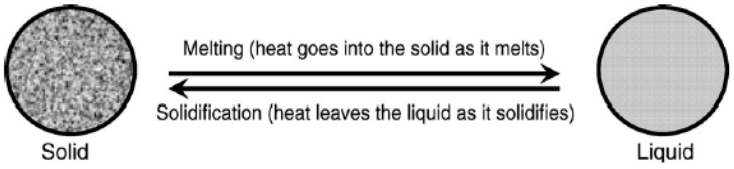

Figure 4.1: Schematic of the phase change process [81].

Criteria for phase change material selection:

A classification of phase change materials can be found in Sharma et al.[5]. They can be broadly categorized as *organics*, *inorganics* or *eutectics*. Some examples of PCMs include

water, paraffins and non-paraffins, salt hydrates, nitrate salts, polyalcohols and other various organic and inorganic compounds. These storage materials have different operating and transition temperatures as well as varying heats of fusion. Therefore, it is important that the thermophysical, kinetic and chemical properties of the PCM be thoroughly investigated before using them for a particular application. Some of these important criteria are listed below [5, 78]:

- Melting point in the desired operating temperature range (temperature range of application).
- High latent heat of fusion per unit mass, so that a smaller amount of material stores a given amount of energy.
- High specific heat to provide additional significant sensible energy storage effects.
- High thermal conductivity, so that the temperature gradients for charging and discharging the storage material are small.
- Small volume changes during phase transition, so that a simple container and heat exchanger geometry can be used.
- Exhibit little or no subcooling (occurs when the PCM begins to solidify at a temperature below its solidification temperature) during freezing.
- Chemically stable, no chemical decomposition and corrosion resistance to construction materials.
- Should consist of non-poisonous, non-flammable and non-explosive elements/compounds.
- Abundantly available at low cost.

4.3 Salt storage system

Any storage system using latent energy storage must comprise three main components. Firstly, it requires a solid-liquid PCM whose phase transition is within the required operating temperature range, and where most of the added heat is stored as latent heat of fusion. Secondly, a suitable container for retaining the storage substance. Lastly, a heat exchanger in order

to transfer heat from the source to the PCM, and from the PCM to the sink. Although latent energy storage is still a developing technology, it seems to have a great deal of potential especially for high temperature storage [82].

4.3.1 $NaNO_3$-KNO_3 binary mixture

The storage system constructed for the work of this thesis consists of a eutectic mixture containing sodium nitrate ($NaNO_3$) and potassium nitrate (KNO_3) in a 50:50 molar percentage. A eutectic mixture is one that consists of two or more substances with a melting point that is lower than the melting point of any other mixture containing the same substances. Eutectics almost always melt and freeze without segregation. This prevents separation of the components. In addition, during melting both components liquefy simultaneously [5]. The $NaNO_3$-KNO_3 binary mixture falls into the category of inorganic PCMs. This nitrate salt combination is also known as "solar salt".

Analysis by Differential Scanning Calorimeter (DSC)

The heat capacities of the $NaNO_3$ and KNO_3 binary mixture can be analyzed using a Differential Scanning Calorimeter (DSC). A typical DSC heating thermogram is shown schematically in Figure 4.2. It is a curve that shows the heat of fusion versus temperature. Latent heat of fusion is the amount of heat added to melt the PCM, and is represented by the area under the peak. The phase change process begins at a temperature T_i, reaches its peak at T_p and ends at T_e.

The melting point of $NaNO_3$ and KNO_3 is 307 °C and 333 °C, respectively [80]. These temperatures are relatively high and in most cases will not be achieved in small scale solar cookers. However, when the $NaNO_3$ and KNO_3 salts are combined into a 50:50 (mol %) binary mixture it has a melting point of 223 °C [83], which is within the suitable range for solar cooking applications. The melting and solidification peaks are shown in Figure 4.3. A 50:50 mole ratio is used since it is the most stable combination and the components will not separate. Some of the pertinent literature listing thermophysical properties of other PCM salts includes Sharma et al.[5], Liu et al.[84], Kenisarin [79], Kenisarin and Mahkamov [85], Farid et al.[86], Lopez et al.[87] and Zalba et al.[80].

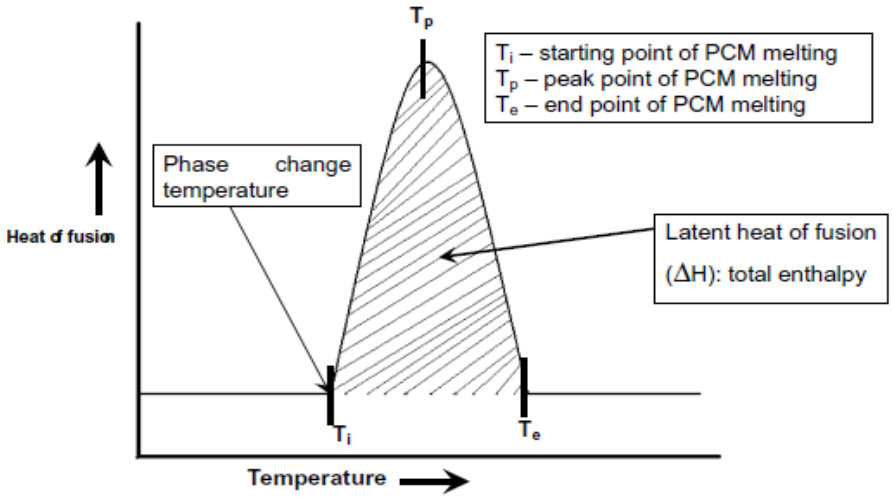

Figure 4.2: Schematic of a DSC heating thermogram for a phase change material [81].

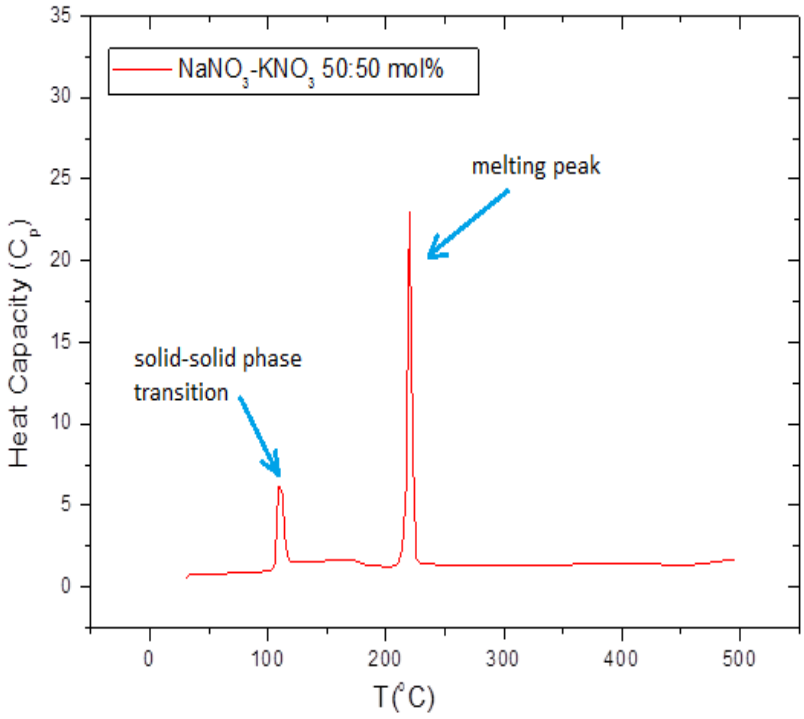

Figure 4.3: DSC heating thermogram of $NaNO_3$ and KNO_3 for 50:50 mol %. The solid-solid phase transition peak and melting peak is at 109 and 220 °C, respectively. Adapted from Foong [83].

4.3.2 Storage geometry

The storage container used for this system is a cylinder of 300 mm height and 300 mm diameter and was constructed from mild steel (grade EN8). Figure 4.4 shows a schematic of the

storage system. The cylinder had a wall thickness of 5 mm and weighed approximately 16 kg. The storage system consists of the cylinder, the top-plate with fin arrangement and the $NaNO_3$-KNO_3 PCM.

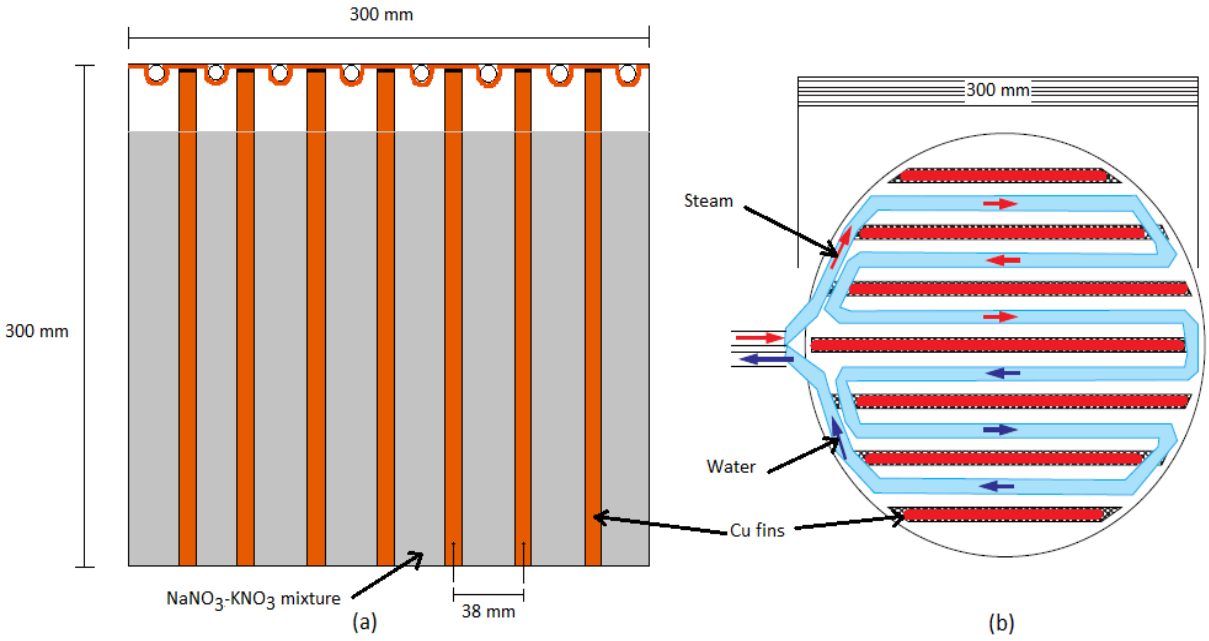

Figure 4.4: Schematic of the salt storage system. (a) Side view of the storage tank filled with $NaNO_3$-KNO_3 binary mixture and copper fins. (b) Top view of aluminium hot-plate with steel pipe clamped to the surface.

The top-plate and fin arrangement are one unit, where the top-plate was made from aluminium (grade 6082) and the fins were made from copper. The copper fins were fitted into slots made in the aluminium plate so that there would be good thermal contact. A total of 7 fins each with 5 mm thickness and 270 mm in length were used. The 7 fins and the 20 mm thick aluminium top-plate weighed 21 and 4 kgs, respectively. The fins have a spacing of 38 mm (center-to-center). A mild steel pipe (grade EN8) of 8 mm/6 mm (OD/ID) was shaped to fit in between the fins and was clamped to the surface of the aluminium plate. A slight groove was made for the pipe to have better contact with the plate. Strips of 0.5 mm thick copper sheet were moulded over the pipes so that a better distribution of heat could be achieved. The total weight of the storage container without the phase change material was 41 kgs. Five thermowells spaced 35 mm apart were welded into the wall, along the height of the container. The probes were positioned parallel to the fins and at a distance of appoximately 19 mm away from the fins. This allowed for the insertion of K-type thermocouple probes for temperature

measurement. Figure 4.5 shows the storage container with the fin arrangement, before the bottom section of the container was fitted and before the dry solar salt mixture was added.

The salt mixture was filled in the gaps between the fins within the storage container. The total mass of salt used was 14.5 kg (6.61 kg of $NaNO_3$ and 7.86 kg of KNO_3), which gave the storage container a total weight of 55.5 kg. The storage container was insulated with Superwool insulation with a total thickness of 75 mm and placed approximately 1100 mm above ground level. One of the requirements of a thermosyphon system is that the storage container be above the receiver so that the hot fluid/steam is allowed to rise and the cold fluid/condensate will sink to the bottom.

As mentioned previously, the water heated within the receiver is converted into steam and circulates through the coiled pipe that is clamped beneath the aluminium plate. The contact with the colder hot-plate causes the steam to transfer its thermal energy by conduction to the plate and condenses. The continuous process of steam flowing through the pipe in contact with the hot-plate causes the temperature of the plate to rise. The energy from the plate is transferred by conduction to the copper fins to heat the solar salt mixture. The copper fins within the storage container serves two purposes. The first is that they transfer the heat from the hot-plate into the salt so that the salt can melt throughout the day. The second is that when the salt solidifies at night and releases its latent energy, the fins transfer this energy from the salt back to the hot-plate where it can be used for water heating or cooking.

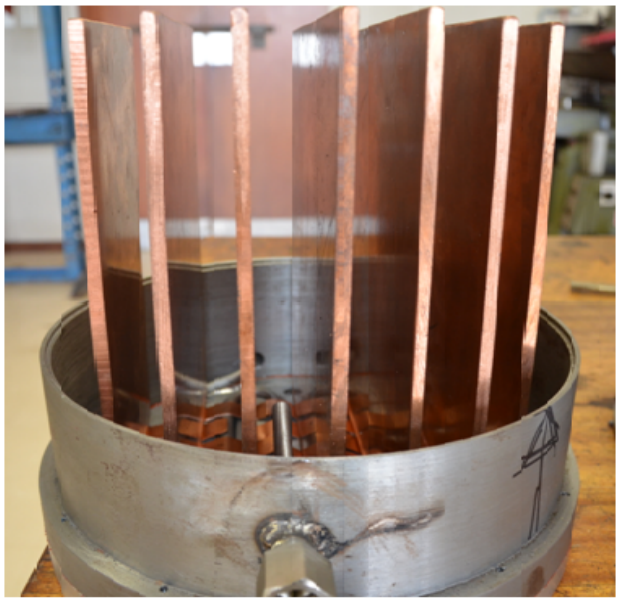

(a)

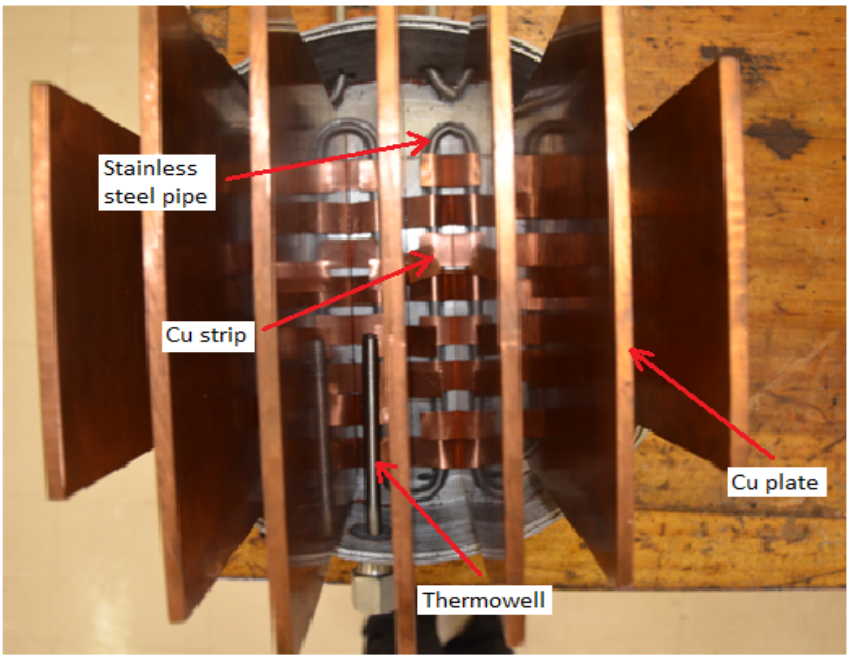

(b)

Figure 4.5: (a) Salt storage container with copper fin arrangement viewed upside down (hot-plate face down). (b) Copper strips cover the stainless steel pipe that is clamped to the hot-plate so that the heat can be distributed evenly. Thermowell welded into the wall of the container to allow for the insertion of K-type thermocouple probe.

4.4 Alternative storage system

In addition to the salt storage system, an alternative storage system was constructed. This was needed because (as will be shown in Chapter 7), leaks in the pipe connections resulted in receiver temperatures significantly lower than 200 °C, so melting of salt was not possible. Furthermore, it was found that there was a settling effect of the salt in the storage container. Therefore, an alternative storage system was constructed and was used to demonstrate the following:

- De-airing of the system.
- Transfer of heat from the receiver to the storage system.

This system consisted of a copper coil, 16 mm/13 mm (OD/ID) (531g), immersed in water and contained in an aluminium pot (625 g). The coil had two turns and was mounted into the pot such that it did not touch the base or the sides of the pot. This system replaced the salt storage and was connected to the inlet and outlet steel pipes. The steam produces a flow through the copper pipe and condenses when in contact with the colder part of the pipe. The heat released during condensation is transferred to the surrounding fluid and raises its temperature. The same procedure was carried out with the water being replaced by cooking oil as the storage medium. A schematic of the alternative storage system and the storage container before the water/oil was filled are shown in Figure 4.6. The storage container was insulated with one layer (25 mm) of Superwool insulation.

4.5 Insulation

Insulation plays a vital role in thermal energy storage systems. It consists of material with high thermal resistance, and its primary purpose is to retard the heat flow rate by conduction, convection and radiation. The way in which this is achieved is by the use of numerous tiny dead-air cells that prevent convective heat transfer. In order to reduce the radiation effects a closed cell structure is created within the insulation material to avoid a large temperature difference. This breaks the radiation "paths" into smaller distances causing the longwave infrared radiation to be absorbed or scattered by the insulating material. However, the decrease in cell size causes an increase in conduction as well as an increase in the material density. Insulation material can be categorized into either *inorganic* or *organic* materials. This can then be further classified into fibrous or cellular materials [88]. Alternatively, they can be classified as

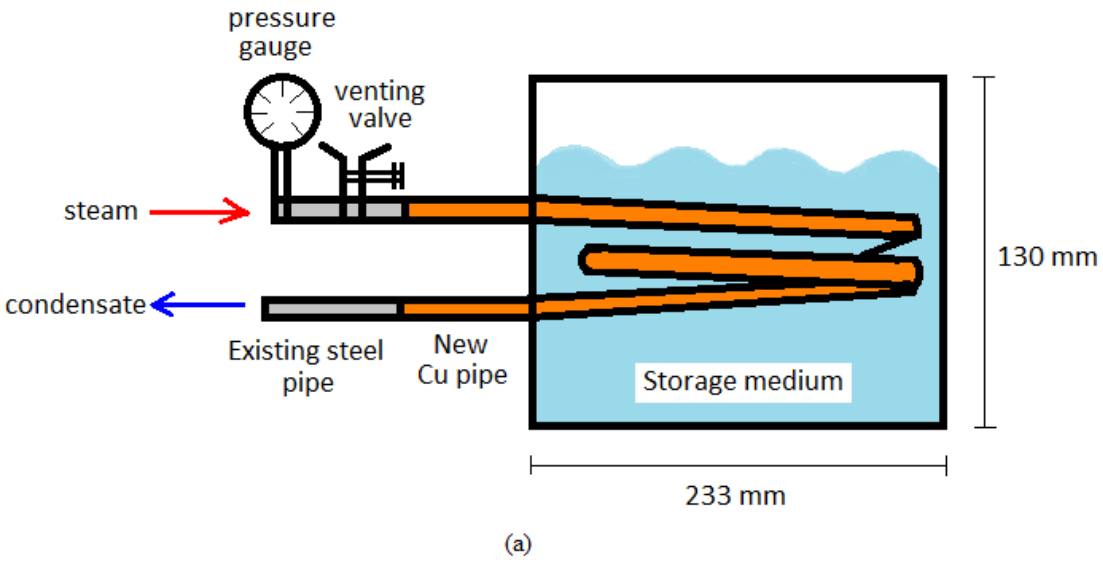

(a)

(b)

Figure 4.6: (a) Schematic of alternative storage system. The copper pipe assembly is connected to the existing steel pipes. (b) Copper coil placed into an aluminium storage container before filling water/oil as the storage medium.

either *high* or *low* temperature. The selection of the appropriate insulation material depends on the type of application as well as the physical and thermal properties of the material.

4.5.1 Thermal conductivity

The most important parameter of insulating material is thermal conductivity, which is a measure of how effective a material is in conducting heat. This is known as the *k-value* and

is expressed in W/m·K. Comparison of the k-values for different insulation materials gives an indication of which material will be more effective for a particular application. Generally, materials with high thermal conductivity values are good heat conductors and materials with low thermal conductivity values are poor heat conductors (or insulators). However, the k-value is temperature dependent and as the temperature increases, the k-value will increase. The thermal conductivity for conduction (in the x-direction) can be expressed by the following

$$k \equiv -\frac{q''}{\partial T/\partial x}, \tag{4.4}$$

where q'' is the *conduction* heat flux (W/m^2) and $\partial T/\partial x$ is the temperature gradient. The negative sign in the above equation indicates that the heat is being transferred in the direction of *decreasing* temperature [71].

There are various factors that need to be considered for the selection of thermal insulation material. Some of these include cost, durability of the material, thermal conductivity, the material's compressive strength, resistance to fire, health and safety hazards and the ease of application. However, when considering the thermal performance of the material, the k-value is of most importance.

As mentioned previously, insulation can also be classified as either high or low temperature. Some common low temperature options include rock/slag/glass wool, vermiculite, cellulose and polystyrene. A comprehensive description of the different low temperature insulating materials and their properties can be found in Bynum [89]. Progress is being made towards superior insulation materials for high temperature applications, which possess lower k-values and are significantly thinner, lighter and less dense. Some of these superior or "state-of-the-art" materials include aerogels, vacuum insulation panels, gas-filled panels, plastic fiber insulation and phase-change materials [90]. Further details can be found in literature such as Jelle et al.[90, 91], Fricke et al.[92, 93], Simmler and Brunner [94], Alam et al.[95] and Baetens et al.[96]. For the purpose of this system, high temperature insulation material has been used.

4.5.2 Superwool

Superwool insulation has been used as part of the thermal energy storage system. It has a chemical composition of 62-68% SiO_2, 26-32% CaO and 3-7% MgO, and can withstand temperatures up to 1200 °C [97]. The insulation used was 25 mm thick with density of 128 kg/m^3. The storage container was insulated with a total Superwool thickness of 75 mm. The unexposed parts of the receiver and transport pipes were insulated with the same material. The variation of thermal conductivity with temperature for the Superwool material for different

densities is shown in Figure 4.7.

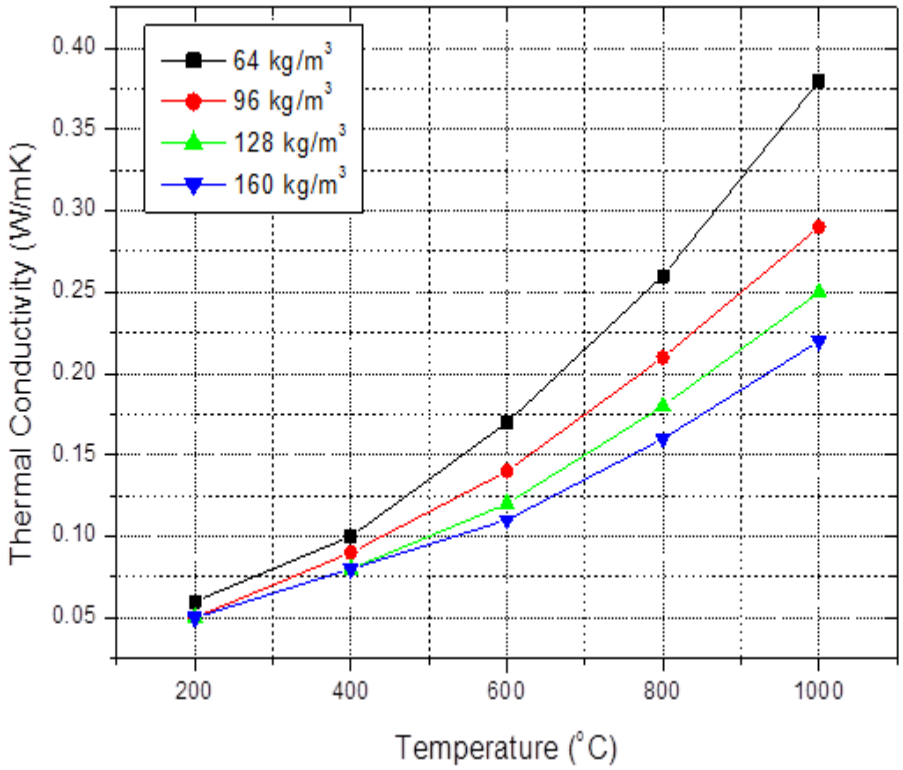

Figure 4.7: Variation of thermal conductivity (k-value) with temperature for different densities of Superwool insulation. Adapted from Superwool datasheet [97].

Chapter 5

System operation and experimental setup

This chapter describes the solar thermal cooker system that was designed and constructed for the work of this thesis, with respect to its experimental setup and operation. Various quantities such as the expected energy input, output and storage capacities, that have been calculated using equations from Chapter 3, will be presented here. The experimental setup includes a description of the type of heat source and storage material used, duration of heating and the importance of a de-airing process. The experimental method in terms of a procedure for the experiments is discussed in Chapter 6. Results from the experiments are presented and discussed in Chapter 7.

5.1 System operation with solar heating

As mentioned in Chapter 3, the concentrator is responsible for capturing the incoming radiation and directing it toward the receiver. Conduction of the incoming radiation through the spherical cap raises the temperature of the inner wall of the receiver. Within the receiver, energy is passed through convection from the inner wall to the water and then throughout the mass of the water. Heat transfer through convection and radiation also occur from the spherical cap of the receiver where the incoming radiation is focused. The heat loss and efficiency of the receiver are calculated using equations (3.12) and (3.13), respectively.

The total energy contained in water, steam or a mixture of the two is referred to as the enthalpy of the fluid and is expressed in kilojoules per kilogram (kJ/kg). These quantities can be found in steam tables which are used to determine the amount of energy available in

water or steam at a given temperature and pressure. The enthalpy of water and steam found in steam tables can be described as follows:

- The *enthalpy of liquid*, (h_f), is a measure of the amount of sensible energy contained in the water at a specific temperature.
- The *enthalpy of evaporation*, (h_{fg}), or *latent heat of vaporization* is the quantity of energy needed to convert one kilogram of water to one kilogram of steam at a given pressure.
- The *enthalpy of steam*, (h_g), is the total latent energy contained in saturated steam at the given pressure. This energy is the sum of the liquid enthalpy and the enthalpy of evaporation and is given by the following equation

$$h_g = h_f + h_{fg}, \tag{5.1}$$

where values for h_f, h_g and h_{fg} are given in Table B.1 (Appendix B) [99]. For the receiver being completely filled (625 ml), the quantity of sensible energy required to raise the temperature of the water from 25 °C (ambient) to 100 °C was calculated using equation (4.1) as follows

$$\begin{aligned} Q_s = (m_w C_p + m_{st} C_{st})\Delta T \; &= \; [(0.625 \text{ kg})(4.19 \text{ kJ/kgK}) \\ &+ (2.5 \text{ kg})(0.486 \text{ kJ/kgK})](373 - 298 \text{ K}) \\ &= 288 \text{ kJ}, \end{aligned} \tag{5.2}$$

where m_w is the mass of the water, m_{st} and C_{st} are the mass and heat capacity of the steel receiver, respectively. The additional vaporization energy, Q_v, required to produce steam was calculated according to

$$Q_v = m_w C_v = (0.625 \text{ kg})(2257 \text{ kJ/kgK}) \; = \; 1410 \text{ kJ}, \tag{5.3}$$

where C_v is the heat capacity of the vapour. Therefore, a total energy, Q_{tot}, of 1698 kJ is required to convert all the water to steam. For an estimated P_{net} of 677 W, the time taken to heat the receiver and convert all the water to steam was approximately 42 minutes according to the following equation

$$t = \frac{Q_{tot}}{P_{net}}, \tag{5.4}$$

where t is the time in seconds and Q_{tot} is the total energy in kJ.

5.1.1 Heat transfer and steam flow

For this system, the receiver is considered to be the heat source and the storage the heat sink. The basic requirement for transfer of heat is the presence of a temperature difference. There can be no net heat transfer between two media that are at the same temperature therefore, it is the temperature difference that is the driving force for the heat transfer. Heat will always flow from a high-temperature medium (heat source) to a low-temperature medium (heat sink) until thermal equilibrium is reached. This is when the two media reach the same temperature and a temperature gradient no longer exists [72].

In order for the steam to flow from the point where it is produced to the point of utilization, there needs to be a difference in pressure. As boiling progresses in the receiver the pressure begins to increase due to the change of volume from liquid to gas. Provided that the system is sealed, as the pressure increases the boiling point of the water also increases according to the Pressure-Temperature (P-T) curve in Figure 5.1. When water is heated at a pressure above atmospheric, the boiling point of the water is higher than 100 °C and the sensible heat required to reach the boiling point will be greater. If water is heated at a pressure below atmospheric, the boiling point will be lower than 100 °C [99]. The boiling point temperature and corresponding energy at a specific pressure can be found in steam tables.

Figure 5.2 depicts the flow of steam within the system. There are two modes of operation, mode A and B, as indicated by level A and B. When the water level in the receiver covers the condensate pipe only, the receiver operates in mode A where the steam produced in the receiver it takes the higher outlet pipe due to the less dense steam molecules. The natural circulation of steam is initiated by the top pipe becoming filled with steam as it gets produced in the receiver. As the steam travels through the coil in the storage it transfers its energy to the surrounding colder medium and eventually condenses. The condensate drips downward into the receiver where it is re-heated. Mode B operation is when the water level in the receiver is at level B, such that both pipes are exposed and the steam travels up both pipes into the storage. When the steam condenses in the storage the condensate is returned to the receiver via the lower pipe due to gravity. This process will continue as long as steam is being produced, and the steam flowing into the storage will be constantly replenished as it condenses. The same amount of energy that is required to produce steam is released back to its surroundings during condensation. This is the useful amount of energy that may be used for heating since it is the total energy in the steam that is extracted when the steam is condensed back to water. The mass of steam, m_s, being produced by the receiver was calculated according to

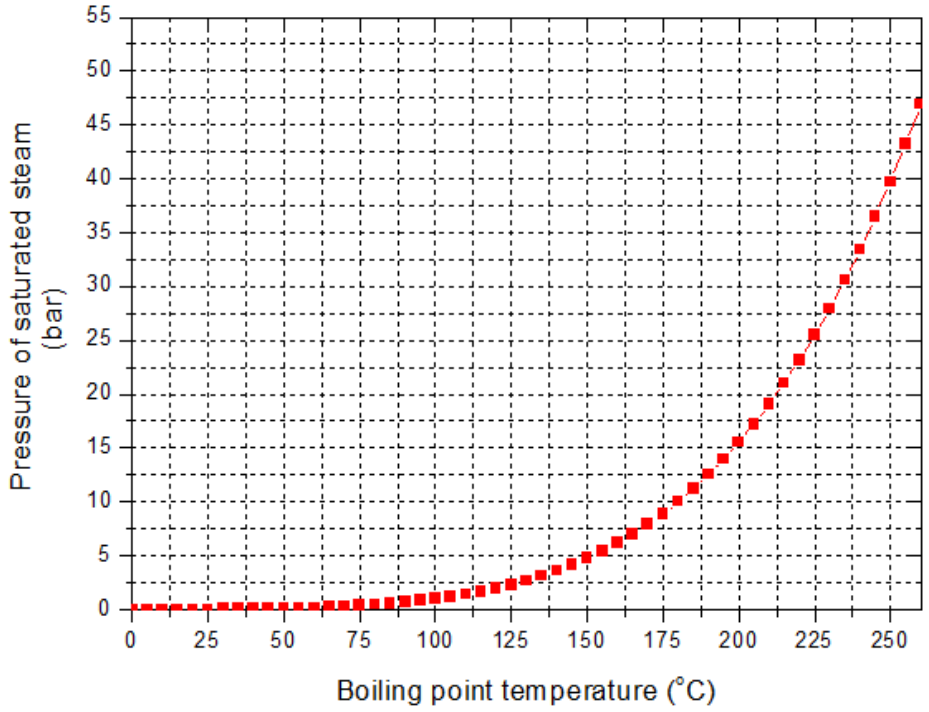

Figure 5.1: Pressure versus boiling point temperature of saturated steam. Adapted from Steam tables [98].

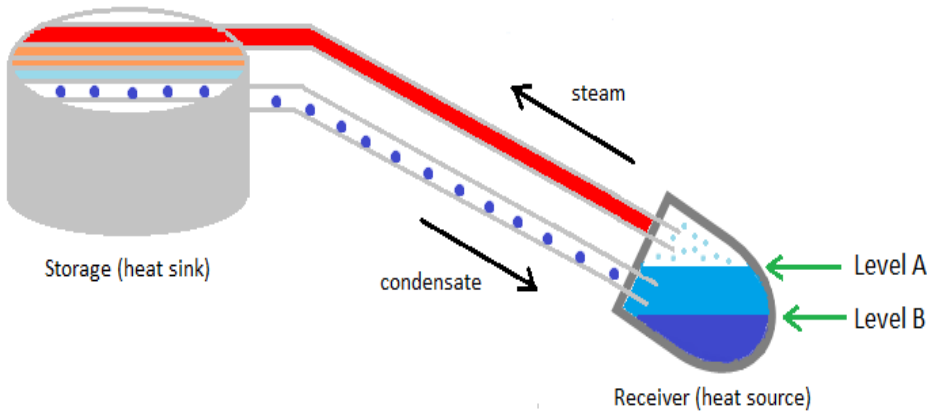

Figure 5.2: Flow of steam within the system as it is produced in the receiver. Mode A (level A): steam produced flows through the upper pipe only to the storage where it condenses. Mode B (level B): steam produced flows through both pipes to the storage where it condensates. During both modes of operation the condensate flows back to the receiver, via the lower pipe due to gravity, where it is re-heated.

the following equation

$$m_s = 3600\frac{q}{h_g}, \tag{5.5}$$

where q is the heat rate in J/s and m_s is in kg/h.

Since there was no flow meter incorporated into the system, the water level in the receiver can be estimated using Figure 5.3. This curve is a relationship between the quantity of water in the receiver and the time it takes for the water to reach 100 °C and boil that quantity of water. The maximum quantity of water that the receiver could contain was 625 ml. If the time taken for the water to reach 100 °C and the boiling time is known, then the amount of remaining fluid in the receiver can be estimated.

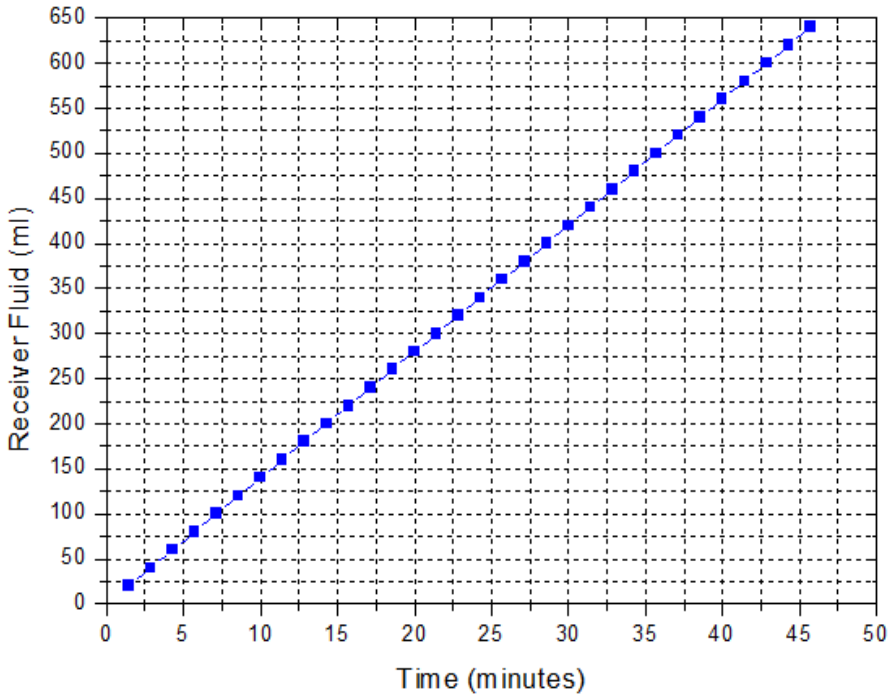

Figure 5.3: Relationship between varying quantities of water in the receiver and the time it takes for each of these quantities to reach 100 °C and boil that quantity of water. The maximum amount of water that the receiver can contain is 625 ml.

The system was designed to produce superheated water in the receiver at a boiling temperature of 250 °C and at a pressure of 40 bar. This was required since the temperature to melt the $NaNO_3$-KNO_3 PCM is 223 °C. Steam produced from the superheated water at a temperature of 250 °C has a pressure of 40 bar as shown in the Pressure-Temperature (P-T) curve in Figure 5.1. It will be shown in Chapter 7 (sections 7.2 and 7.3) that the expected pressure of 40 bar at 250 °C could not be attained due to leaks in the pipe connections.

For the salt storage system, the amount of sensible energy, Q_s, needed to heat the storage from 80-250 °C was calculated according to the general equation (equation (4.1)) which incorporates the heat capacities of the relevant materials

$$\begin{aligned} Q_s &= (m_{salt}C_{p1} + m_{st}C_{p2} + m_{Cu}C_{p3} + m_{Al}C_{p4})\Delta T \\ &= [(14.5\text{ kg})(1500\text{ J/kgK}) + (16\text{ kg})(486\text{ J/kgK}) \\ &+ (21\text{ kg})(385\text{ J/kgK}) + (4\text{ kg})(900\text{ J/kgK})](170\text{ K}) = 1.9\text{ kWh}, \end{aligned} \tag{5.6}$$

where the values for C_{p1}, C_{p2}, C_{p3} and C_{p4} are listed in Table B.2 (Appendix B) and the mass for the different materials can be found in Chapter 4. The total sensible energy was calculated to be 1.9 kWh. The latent energy, Q_l, was calculated by multiplying the latent heat capacity, C_{lp}, of the salt by the mass as follows

$$Q_l = m_{salt}\,C_{lp} \ = (14.5\text{ kg})(120\text{ kJ/kg}) \ = 0.5\text{ kWh}. \tag{5.7}$$

The latent heat energy was calculated to be 0.5 kWh, giving the salt storage a total heat capacity of 2.4 kWh.

As mentioned in Chapter 4 the salt storage container was insulated with 75 mm thick Superwool insulation. This required 3 layers of the 25 mm thick Superwool material. Since the storage tank is cylindrical in shape the heat loss rate was calculated using equation (3.36) and the thermal resistances due to conduction and convection were calculated by equations (3.37) and (3.45), respectively. The conduction through the composite layers of insulation involves adding the individual thermal resistance for each layer of insulation, to find the total thermal resistance for the container wall and insulation layers. For the 3 layers of insulation and a storage container wall thickness of 5 mm, the total thermal resistance due to conduction and convection was calculated to be 4.4 K/W. The thermal conductivity for the relevant insulation density was estimated using Figure 4.7. The convection coefficient, h_a, was assumed to be the highest for natural convection at 25 W/m^{2}K.

5.1.2 Importance of de-airing

A de-airing process is an essential part of the experimental setup. To de-air the system means to remove the air so that only steam is present. Air is considered an insulator. Due to the high resistance of air, it cannot maintain the temperature or the latent heat of steam. This causes a reduction in temperature thus, making its presence within the system undesirable. A layer of air that is 1 mm thick can offer the same resistance to heat flow as a layer of water

25 mm thick [100]. Therefore, in order to obtain an efficient transfer of heat from the receiver to the storage the system has to be de-aired. The de-airing method is discussed in Chapter 6.

5.1.3 Energy loss through leaks

Steam leaks are a significant loss of energy. Steam has a higher heat carrying capacity than water therefore, the energy loss from a steam leak would be greater than a condensate leak [99]. For the purpose of this thesis, all the leaks in the system are treated as one leak. Assuming 10% of the mass of steam produced is lost, then the amount of energy lost through the leak, P_{leak}, was estimated according to

$$P_{leak} = 0.1 m_s h_{fg}, \tag{5.8}$$

where P_{leak} is in kJ/h and h_{fg}, which is the latent heat energy at a specific pressure, can be found in steam tables [99].

5.2 System operation with alternative heating

For the alternative heating of the receiver a blowtorch was used as the heat source. The reason for using an alternative heat source was so that it could be established whether all the energy reflected from the concentrator was actually reaching the receiver. Also, if only the solar source was used the de-airing process could not be achieved even after an entire day, due to the present leaks in the system. The blowtorch provided a high energy source at the receiver so that the water could boil and the air could be expelled from the system within a short period of time. If there were no leaks in the system the solar source could have been used for the de-airing process.

The power from the blowtorch was estimated by heating a flat plate coated with high temperature resistant black paint for a short time period. The reason for heating for a short period was so that the heat loss from the plate would be minimum. The sensible heating of the flat plate was calculated according to equation (4.1). The amount of sensible energy required to raise the temperature of the plate from 42-123 °C in 60 seconds was 39 kJ. Therefore, the amount of power provided by the blowtorch was 654 W.

5.2.1 Alternative storage system

The amount of energy required to heat the alternative storage system with water as the storage medium was calculated using equation (4.1) together with the relevant heat capacity values

from Table B.2 (Appendix B). The amount of sensible energy required to raise the temperature of the water from 25 to 100 °C was 1315 kJ. Replacing the water with oil, the energy required to heat the oil to the same temperature was 534 kJ. The water requires approximately 2.5 times more energy than the oil to be heated to 100 °C. In addition, using equation (5.4) and an input power of 654 W, the heating time for the water and oil storage was calculated to be approximately 34 and 14 minutes, respectively. The heating time of the water was more than twice that of the oil. This is due to the heat capacity of the water being approximately 2.5 times greater than the heat capacity of the oil. Heat loss from the storage system was calculated using equations (3.37) and (3.45). The total thermal resistance for the pot having 1.5 mm wall thickness and one layer of 25 mm thick Superwool insulation was calculated to be 5.1 K/W. The convection coefficient, h_a, was assumed to be 25 W/m^{2}K.

Chapter 6

Experimental method

This chapter outlines the experimental procedure, using the experimental setup described in Chapter 5, to investigate the performance of the solar thermal cooker system that was constructed for the work of this thesis. The test site for the experiments was on a roof platform at the School of Chemistry and Physics, at the Westville campus, University of KwaZulu-Natal. The roof platform is 205 m above sea level on latitude S29 °49'2" and longitude E30 °56'40". This site was chosen since it had an unobstructed view of the horizon and no shading from the nearby buildings. The direct normal radiation (DNI) and wind speed being received at the site were monitored together with the temperature of the water within the receiver and temperature of the storage media.

6.1 Test schedule

Several tests were conducted for the investigation of the receiver. Five tests were conducted using the solar source and three tests were conducted using a blowtorch. The tests conducted with the solar source on the receiver were done in two parts: open system and closed system. The first two days were conducted with the system open. This was where the outlet pipe carrying the steam was disconnected from the storage container. The reason for doing this was so that the system could be de-aired as the steam was produced. De-airing the system is needed in order to ensure good heat transfer between the steam and the storage material. The remaining six days of the tests were conducted with the system closed. This was when the outlet steam pipe was connected to the storage tank so that the steam produced can circulate through the pipe clamped beneath the top-plate.

The last three tests were conducted using a blowtorch. The blowtorch was clamped ap-

proximately 5 cm in front of the receiver and a soot-free blue flame was used to heat the receiver. This was a controlled test since the heat flow from the blowtorch was kept constant as well as the position of the blowtorch relative to the receiver. A summary of the test schedule is given in Table 6.1. It includes the type of test conducted, the heat source and storage medium used, approximate duration of the test and whether the system was open or closed.

Table 6.1: Summary of the experimental test schedule.

Date of test	Type of test	Heat source	Storage Type	Duration
14 February 2013	Open system	Solar	PCM salt	5 hours
6 March 2013	Open system	Solar	PCM salt	2 hours
13 March 2013	Closed system	Solar	PCM salt	4 hours
18 March 2013	Closed system	Solar	PCM salt	4 hours
22 March 2013	Closed system	Solar	PCM salt	3.5 hours
4 April 2013	Closed system	Blowtorch	PCM salt	11 minutes
25 April 2013	Closed system	Blowtorch	Water [1]	2 hours 26 minutes
25 April 2013	Closed system	Blowtorch	Oil	1 hour 48 minutes

For all of the solar heating tests conducted, manual tracking of the concentrator was used. This was due to the following reasons:

- The sensor that was used to determine the sun's position was connected to the motor of the chaindrive. The motor was activated when the sun was out of position which was every 5 - 10 minutes. However, since the chaindrive consisted of a bicycle chain and sprockets, the teeth were relatively far apart. This caused the motor to move further than the exact focal position and hence, resulted in the concentrator being out of focus. Manual tracking was used to correct this and keep the dish focused on the receiver at all times.

- The swing gate motor used with the chaindrive ceased at some time during the tracking. This was due to the load of the dish and supporting arms being too heavy. This in turn caused the sensor to jog the motor back and forth trying to find the exact position of

[1] Water and oil were used as storage mediums with the alternative storage system described in Chapter 4.

the sun. This resulted in the focal image being shifted off the receiver hence, lowering the receiver temperature.

6.2 De-airing the system

De-airing the system was important for ensuring good heat transfer. This was done by first overflowing the system with de-aired water so that the air trapped in the pipes could be expelled. The valve situated next to the pressure gauge was left open and the pipes were connected to close the system. The water was then heated until it started to boil and steam was produced. At first there was steam together with a spray of water droplets. Once the water droplets stopped and only clean, dry steam was seen escaping from the valve, the valve was closed and the steam was allowed to circulate through the system. For the alternative storage system with oil as the storage medium the above method was carried out. The oil was filled into the storage container before the de-airing process began. With water as the storage medium the method was slightly altered as follows:

- The system was filled with water until it reached an overflow condition. During this time the storage container was empty.
- The valve was left open and water in the receiver was heated until boiling started and steam was being produced.
- Once clean steam was observed leaving the valve, the valve was shut off so that the system was closed.
- The storage container was filled with water.

It will be shown that the system could not be completely de-aired due to leaks in the pipe connections.

6.3 Data Acquisition system

The data logging and acquisition for the temperatures were done using a Hewlett Packard (HP) 34970A Datalogger (20 channel multiplexer), with *Benchlink* software. Figure 6.1 shows the positions of the thermocouples within the system, denoted by 'X,' and how the thermocouples were connected to the multiplexer, data logger and computer. One thermocouple was placed

at the receiver and five along the height of the storage container. Figure 6.2 shows the thermocouples for the storage. Probes together with thermowells were the type of thermocouples used. Temperatures from the receiver and storage were logged in 1 minute intervals by the HP data logger. All of the thermocouples used within the system were K-type (Chromel-Alumel). The outside surface temperature of the receiver was measured using a thermal imaging camera (FLIR model T335 with *QuickReport* software, 2% accuracy) and the temperatures were recorded in 15 minute intervals. The viewing angle of the thermal images had to be taken at approximately 45 ° to the target to avoid obstructing the incoming radiation on the concentrator.

To monitor the pressure within the system a glycerine-filled pressure gauge (0-10 MPa) was used. This was positioned along the water pipe of the system, close to the storage tank. In addition, a venting valve, mounted next to the pressure gauge, was incorporated within the system for venting steam if the pressure were to reach the maximum level. The positions of the pressure gauge and valve within the system are indicated in Figure 6.2 .

The direct, diffuse and global radiation were monitored by a Kipp and Zonen pyrheliometer and pyranometers, respectively. The daily, hourly and minute data were logged by a CR1000 data logger (with *LoggerNet* software). A weather station (Vantage Pro2 with *Weatherlink* software, 5% accuracy) was used to monitor the wind speed at the test site. Wind speeds were logged every 15 minutes.

The complete solar cooker system that was constructed is shown in Figure 6.3. The system is situated facing North on the roof platform of the Physics building. Detailed dimensions of system components are given in Appendix C.

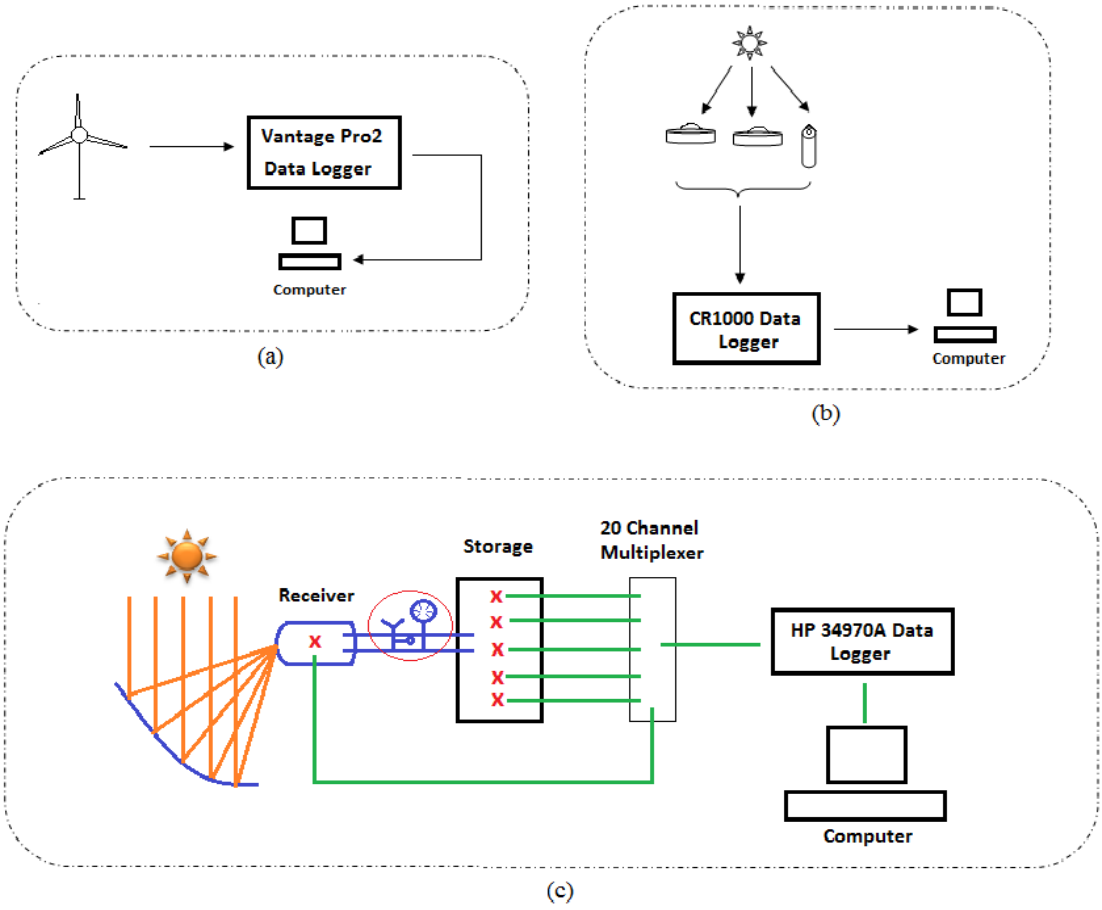

Figure 6.1: Instrument setup at the test site. (a) Wind station using the Vantage Pro2 data logger. (b) Radiometric instruments (pyrheliometer and shaded and unshaded pyranometers) connected to CR1000 data logger. (c) Solar thermal cooker connected to the HP 34970A data logger through a 20 channel multiplexer. Positions of thermocouples within the system denoted by 'X,' one thermocouple at the receiver and five along the height of the storage cylinder. Pressure gauge and venting valve circled in red.

(a)

(b)

Figure 6.2: (a) Storage tank containing $NaNO_3$-KNO_3 phase change material covered by Superwool insulation. Five thermocouples place along the height of the container. (b) Pressure gauge and venting valve.

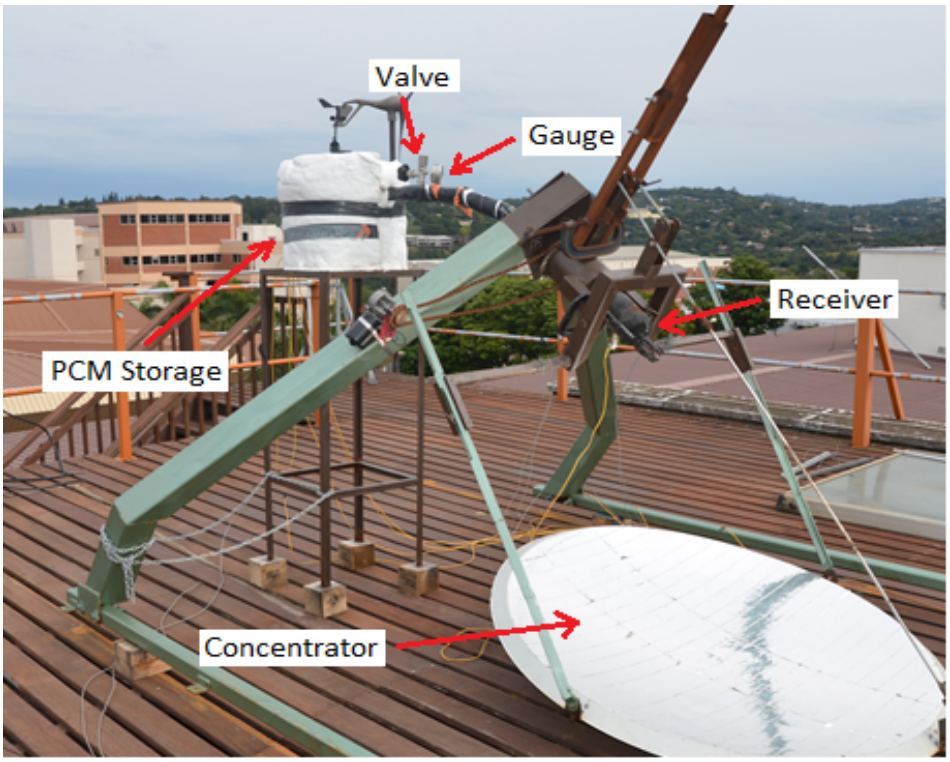

Figure 6.3: Solar thermal cooker system situated on the roof platform of Physics building at the Westville Campus, UKZN. The support structure is positioned facing North and the storage system is situated at the back.

Chapter 7

Experimental results and discussion

The results of the experimental tests and a discussion of these results are presented in this chapter. There were five tests conducted for the solar heating of the receiver. The first two were with the system left open and the remaining tests were with the system closed. There were also two tests conducted on the system with an alternative heat source and an alternative storage system. The heating of the receiver and storage are shown, and details of the temperatures reached within the receiver and the storage are listed. Thermal images of the surface during heating and a comparison between receiver surface temperature and wind speed, are also included.

7.1 Solar heating

Test for 14 February 2013 - Open system with solar source and PCM storage: The variation of the temperature of the water heated within the receiver is shown in Figure 7.1. The receiver was filled with 625 ml of water and approximately 300 ml more was used to overflow the system. The water was heated for 5 hours by the sun where the average DNI for the test period was 896±1 W/m^2. The initial heating period was between 9:15 and 12:00, after which the receiver temperature began to flatten out. The water reached a maximum temperature of $98 \pm 1\,^{\circ}$C, after approximately 4 hours of heating, at 12:54. The system during the test period was left open i.e disconnected from the storage tank and water vapour was allowed to escape to the atmosphere. The reason for this was so that the air within the system could be boiled out. Since the water did not attain 100 °C, steam was not produced to expel the air from the system. The fluctuation in water temperature was due to the re-positioning of the collector during manual tracking.

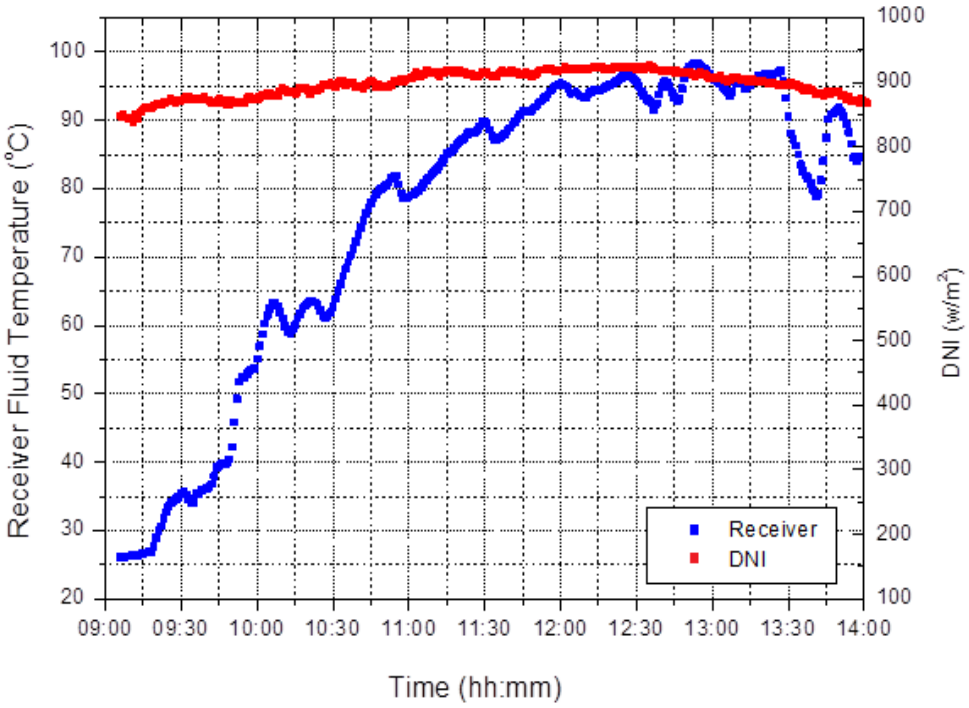

Figure 7.1: Test conducted on 14 February 2013. Variation of the water temperature within the receiver for the system open with solar source and PCM storage. Water vapour produced escaped to the atmosphere and the water in the receiver attained a maximum temperature of 98 °C after 5 hours of heating. The average DNI during the test period was 896 W/m^2.

Test for 6 March 2013 - Open system with solar source and PCM storage: A second test was carried out on the receiver with the system open and with the remaining amount of water from the previous test. The purpose of this test was to verify the previous test, where steam could not be produced and the air could not be boiled out of the system. The variation of the water temperature is shown in Figure 7.2. The maximum temperature of the water was 87 ± 2 °C at 12:17, which was approximately 90 minutes after the initial heating began. The approximate heating period was between 11:05 and 12:07 thereafter, the receiver temperature began to flatten out, similar to the previous test. The average DNI for the test period was 892±1 W/m^2. Similarly to the test conducted on 14 February 2013, the temperature of the water did not reach 100 °C and only water vapour was observed.

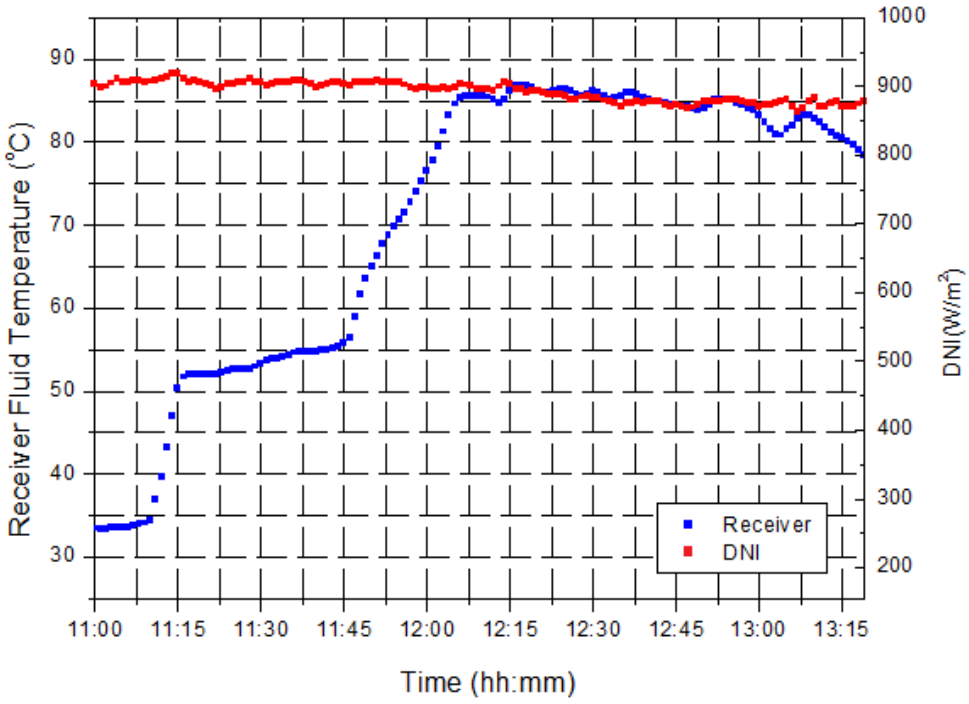

Figure 7.2: Test conducted on 6 March 2013. Variation of the water temperature within the receiver for the system open with solar source and PCM storage. The maximum temperature the water attained was 87 °C. Only water vapour was observed. Average DNI for the test period was 892 W/m^2.

Test for 13 March 2013 - Closed system with solar source and PCM storage: During this test the system was closed (steam pipe connected to the storage) and the receiver was heated. Any water vapour or steam produced was allowed to circulate through the storage. The variation of the water temperature is shown in Figure 7.3. The water reached 100 °C approximately 1 hour and 15 minutes after the initial heating began. It attained a maximum temperature of 108 ± 1 °C at 11:25. This indicated that there was steam produced within the system. However, the steam production was not maintained for the entire test period and the temperature of the water decreased to maintain an average of 87 ± 0.4 °C, for the remainder of the test period. The heating up phase of the receiver was between 10:00 and 11:45. Thereafter, there was a decrease followed by a flattening out in the receiver temperature which was an indication of the heat being transferred to the storage. The incoming energy was first used to heat the receiver and once the receiver was heated the excess energy was transferred to the storage.

The fluctuation in water temperature was again due to the manual tracking of the collector. There was also fluctuation in the DNI due to the presence of clouds which may have also

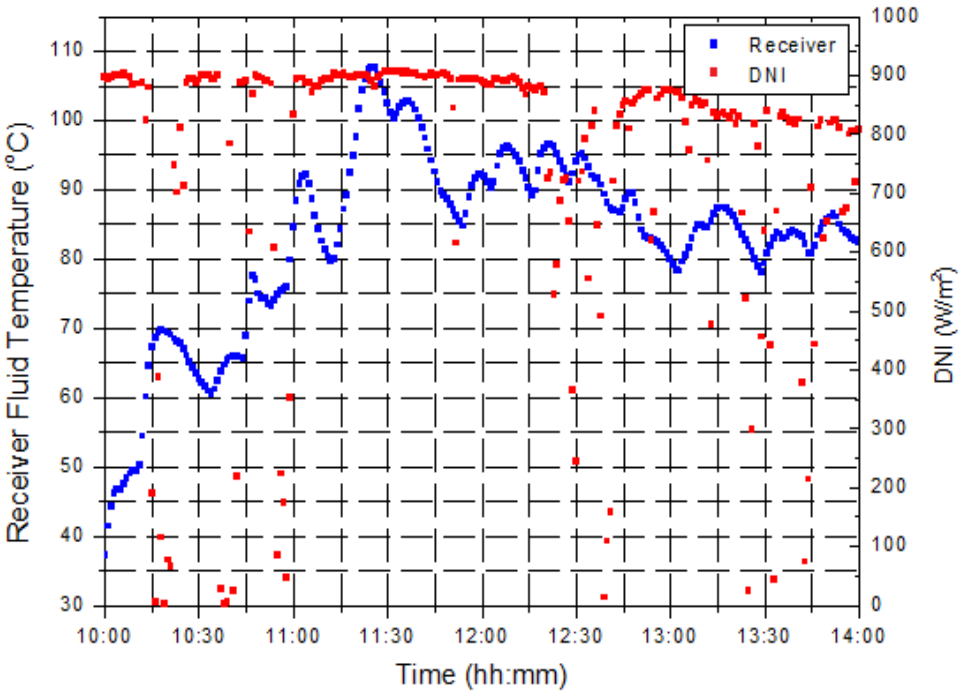

Figure 7.3: Test conducted on 13 March 2013. Variation of the water temperature within the receiver for the system closed with solar source and PCM storage. A maximum temperature of 108 °C was attained at 11:25. Average DNI was 975 W/m^2 during the test period.

contributed to the decrease in the receiver temperature. The average DNI for the test period was 975±1 W/m^2. However, despite the presence of clouds and the use of manual tracking, the receiver was still able to produce steam in less than 2 hours of heating.

The variation of the receiver's spherical surface temperature with wind speed is shown in Figure 7.4. The receiver surface temperature and wind speed were recorded at 15 minute intervals. At each interval, it can be seen that generally, when the wind speed increases the receiver surface temperature decreases and vice versa. This was due to heat being lost from the receiver surface due to convection. High wind speeds cool the spherical surface of the receiver by carrying away heat, hence lowering the temperature. The average surface temperature of the spherical cap reached a maximum of 115 ± 2 °C at 11:15. The heat loss due to convection at this temperature was found to be 36±1 W, while the radiative loss was 13±0.4 W. This indicated that convection was the dominant heat loss component. Convective and radiative heat loss occur in parallel from the receiver's spherical surface and the total heat loss from the spherical cap was 49±2 W, at the maximum average temperature of 115 °C and a wind speed of 5.4 m/s. The variation of the heat loss with wind speed, for the entire test period, is

shown in Figure 7.4.

The cylindrical portion of the receiver was not exposed to concentrated radiation and was insulated with a 25 mm thick layer of insulation. According to equations 3.37 and 3.45 (and neglecting radiative heat loss) the rate of heat transfer from from the inner cylinder wall to ambient at maximum water temperature of 108 °C, was calculated to be 7±0.04 W. This brought the total heat loss for the entire receiver (spherical and cylindrical parts) to 56±2 W. The thermal conductivity for the Superwool insulation was estimated to be 0.05 W/m^2K from Figure 4.7.

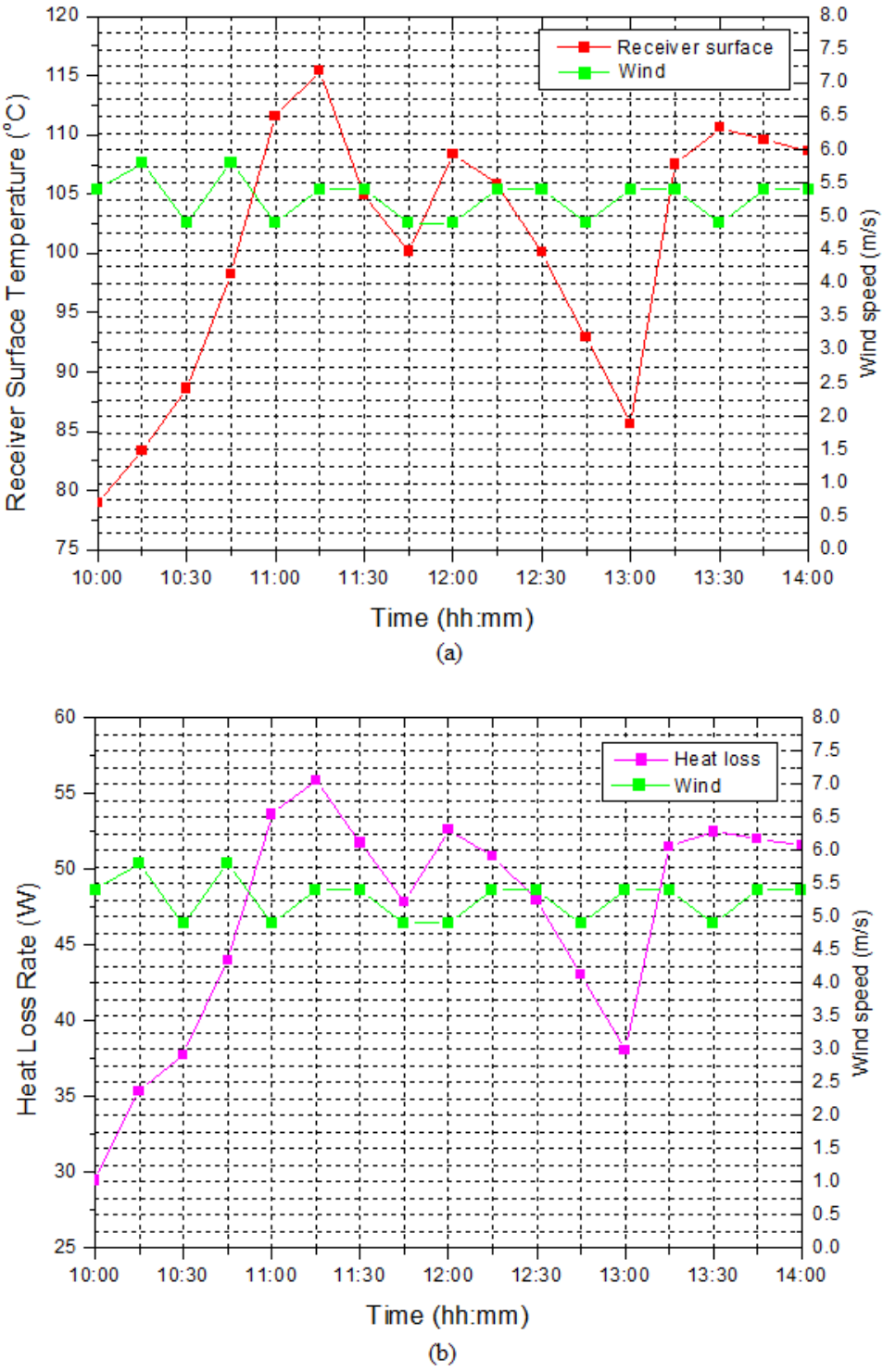

Figure 7.4: Test conducted on 13 March 2013. (a) Variation of receiver surface temperature with wind speed. An overall maximum surface temperature of 115 °C was reached at approximately 11:15. (b) Variation of the total heat loss rate for the receiver which reached a maximum value of 56 W and when the average receiver surface temperature reached a maximum of 115 °C. Wind speed and ambient temperature were 5.4 m/s and 25 °C, respectively.

Test for 18 March 2013 - Closed system with solar source and PCM storage: For this test, the temperature of the water in the receiver reached 100 °C approximately 30 minutes after the initial heating began and steam was produced, as shown in Figure 7.5. It reached a maximum temperature of 136 ± 1 °C at 10:53 and maintained temperatures above 100 °C between 11:30 and 13:50. During this time there was a constant production of steam from the receiver. However, the pressure within the system still remained close to 0 MPa which indicated that the water was still boiling at atmospheric pressure. The significant decrease followed by the flattening out in the receiver temperature after 11:00 was again an indication of heat transferred to the storage. The average DNI for the test period was 912±1 W/m^2. The illuminated receiver is shown in Figure 7.6. The fluctuation in water temperature throughout the test period was due to the misalignment of the concentrator during manual tracking.

Thermal images of the heated receiver surface at the start, middle and end of the test period are shown in Figure 7.7. These were taken at 15 minute intervals using the FLIR thermal camera. The receiver surface temperature was maintained at an average of 117 ± 4 °C during the test period and reached a maximum temperature of 131 ± 3 °C at 12:30. The average temperature of the receiver surface at the start, middle and end of the test period was 55 ± 1 °C, 125 ± 3 °C and 101 ± 2 °C degrees, respectively. From the thermal images it can be seen that the receiver was not always uniformly illuminated and instead a hot-spot exists. The temperature of the hot-spot was significantly higher than the rest of the cap. The temperature of the hot-spot was, 243 ± 5 °C which was approximately 125 °C higher than the average temperature of other parts of the spherical cap. The heat loss from the hot-spot was approximately 36% higher than other parts of the spherical cap.

The temperature of the receiver surface during the test period is shown in Figure 7.8. There was a significant correlation between surface temperature and wind speed. Surface temperature decreases with increasing wind speed and vice versa. The variation of total heat loss from the receiver's spherical surface with wind speed is also shown in Figure 7.8. The heat loss for the highest receiver surface temperature of 131 °C was 26±1 W. For the insulated cylindrical part of the receiver, the heat loss at this temperature was 9±0.1 W. Therefore, the total heat loss from the entire receiver was 34±1 W. This indicated that convection was the dominant heat loss mechanism. The average wind speed for the test period was 2.4 m/s and the pressure within the system remained close to 0 MPa (0 ± 0.02 bar).

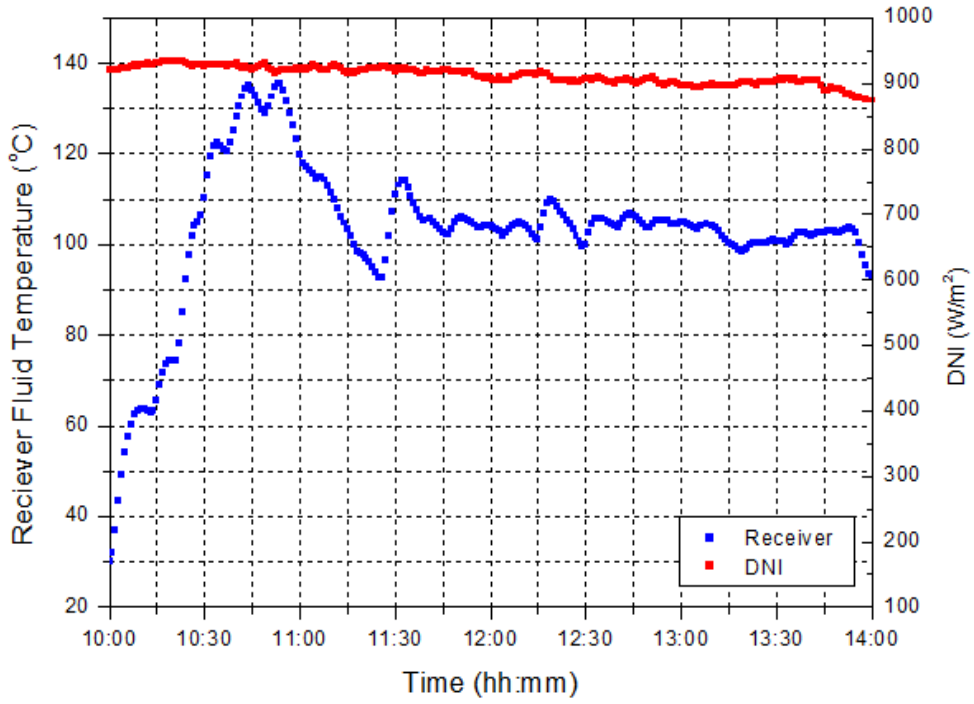

Figure 7.5: Test conducted on 18 March 2013. Variation of the water temperature within the receiver for the system closed with solar source and PCM storage. The water reached 100 °C, steam production began during the initial 30 minutes of the test period and reached a maximum of 136 °C. The production of steam was maintained for more than an hour during the test period.

Figure 7.6: Sun illuminated receiver during test conducted on 18 March 2013 taken at 12:28. The cylindrical part of the receiver was insulated with 25 mm thick Superwool insulation and the spherical part of the receiver was exposed to the concentrated radiation. The average receiver surface temperature reached a maximum of 131 °C at 12:30. The DNI was at an average of 912 W/m^2 during the test period.

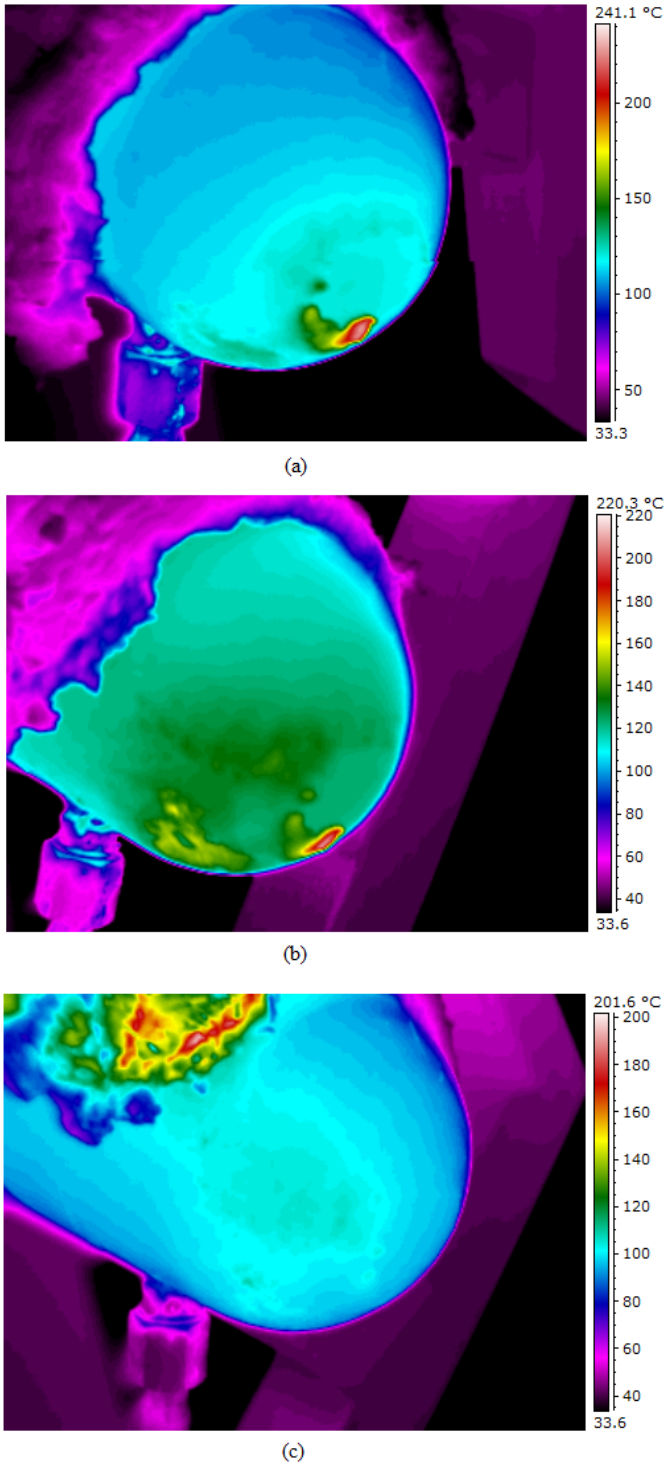

Figure 7.7: Thermal temperature profile of the receiver surface for test conducted on 18 March 2013 with the solar source. Temperature profile (a) at the start of the test period at average temperature of 55 °C, (b) at the middle of the test period at average temperature of 125 °C and (c) at the end of the test period at average temperature of 101 °C. The maximum surface temperature during the test period was 131 °C at 12:30. A distinct hot spot can the seen on the receiver surface.

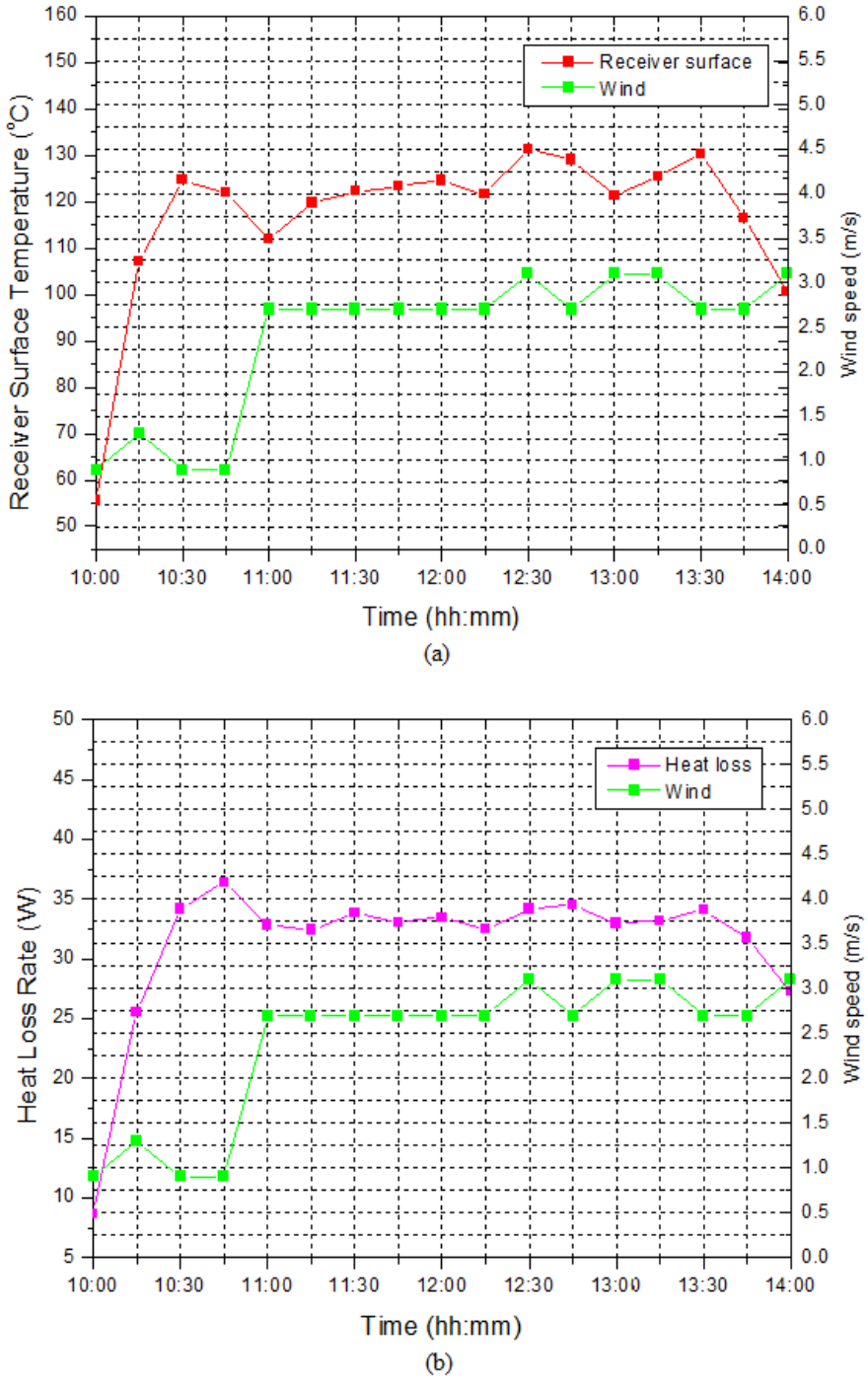

Figure 7.8: Test conducted on 18 March 2013. (a) Variation of the receiver's spherical surface temperature with wind speed. (b) Variation of the heat loss rate with wind speed for the receiver surface.

Test for 22 March 2013 - Closed system with solar source and PCM storage: This was the third test of the heating of the water in the receiver with the system closed. Figure 7.9 shows the heating of the water where steam production began at 11:05, approximately 34 minutes after the initial heating began. The water reached a maximum temperature of $118 \pm 2\,^{\circ}\mathrm{C}$ at 11:30. The period between 12:15 and 14:00 indicated heat transferred to the storage. Average DNI for the test period was 856±3 W/m^2. The heat loss variation, from the receiver's spherical cap, with the wind speed is shown in Figure 7.10. The heat loss from the spherical cap was calculated to be 53.0±1.7 W at the highest average surface temperature of $123 \pm 3\,^{\circ}\mathrm{C}$. The heat loss from the cylindrical portion of the receiver at this temperature was 10±0.1 W, making the total heat loss from the receiver 63±2 W.

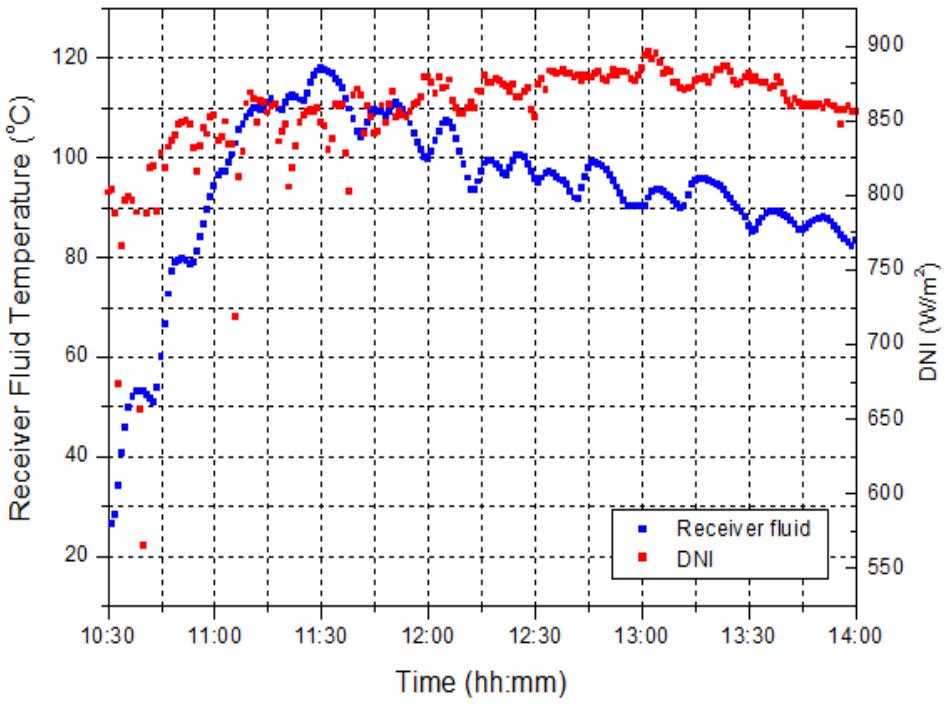

Figure 7.9: Test for 22 March 2013. Variation of the water temperature within the receiver for the system closed with solar source and PCM storage. Steam production began at 11:05 and reached a maximum of $118\,^{\circ}\mathrm{C}$ at 11:30. Average DNI for the test period was 856 W/m^2.

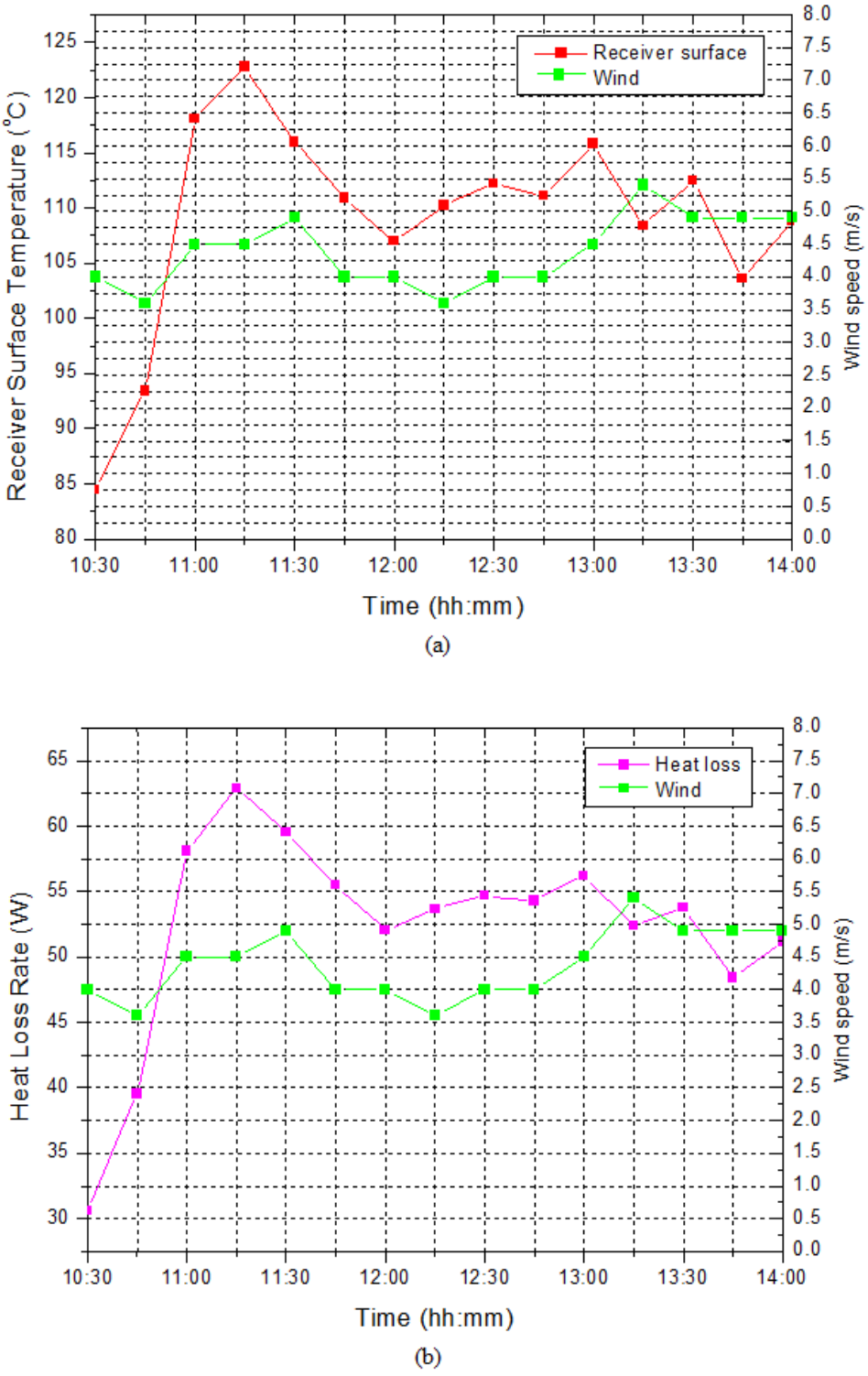

Figure 7.10: Test conducted on 22 March 2013. (a) Variation of the receiver's spherical surface temperature with wind speed. Average surface temperature attained was 123 °C. (b) Variation of the heat loss rate with wind speed for the receiver surface.

7.2 Alternative heating

Test for 4 April 2013 - Alternative heat source (blowtorch) and PCM storage: Figure 7.11 shows the heating of the receiver with the blowtorch. When heating began the water reached a temperature of 105 °C in 6 minutes. It reached a maximum of 133 °C for the duration of the test which was 13 minutes. During this time the pressure in the system had risen to 1 MPa (10 ± 0.2 bar). Due to leaks in the pipe connections and since steam was being rapidly produced the test was stopped due to safety reasons. The thermal temperature profile of the heated receiver is shown in Figure 7.11. The average surface temperature of the receiver was 169 ± 3 °C. The temperature of the hot spot where the blowtorch was concentrated on was 360 ± 7 °C.

Test for 25 April 2013 - Alternative storage system with blowtorch and water storage: The alternative storage was used to demonstrate if there was an effective transfer of heat taking place within the system. This was an easier system to measure and analyze compared to the salt storage. As described in Chapter 4 (section 4.4), this consisted of a copper coil connected to the existing transport pipes and immersed in water or oil. The steam flowing through the copper pipe condenses when it comes into contact with the colder environment which is the pipe wall and the surrounding liquid.

The test was conducted with the blowtorch as the heat source. After the system was de-aired, the water in the receiver was heated until it started to boil. It took 46 minutes for the water in the receiver to reach 100 °C. The heating curve for the water in the receiver and storage is shown in Figure 7.12. It can be seen that when the water temperature began to decrease, at approximately 13:39, the temperature of the water in the storage continued to increase where it reached a maximum temperature of 70 °C. This indicated that there was heat being transferred to the storage medium. It took 1 hour and 48 minutes for the water (4 kg) in the storage container to reach its maximum temperature of 70 °C at 13:58.

There was an average temperature difference of 42 ± 1 °C between the water in the receiver and the water in the storage. The amount of energy used to heat the storage during this time was 754 kJ. The storage could not be heated to 100 °C since this required an additional 561 kJ. Some of the additional energy required was being lost to the environment due to leaks in the pipe connections. The heat loss rate from the storage was 9 W when the maximum storage temperature was reached.

The process was repeated with cooking oil (3.8 kg) as the storage medium. The heating

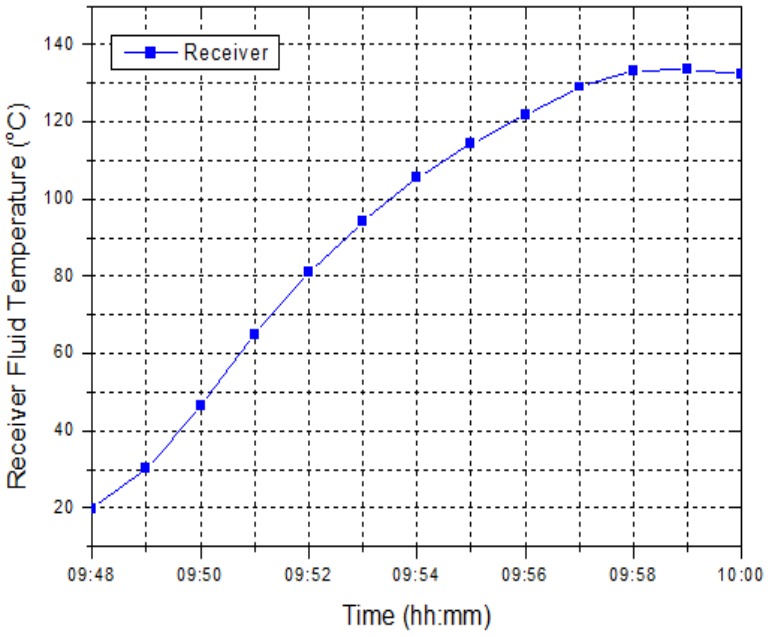

(a)

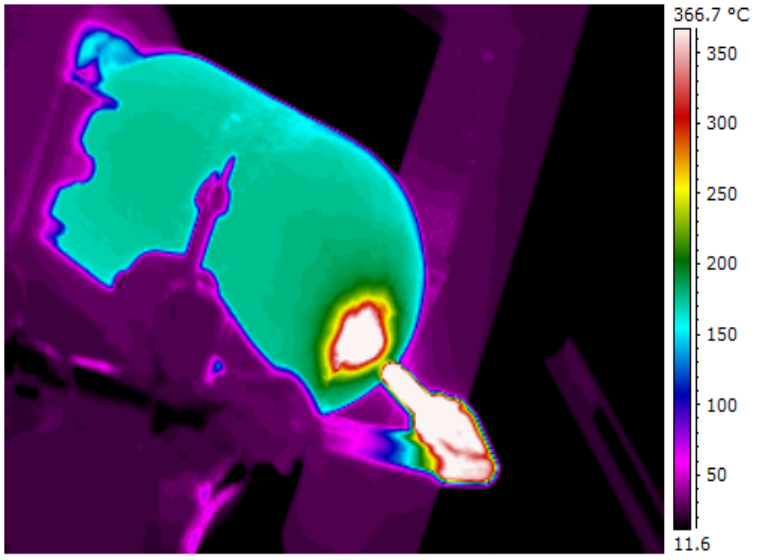

(b)

Figure 7.11: Blowtorch heating of the receiver for 2 April 2013. (a) Variation of the water temperature in the receiver with PCM storage. Steam production began within 6 minutes of the initial heating. (b) Thermal temperature profile for the receiver surface during the test.

curve for the oil is shown in Figure 7.13. The water in the receiver reached 100 °C in 14 minutes. The oil reached a maximum temperature of 96 ± 2 °C after 1 hour and 42 minutes. Although, the initial heating of the oil to 70 °C took 23 minutes, which is 9 minutes more than the theoretical heating time. Steam production was maintained throughout most of the test

period.

The quantity of energy used during the heating period of the oil was 505 kJ. Initially the water in the receiver heated up rapidly and then began to level out. The fluctuations in the receiver temperature were caused by the interruption of the heat from the blowtorch due to wind. The water in the receiver took 14 minutes to start boiling, a significantly shorter time than for the test conducted with the water storage. The average temperature difference between temperature of the water in the receiver and the oil was $40 \pm 2\,^{\circ}\mathrm{C}$. The oil storage reached a temperature that was $26\,^{\circ}\mathrm{C}$ higher than the water storage in a shorter time. This was due to the heat capacity of oil being 2.5 times lower than the heat capacity of water. The heat loss rate from the storage when the oil was at the maximum temperature of $96\,^{\circ}\mathrm{C}$ was 14 W. It can be seen from Figure 7.13, at approximately 11:25, there was a sharp increase in receiver temperature. This was an indication of the water being boiled out of the receiver and as a result only air was being heated. This caused the oil temperature to decrease since there was no longer steam being produced. Therefore, the heating of the oil was limited by the steam leaking from the system. The oil being heated to $200\,^{\circ}\mathrm{C}$ was achievable if the system were leak free.

The experimental heating time for the water and oil storage was significantly longer than the theoretical heating time, as calculated in Chapter 5. This was due to energy being lost through leaks in the system and as a result the heating time was increased. The estimated energy loss from the system through the leaks, P_{leak}, during the the heating of the oil and water storage was 235 kJ/h. This appears to be reasonable since in approximately 2 hours the energy available to the water storage medium could have been raised from 754 kJ to 1224 kJ and correspondingly, the oil storage medium from 505 kJ to 975 kJ. This would result in the water storage reaching a higher temperature of $98\,^{\circ}\mathrm{C}$ and the oil storage reaching a temperature of $162\,^{\circ}\mathrm{C}$, in the same time period.

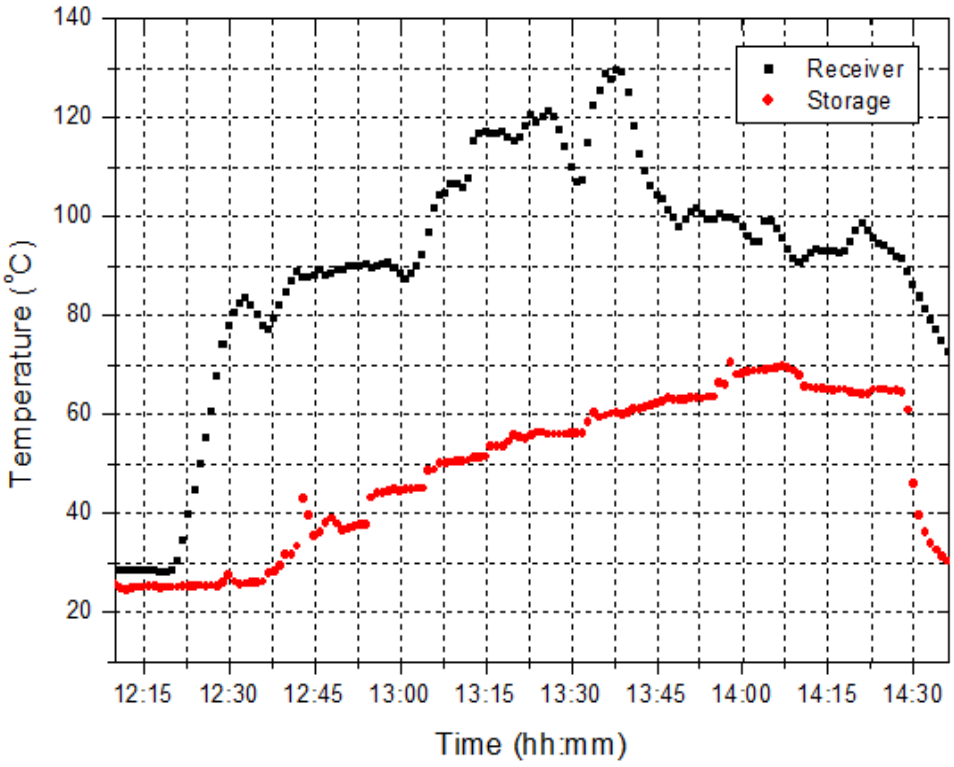

Figure 7.12: Alternative heating for 25 April 2013. Heating of the water in the receiver with the blowtorch and the alternative storage system with water as the storage medium. The water in the receiver reached a maximum of 130 °C at 13:38, while the water in the storage reached a maximum of 70 °C at 13:58.

Summary: A summary of the experimental tests conducted on the receiver is given in Table 7.1. The purpose of the first two tests that were conducted with the system open was to boil out the air from the system. There were no temperatures of the receiver surface recorded since the aim was to attain temperatures above 100 °C so that the water would start to boil. For the remainder of the tests, where the system was closed, the water reached 100 °C and more, the receiver surface temperatures were recorded and corresponding heat loss values were found. The blowtorch was used as an alternative heat source together with an alternative storage system to investigate whether a transfer of heat was occurring within the system. The summary of the maximum temperatures and heat loss values given in Table 7.1 are for the receiver only. Average receiver surface temperature for the first two tests were not recorded since only de-airing of the system was being conducted and hence, the total heat loss values were not included. The total heat loss for the last test was not included since the blowtorch was used as the heat source and the insulation had to be omitted to avoid burning.

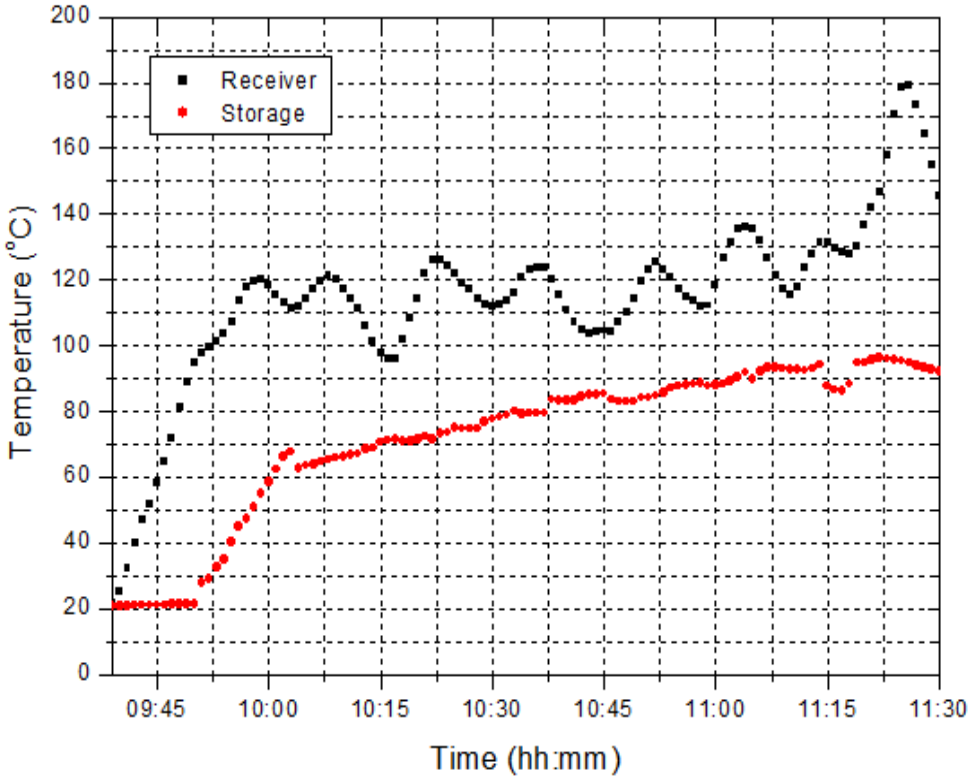

Figure 7.13: Alternative heating for 25 April 2013. Heating of the water in the receiver with the blowtorch and the alternative storage system with oil as the storage medium. The water in the receiver maintained an average above 100 °C throughout most of the test period, while the oil in the storage reached a maximum of 96 °C at 11:22.

7.3 Discussion

7.3.1 Solar heating

The amount of sensible heat required to raise the temperature of water from ambient (25 °C) to 100 °C is 314 kJ/kg. The amount of heat required to vaporize the water is 2257 kJ/kg. Therefore, using equation (5.1) a total enthalpy, h_{fg}, of 2571 kJ/kg (714 Wh) was required to convert water to steam at 100 °C. In addition, the energy required to heat the steel receiver to 100 °C was 91 kJ.

For an average DNI of 800 W/m^2, the power available to the receiver according to equation (3.50) was approximately 677 W. Therefore, since in one hour there was only 677 W being captured by the concentrator, it was insufficient energy to raise the temperature of the water

Table 7.1: Summary of experimental results for the receiver. These were the maximum values attained for the receiver's water temperature and surface temperature. Other values include total heat loss from the receiver as well as the average DNI and ambient temperature at the test site.

Test date	**Maximum water Temp (°C)**	**Average surface Temp (°C)**	**Total heat loss (W)**	**Ave DNI (W/m^2)**	**Ambient (°C)**
14 February 2013	98	-	-	896	31
6 March 2013	87	-	-	892	28
13 March 2013	108	115	55.9	975	25
18 March 2013	136	131	34.2	912	27
22 March 2013	118	123	62.9	856	26
4 April 2013	133	169	-	-	-

above 100 °C. However, in two hours there was 1252 W of energy being captured which was sufficient energy to heat the water above 100 °C and convert it to steam. The mass of steam being produced for a heat rate of 677 W was 1.1 kg/h (0.3 g/s).

When the system was left open and after 4 hours of heating, the water did not attain 100 °C. This may be due to the energy carried in the water vapour being lost to the atmosphere from the open pipe. When water is heated, water vapour is produced. This vapour carries 2257 kJ/kg of energy. Therefore, 2257 kJ/kg of energy was continuously being lost to the environment as it was being produced. Therefore, the water does not reach 100 °C since the amount of energy being put in was insufficient to overcome the amount being lost by the vapour. However, when the system was closed, the temperature of the water reached 100 °C within the first hour of the test period. This was due to the energy from the vapour and steam no longer being lost to the atmosphere but allowed to circulate through the hot-plate clamped to the top of the storage.

In Figures 7.3, 7.5 and 7.9, there was an initial heating up of the water curve followed by a decrease in temperature and then a flattening out. The flattening out in the curve was an indication of the heat being transferred to the storage which was at a lower temperature. The heat from the receiver wall was transferred to the water and steam was produced. When the steam came into contact with a colder storage surface it condensed and transferred its energy to the storage. This continued until the temperature of the storage reached the same

temperature as the receiver such that thermal equilibrium was established.

The pressure within the system, as measured by the gauge, during the solar heating tests remained close to 0 MPa (0 ± 0.02 bar). The system was unable to build significant overpressure (as measured by the gauge) due to the leaks in the pipe connections. Therefore, the temperature of the water in the receiver could not increase higher than the maximum of 136 °C. As a result, the receiver was not able to produce superheated water required to melt PCM salt. The slight overpressure that was present within the system, which was too small to be measured by the gauge, was used to drive the leaks.

The highest water temperature attained on the days using solar heating was found to be 136 ± 1 °C for an average DNI of 912±1 W/m^2. The corresponding average surface temperature and total heat loss of the receiver were 112 ± 2 °C and 34 W, respectively. The pressure measured by the gauge remained close to 0 MPa (0 ± 0.02 bar) although the P-T curve indicates a pressure of 3 bar at this temperature.

Heat loss from the receiver was mainly due to air convection from the spherical cap. The efficiency of the receiver according to equation (3.13) was calculated to be 66%. This was the highest receiver efficiency attained from all the solar heating tests. When the temperature of the water was 28 °C lower, at 108 ± 2 °C the receiver efficiency was 64%. The lowest efficiency of the receiver was 63% which was when the temperature of the water was 118 ± 1 °C.

It can be seen that throughout the tests, the time required to heat the water in the receiver decreased. This was due to the decreasing water level. From Figure 7.5 and 7.9, the time required to boil the water decreased to 30 and 34 minutes, respectively. From Figure 5.3 the estimated water level in the receiver had decreased by 200 ml and was now 425 ml. The difference of 4 minutes in the heating time was due to the lower average DNI available during the second test.

Storage temperatures

Due to the leaks in the system, there was the possibility of water leaking into the storage causing a cooling of the PCM. Due to this the storage was then opened to investigate the condition of the PCM. It was found that the salt mixture had caked significantly and there were air gaps within the material. The caking was due to moisture since the container was not completely air-tight. The air gaps were due to the top-plate and fin combination being placed into the dry mixture. This combined with an error in the measurement system meant that the data collected from the PCM storage had to be discarded. An analysis of the efficiency of

the system as a function of temperature could not be performed due to data from the PCM storage being discarded.

From the tests being conducted on the receiver it was evident that temperatures of the order of 250 °C were not going to be achieved due to leaks in the system and the inability of the system to be pressurized. Therefore, an alternative storage system was constructed.

Reciever hot-spot

For this system, the uneven flux distribution and hence, the hot-spot shown in Figure 7.7 was caused by the inaccuracy in the shape of the concentrator. The inaccuracy could not be corrected since reflective film was used on the concentrator surface and this took the shape of any aberrations on surface. A similar situation was experienced by Van den Heetkamp [18], where strips of acrylic mirror material was used as the reflective surface which produced a non-uniform flux distribution on the receiver. As discussed in Chapter 1, this problem can be overcome by using individual mirror tiles.

The presence of the hot-spot also indicated the effect of the lower thermal conductivity of mild steel as compared to other metals such as copper and aluminium. Therefore, in order to ensure an even distribution of heat on the receiver, metals with high thermal conductivity such as copper, iron and aluminium are preferred. The presence of a hot-spot for this type of receiver did not pose any problems since the wall of the receiver was 4 mm thick and mild steel has a melting temperature in excess of 1000 °C. However, for a fiber-based receiver the hot-spot will burn through the material and cause severe degradation to the receiver.

The advantage of having the receiver with a spherical portion was that the rays intercepting the cap from a point above the receiver was absorbed. This is due to a sphere having a larger capture area than a flat plate. These rays would be lost if a flat plate receiver were to be used since the area of the flat circular receiver is the same as only the base of the spherical cap. This boiler type receiver intended to generate steam can be connected directly to a pressure cooker, similar to what was done by Oommen and Jayaraman [45].

7.3.2 Alternative heating

When heating of the receiver was conducted using a blowtorch, the temperature of the water reached 100 °C in 6 minutes. The average surface temperature of the receiver was 169 ± 7 °C, while the temperature of the hot-spot where the heat from the blowtorch was directed at, was 360 ± 7 °C. The water reached a maximum temperature of 134 ± 4 °C during the 6 minutes.

During this time there was a constant production of steam and the pressure in the system had risen to 1 MPa (10 ± 0.2 bar), despite the present leaks in the threaded pipe connections. However, according to the P-T curve in Figure 5.1, the pressure should be approximately 2.7 bar. This indicated that there was still air within the system therefore, the pressure measured by the pressure gauge was significantly higher. For most of the tests the pressure measured by the pressure gauge was close to 0 MPa (0 ± 0.02 bar). This suggested that there may be a pressure within the system that was not being measured due to the range on the gauge being too large.

Tests were carried out on the alternative storage system with the blowtorch as the heat source. The reason for using the blowtorch was so that the de-airing process could be carried out and to investigate if there was a successful transfer of heat from the receiver to the storage. De-airing was not possible using solar heating as was shown in the first two tests conducted. The mass of steam, m_s, produced when using the the blowtorch was 1.0 kg/h (0.3 g/s).

For the receiver temperatures, the temperature measured by the thermocouple in the receiver may also be influenced by the heating of the thermowell from the outside. Even though the thermowell was situated away from the concentrated radiation its temperature may be raised by heat being conducted along the length of the receiver cylinder. If this was the case, then the temperature measured may be an average temperature between the water inside the receiver and the exposed thermowell.

From the experimental tests carried out on the solar thermal cooker system, it can be seen that the expected temperature of 250 °C and pressure of 40 bar could not be achieved. The aim was to produce superheated water in the receiver at at boiling temperature of 250 °C, and the steam would be used to melt $NaNO_3$-KNO_3 PCM. The main reason for this not being achieved was due to the leaks in the pipe connections which prevented the system from being completely de-aired and pressurized. However, despite the leaks there was successful heat transfer to the storage. As it stands, only low temperature, low pressure steam was produced by the receiver which is unable to melt PCM salt.

Chapter 8

Conclusions and recommendations

8.1 Conclusions

Using a 1.2 m satellite dish as a concentrator, a receiver that serves as a boiling chamber was heated. The highest temperature the water inside the receiver obtained during the solar heating tests was 136 °C. The overall receiver surface temperature was a maximum of 131 °C and the maximum operating efficiency of the receiver was 66%. It was found that generally when the wind speed is high the surface temperature of the receiver decreases. This indicated a definite correlation between wind speed and surface temperature, and it was found that the heat loss due to convection was the most significant. The maximum heat loss from the receiver was 63 W. The receiver constructed for the system has proven to be an effective boiling chamber.

The alternative storage system was tested with water and oil as the storage medium. When water was used as the storage medium the temperature reached a maximum of 70 °C. When oil was used as the storage medium, the temperature reached a maximum of 96 °C. It was proven that there has been successful heat transfer to the storage when water and oil were used as the storage medium.

The receiver needed to produce superheated water at a boiling temperature of 250 °C, in order to melt $NaNO_3$-KNO_3 PCM in the storage. Due to leaks in the system, this could not be achieved. Therefore, the expected temperature of 250 °C and pressure of 40 bar was not attained. Instead there was only low temperature, low pressure steam being produced by the receiver, which was unable to melt $NaNO_3$-KNO_3 PCM.

The off-axis parabolic dish (satellite dish) covered with Reflectech mirror film makes a relatively good solar concentrator despite its inaccurate curvature.

8.2 Considerations for future work

- If a satellite dish is to be used as a concentrator, adequate inspection of the dish surface with respect to its curvature should be investigated using ray-tracing techniques, in order to determine how accurately it has been manufactured. Any geometrical defects during fabrication should then be taken into consideration when estimating the smallest flux distribution for designing of the receiver.

- A two-axis automatic tracking of the concentrator should be included so that it is accurately focused on the receiver at all times.

- The receiver should incorporate a wind barrier to prevent convective heat loss due to high wind speeds.

- A pressure saftety valve must be included into the system.

- A flow meter is required to monitor the flow rate of the heat transfer fluid. Also, a digital pressure gauge should be used instead of the present one so that small fluctuations in pressure can be measured.

- In order for the system to operate at high pressure and to avoid leaks, other methods for properly sealing the system are necessary. This may be in the form of specialized welding, instead of threaded pipe connections. In addition, seamless pipes should be used to ensure that there are no pin holes that could cause leaks. All pipes should be pressure tested before being used in the system.

- If phase change material is to be used as a storage medium, it needs to be completely melted and thoroughly mixed to produce a homogeneous mixture. Dry mixing of the material should be avoided.

Bibliography

[1] Kalogirou S.A., "Solar thermal collectors and applications", Progress in Energy and Combustion Science 30 (2004) 231-295.

[2] Brakmann G., Aringhoff R., Geyer M., Teske S., "Concentrated solar thermal power-now!". Accessed 24 January 2012 at http://www.fichtnersolar.com.

[3] Edkins M., Winkler H., Marquard A., "Large-scale rollout of concentrating solar power in South Africa". Accessed 14 April 2011 at http://www.erc.uct.ac.za.

[4] Fluri T.P., "The potential of concentrating solar power in South Africa", Energy Policy 37 (2009) 5075-5080.

[5] Sharma A., Tyagi V.V., Chen C.R., Buddhi D., "Review on thermal energy storage with phase change materials and applications", Renewable and Sustainable Energy Reviews 13 (2009) 318-345.

[6] Muthusivagami R.M., Velraj R., Sethumadhavan R., "Solar cookers with and without thermal storage-A review", Renewable and Sustainable Energy Reviews 14 (2010) 691-701.

[7] http://www.solarcooking.org/saussure.htm.

[8] Wentzel M., Pouris A., "The development impact of solar cookers: A review of solar cooking impact research in South Africa", Energy Policy 35 (2007) 1909-1919.

[9] Panwar N.L., Kaushika S.C., Kothari S., "State of the art of solar cooking: An overview", Renewable and Sustainable Energy Reviews 16 (2012) 3776-3785.

[10] Saxena A., Varun G., Pandey S.P., Srivastav G., "A thermodynamic review on solar box type cookers", Renewable and Sustainable Energy Reviews 15 (2011) 3301-3318.

[11] Pulfer J., "Small marmalade factory in Argentina working with Scheffler type industrial cooker". Accessed 19 June 2012 http://www.solare-bruecke.org.

[12] http://www.solarcooking.wikia.com/wiki/WolfgangScheffler.

[13] Scheffler W., "Introduction to the revolutionary design of Scheffler reflectors", Proceedings of the 6th International Conference on Solar Cooker, Spain, 2006.

[14] Kimambo C.Z.M., "Development and performance testing of solar cookers", Journal of Energy in Southern Africa 18 (2007) 41-51.

[15] Funk P.A., "Evaluating the international standard procedure for testing solar cookers and reporting performance", Solar Energy 68 (1999) 1-7.

[16] Duffie J.A., Beckman W.A., (1991). "Solar Engineering of Thermal Processes", second edition, John Wiley and Sons, NY.

[17] Hischier I., Poživil P., Steinfeld A., "A modular ceramic cavity-receiver for high-temperature high-concentration solar applications", ASME Solar Energy Engineering 134 (2012) 1-6.

[18] Van den Heetkamp R.R.J., "The Development of Small Solar Concentrating Systems with Heat Storage for Rural Food Preparation", Physica Scripta T97 (2001) 99-106.

[19] Koroneos C.J., Piperidis S.A., Tatatzikidis C.A., Rovas D.C., "Life Cycle Assessment of a Solar Thermal Concentrating system", Proceedings of WSEAS, World Scientific and Engineering Academy Society Conference, Spain, 2008.

[20] Price H., Lupfert E., Kearney D., Zarza E., Cohen G., Gee R., Mahoney R., "Advances in Parabolic Trough Solar Power Technology", ASME Solar Energy Engineering 124 (2002) 109-125.

[21] Kennedy C.E., Price H., "Progress in development of high-temperature solar-selective coating", Proceedings of ISEC, International Solar Energy Conference, Florida, 2008.

[22] Reddy K.S., Sendhil Kumar N., "Convection and surface radiation heat losses from modified cavity receiver of solar parabolic dish collector with two-stage concentration", Heat Mass Transfer 45 (2009) 363-373.

[23] Sareshpande V.R., Chandak A.G., Pillai I.R., "Procedure for thermal performance evaluation of steam generating point-focus solar concentrators", Solar Energy 85 (2011) 1390-1398.

[24] Kalbande S.R., Kothari S., Nadre G.R., Mathur A.N., "Design theory and performance analysis of paraboloidal solar cooker", Applied Solar Energy 44 (2008) 103-112.

[25] Habeebullah M.B., Khalifa A.M., Olwi I., "The Oven Receiver: An approach toward the revival of concentrating solar cookers", Solar Energy 54 (1995) 227-237.

[26] Sonune A.V., Philip S.K., "Development of a domestic concentrating cooker", Renewable Energy 28 (2003) 1225-1234.

[27] Mlatho J.S.P., "Experimental performance of solar receivers designed to use oil as a heat transfer fluid". Accessed 13 June 2012 at http://www.isrn.com.

[28] Kribus A., Doron P., Rubin R., Reuven R., Taragan E., Duchan S., Karni J., "Performance of the directly-irradiated annular pressurized receiver (DIAPR) operating at 20 bar and $1,200\,^{\circ}\mathrm{C}$", ASME Solar Energy Engineering 123 (2001) 10-17.

[29] Kribus A., Doron P., Rubin R., Karni J., Duchan S., Taragan E., "A Multistage solar receiver: The route to high temperature", Solar Energy 67 (1999) 3-11.

[30] Karni J., Kribus A., Rubin R., Doron P., "The 'Porcupine': A novel high-flux absorber for volumetric solar receivers", ASME Solar Energy Engineering 120 (1988) 85-95.

[31] Taumoefolau T., Paitoonsurikarn S., Hughes G., Lovegrove K., "Experimental investigation of natural convection heat loss from a model solar concentrator cavity receiver", ASME Solar Energy Engineering 126 (2004) 801-807.

[32] Fend T., Pitz-Paal R., Reutter O., Bauer J., Hoffschmidt B., "Two novel high-porosity materials as volumetric receivers for concentrated solar radiation", Solar Energy Materials and Solar Cells 84 (2004) 291-304.

[33] Ávila-Marín A.L., "Volumetric receivers in solar thermal power plants with Central Receiver System technology: A review", Solar Energy 85 (2011) 891-910.

[34] Jørgen Løvseth, "Personal Notes", (2011).

[35] Zeghib I., Chenni R., Kerbache T., "Design and construction of a thermal collector of high temperature", Engineering and Applied Sciences 2 (12) (2007) 1827-1833.

[36] Kaushika N.D., Reddy K.S., "Performance of a low cost solar paraboloidal dish steam generating system", Energy Conversion and Management 41 (2000) 713-726.

[37] Sendhil Kumar N., Reddy K.S., "Comparison of receivers for solar dish collector system", Energy Conversion and Management 49 (2008) 812-819.

[38] Prakash M., Kedare S.B., Nayak J.K., "Investigations on heat losses from a solar cavity receiver", Solar Energy 83 (2009) 157-170.

[39] Badran A.A., Ibrahim A.Y., Noureddine K.J., Rami A., Halawa H., "Portable solar cooker and water heater", Energy Conversion and Management 51 (2010) 1605-1609.

[40] Bellel N., "Study of two types of cylindrical absorber of a spherical concentrator", Energy Procedia 6 (2011) 217-227.

[41] Bhirud N., Tandale M.S., "Field evaluation of a fixed-focus concentrators for industrial oven", Proceedings of Advances in Energy Research (AER), Mumbai, 2006.

[42] Jayasimha B.K., "Application of Scheffler reflectors for process industry", Proceedings of the 6th International Conference on Solar Cooker, Spain, 2006.

[43] Scheffler W., "Development of a solar crematorium", Proceedings of the 6th International Conference on Solar Cooker, Spain, 2006.

[44] Tyroller M., "Solar steam sterilizer for rural hospitals". Accessed 19 June 2012 at http://www.katharinehamnett.com.

[45] Oommen R., Jayaraman S., "Development and performance analysis of compound parabolic solar concentrators with reduced gap losses-oversized reflector", Energy Conversion and Management 42 (2001) 1379-1399.

[46] Senthilkumar S., Perumal K., Srinivasan P.S.S., "Construction and performance of a three-dimensional compound parabolic concentrator for a spherical absorber", Scientific and Industrial Research 66 (2007) 558-564.

[47] Popoola O.I., Ayanda J.D., "Design, construction and study of the performance of a conical solar concentrator", Nigerian Journal of Physics 17S (2005) 275-284.

[48] Kothandaraman C.P., (2006). "Fundamentals of heat and mass transfer", third edition, New Age International, DL.

[49] Franco J., Cadena C., Saravia L., "Multiple use communal solar cookers", Solar Energy 77 (2004) 217-223.

[50] Franco J., Saravia L., Javi V., Caso R., Fernandez C., "Pasteurization of goat milk using a low cost solar concentrator", Solar Energy 82 (2008) 1088-1094.

[51] Lysko M.D., "Measurement and Models of Solar Irradiance", PhD Thesis, Norwegian University of Science and Technology, Faculty of Natural Sciences and Technology, Department of Physics, 2006.

[52] Myers D.R., "Solar radiation modeling and measurements for renewable energy applications: data and model quality", Energy 30 (2005) 1517-1531.

[53] http://www.physicalgeography.net

[54] Twidell J., Weir T., (2006). "Renewable energy resources", second edition, Taylor and Francis, NY.

[55] Goswami D.Y., Kreith F., Kreider J.F., (1999). "Principles of solar engineering", second edition, Taylor and Francis, PA.

[56] "Photometry and Radiometry-A tour guide for computer graphics enthusiasts". Accessed 4 April 2011 at http://www.helios32.com/Measuring%20Light.pdf.

[57] http://www.kippzonen.com.

[58] Roth P., Georgiev A., and Boudinov H., "Cheap two axis sun following device", Energy Conversion and Management 46 (2005) 1179-1192.

[59] Tiwari G.N., Mishra R.K., Solanki S.C., "Photovoltaic modules and their applications: A review on thermal modelling", Applied Energy 88 (2011) 2287-2304.

[60] Mora Associates, research report March 2009. "CSP: Concentrated Solar Power". Accessed 28 Febuary 2011 at http://www.moraassociates.com/publications/.

[61] http://www.solarthermalmagazine.com/2012/11/07/construction-begins-on-parabolic-and-tower- concentrated-solar-thermal-power-projects-in-south-africa/.

[62] http://en.citizendium.org/wiki/Steam_generator.

[63] http://www.earthtimes.org.

[64] Romero-Alvarez M., Zarza E., "Concentrating solar thermal power". Accessed 5 November 2012 at http://www.scribd.com/doc/69721869/Concentrating-Solar-Thermal-Power.

[65] Munir A., Hensel O., Scheffler W., "Design principle and calculations of a Scheffler fixed focus concentrator for medium temperature applications", Solar Energy 84 (2010) 1490-1502.

[66] "Parabolic antennas". Accessed 5 August 2011 at http://www.montgomerycollege.edu.

[67] Reflectech Mirror Film datasheet. Accessed 21 November 2011 at http://www.reflectechsolar.com/technical.html.

[68] Pottler K., Lupfert E., Johnston G.H.G., Shortis M.R., 'Photogrammetry: A powerful tool for geometric analysis of solar concentrators and their components', ASME Solar Energy Engineering 127 (2005) 94-101.

[69] Garcia R.F., Formoso R.B., Catoira A.D., Gomez J.R., "Pressurized concentrated solar power receiver designed to operate with closed Brayton cycles", International Conference on Renewable Energies and Power Quality, Spain, 2012.

[70] Solvalitt datasheet. Accessed 2 April 2012 at http://www.jotun.com.

[71] Incropera F.P., DeWitt D.P., (2002). "Fundamentals of heat and mass transfer", fifth edition, John Wiley and Sons, NY.

[72] Cengel Y.A., "Heat transfer: A practical aproach". Accessed 13 Febuary 2012 at www.mhhe.com/cengel/.

[73] Pitts D.R., Sissom L.E., (1988). "Schaums outline of theory and problems of heat transfer", second edition, McGraw Hill, NY.

[74] Bakos G.C., "Design and construction of a two-axis Sun tracking system for parabolic trough collector (PTC) efficiency improvement", Renewable Energy 31 (2006) 2411-2421.

[75] Chong K.K., Wong C.W., "General formula for on-axis sun-tracking system and its application in improving tracking accuracy of solar collector", Solar Energy 83 (2009) 298-305.

[76] Iqbal M., (1983). "An introduction to solar radiation", Academic Press, CA.

[77] Gil A., Medrano M., Martorell I., Lázaro A., Dolado P., Zalba B., Cabeza L.F., "State of the art on high temperature thermal energy storage for power generation. Part 1 - Concepts, materials and modellization", Renewable and Sustainable Energy Reviews 14 (2010) 31-55.

[78] Agyenim F., Hewitt N., Eames P., Smyth M., "A review of materials, heat transfer and phase change problem formulation for latent heat thermal energy storage systems (LHTESS)", Renewable and Sustainable Energy Reviews 14 (2010) 615-628.

[79] Kenisarin M.K., "High-temperature phase change materials for thermal energy storage", Renewable and Sustainable Energy Reviews 14 (2010) 955-970.

[80] Zalba B., Marin J.M., Cabeza L.F., Mehling H., "Review on thermal energy storage with phase change: materials, heat transfer analysis and applications", Applied Thermal Engineering 23 (2003) 251-283.

[81] Mondal S., "Phase change materials for smart textiles - An overview", Applied Thermal Engineering (2007), doi:10.1016/j.applthermaleng.2007.08.009.

[82] Hasnain S.M., "Review on sustainable thermal energy storage technologies, Part I: Heat storage materials and techniques", Energy Conversion Management 39 (1998) 1127-1138.

[83] Foong C.W., Nydal O.J., Løvseth J., "Investigation of a small scale double-reflector solar concentrating system with high temperature heat storage", Applied Thermal Engineering (2011), doi:10.1016/j.applthermaleng.2011.02.026.

[84] Liu M., Saman W., Bruno F., "Review on storage materials and thermal performance enhancement techniques for high temperature phase change thermal storage systems", Renewable and Sustainable Energy Reviews 16 (2012) 2118-2132.

[85] Kenisarin M.K., Mahkamov K., "Solar energy storage using phase change materials", Renewable and Sustainable Energy Reviews 11 (2007) 1913-1965.

[86] Farid M.M., Khudhair A.M., Razack S.A.K., Al-Hallaj S., "A review on phase change energy storage: materials and applications", Energy Conversion and Management 45 (2004) 1597-1615.

[87] Lopez J., Acem Z., Palomo Del Barrio E., "$KNO_3/NaNO_3$ Graphite materials for thermal energy storage at high temperature: Part II - Phase transition properties", Applied Thermal Engineering 30 (2010) 1586-1593.

[88] Al-Homoud M.S., "Performance characteristics and practical applications of common building thermal insulation materials", Building and Environment 40 (2005) 353-366.

[89] Bynum Jr. R.T., (2001). "Insulation Handbook", McGraw-Hill, NY.

[90] Jelle B.P., "Traditional, state-of-the-art and future thermal building insulation materials and solutions - Properties, requirements and possibilities", Energy and Buildings 43 (2011) 2549-2563.

[91] Jelle B.P., Gustavsen A., Baetens R., "The path to high performance thermal building insulation materials and solutions of tomorrow", Building Physics 34 (2010) 99-123.

[92] Fricke J., Heinemann U., Ebert H.P., "Vacuum insulation panels - From research to market", Vacuum 82 (2008) 680-690.

[93] Fricke J., Schwab H., Heinemann U., "Vacuum Insulation Panels - Exciting thermal properties and most challenging applications", Thermophysics 27 (2006) 1123-1139.

[94] Simmler H., Brunner S., "Vacuum insulation panels for building application basic properties, aging mechanisms and service life", Energy and Buildings 37 (2005) 1122-1131.

[95] Alam M., Singh H., Limbachiya M.C., "Vacuum Insulation Panels (VIPs) for building construction industry - A review of the contemporary developments and future directions", Applied Energy 88 (2011) 3592-3602.

[96] Baetens R., Bjørn P.J., Thue J.V., Tenpierik M.J., Grynning S., Uvsløkk S., Gustavsen A., "Vacuum insulation panels for building applications: A review and beyond", Energy and Buildings 42 (2010) 147-172.

[97] Superwool datasheet. Accessed 16 May 2012 at http://www.captiveaire.com /CATALOGCONTENT/DUCTWORK/doc/Superwool%20Plus%20Datasheet.pdf.

[98] Steam tables. Accessed 6 March 2013 at http://www.chem.mtu.edu/~tbco/cm3230/steamtables.pdf.

[99] "Steam and condensate systems, Energy Management Series 8". Accessed 8 May 2013 at http://oee.nrcan.gc.ca/sites/oee.nrcan.gc.ca/files/pdf/commercial/password/downloads/EMS_08_steam_and_condensate.pdf.

[100] Spirax Sarco Inc. "Design of fluid systems". Accessed 10 May 2013 at http://www.spiraxsarco.com/us/pdfs/training/Steam-utilization.pdf.

[101] http://www.engineeringtoolbox.com/.

Appendix A

Radiometry data for Westville station

Radiometery data for a typical clear sky day received by the Westville radiometry station. Figure A.1 shows the direct normal irradiation (DNI), diffuse radiation and global radiation for 14 January 2013.

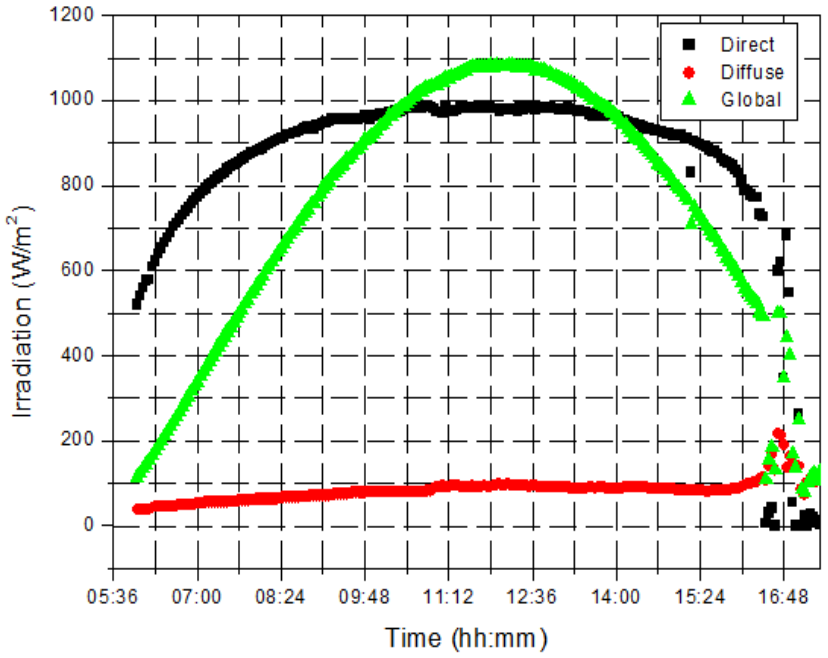

Figure A.1: Direct, diffuse and global radiation received at the Westville station for a typical clear sky day.

Appendix B

Thermophysical properties of water and storage materials

Liquid	T (K)	ρ (kg/m^3)	k (W/m · K)	c_p (J/kg · K)	$\mu \times 10^3$ (Pa · s)	$\beta \times 10^6$ (K^{-1})
Water	273.15	1000	0.569	4217	1.750	−68.05
	280	1000	0.582	4198	1.422	46.04
	290	999.0	0.598	4184	1.080	174.0
	300	997.0	0.613	4179	0.855	276.1
	310	993.0	0.628	4178	0.695	361.9
	320	989.1	0.640	4180	0.577	436.7
	330	984.3	0.650	4184	0.489	504.0
	340	979.4	0.660	4188	0.420	566.0
	350	973.7	0.668	4195	0.365	624.2
	400	937.2	0.688	4256	0.217	896
	500	831.3	0.642	4660	0.118	—
	600	648.9	0.497	7000	0.081	—
	647.3	315.5	0.238	∞	0.045	—

Figure B.1: Thermophysical properties of water. Adapted from Incropera and DeWitt [71].

Table B.1: Enthalpy of water at different phases at a saturation temperature of 100 °C and standard atmospheric pressure. Adapted from Incropera and DeWitt [71].

State	**Enthalpy (kJ/kg)**
Liquid (sensible heat), (h_f)	4.19
Evaporation (latent heat), (h_g)	2257
Saturated steam (total heat), (h_{fg})	2767

Table B.2: Thermosphysical properties of the materials used in the $NaNO_3$-KNO_3 storage and the alternative storage system [71, 83, 101].

Material	**Heat capacity (J/kg·K)**	**Thermal conductivity (W/m·K)**
Aluminium (6082), C_{p4}	900	204
Copper, C_{p3}	385	386
Mild steel (EN8), C_{p2}	486	51.9
$NaNO_3$-KNO_3 (50:50 mol %), C_{p1}	1500	-
Oil (cooking grade)	1670	0.02

Appendix C

System drawings

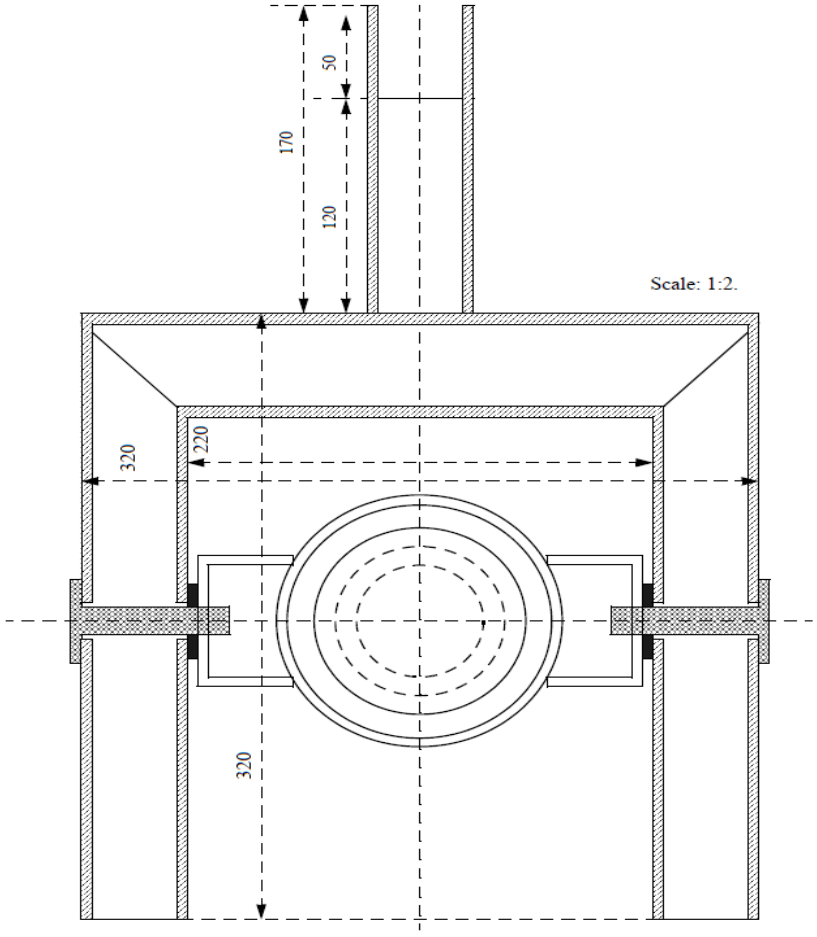

Figure C.1: Front-view of the dish-carrying frame with extended vertical bar for declination adjustment. Receiver positioned at center of the frame. (Courtesy of Jørgen Løvseth).

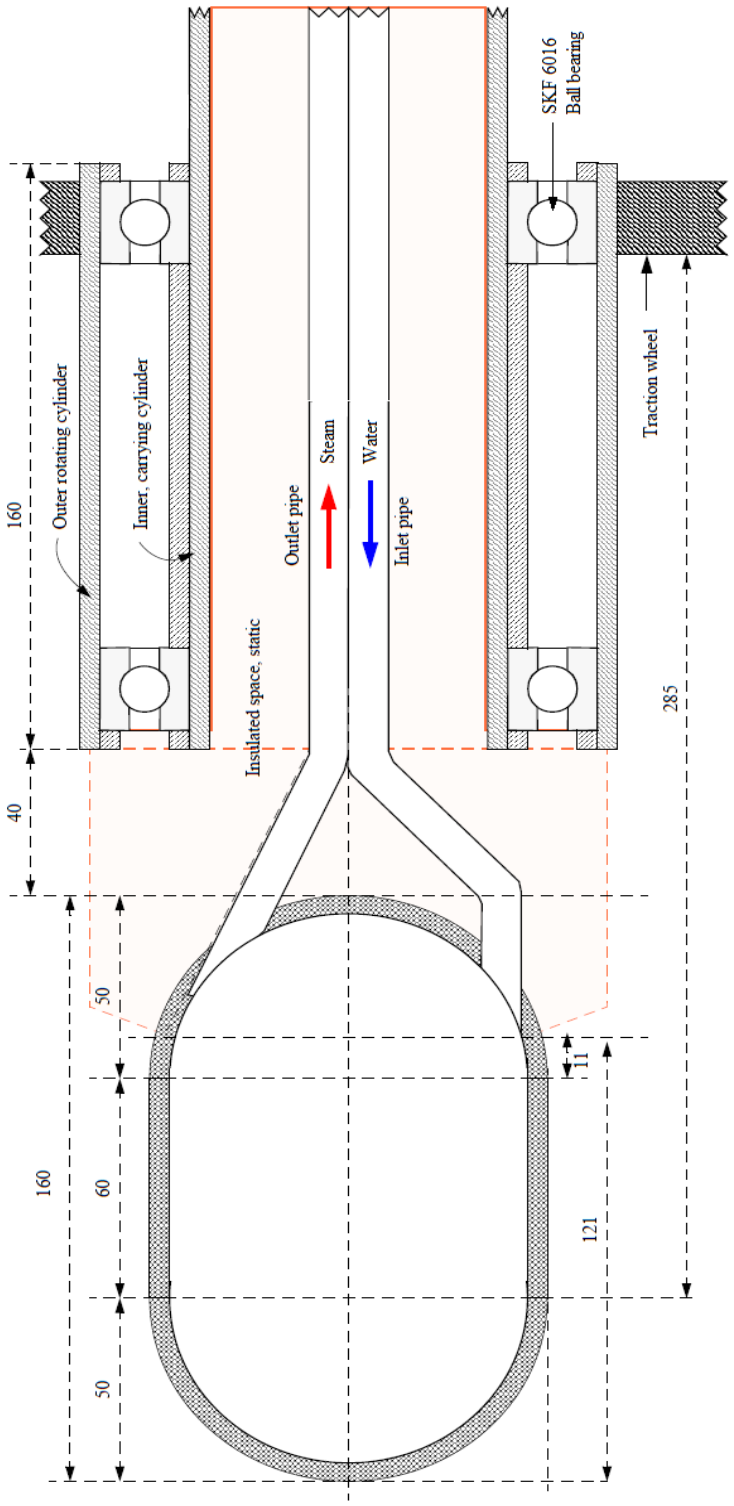

Figure C.2: Side-view of receiver boiling chamber with static and rotating cylinders. Mild steel (grade EN8) receiver boiling chamber with 4 mm wall thickness. (Courtesy of Jørgen Løvseth).

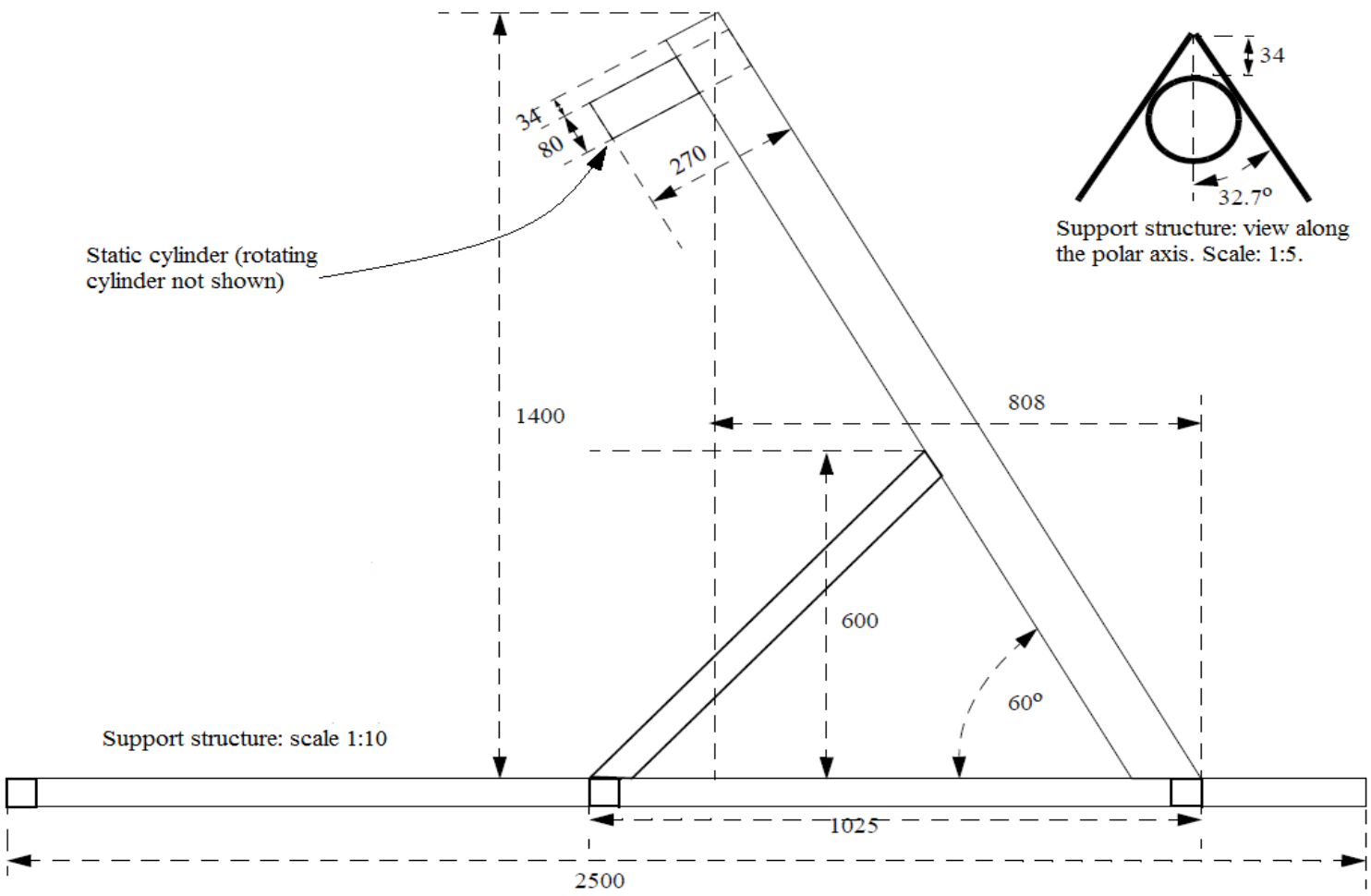

Figure C.3: Side-view of solar cooker system support structure. Inner static cylinder fixed to the top of the triangular structure is shown. Material used for all parts was mild steel (grade EN8). (Courtesy of Jørgen Løvseth).

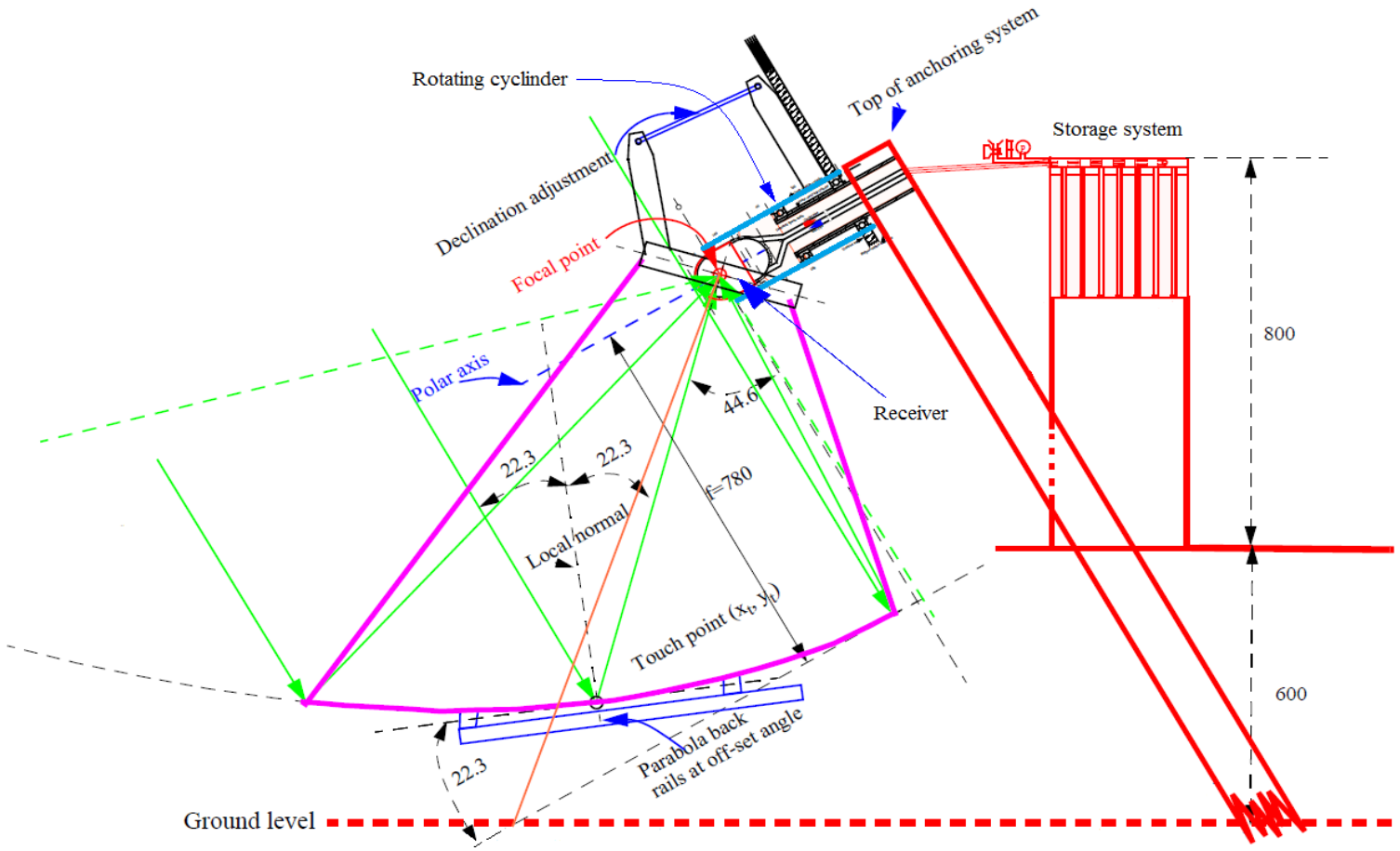

Figure C.4: Solar cooker system with polar axis at 30 ° for Durban. Green solid lines indicate the reflected rays. Declination adjustment is done by the square frame which rotates with the dish and vertical bar mounted onto the rotating cylinder. Parts shown in red are static. Rotating cylinder shown in blue. Inner static cylinder carries the receiver and joined to the outer rotating cylinder through ball bearings. (Courtesy of Jørgen Løvseth).